ISBN 978-94-6295-440-3

TU Delft Faculty of Applied Sciences

TBE - Cover Doctoraat-DEF.indd 1

Reactivity Monitoring of Accelerator-Driven Nuclear Reactor Systems

Wim Uyttenhove

Reactivity Monitoring of Accelerator-Driven Nuclear Reactor Systems

Wim Uyttenhove

Department of Radiation Science and Technology

16/12/15 10:02

INVITATION

For the public defense
of my PhD thesis

Reactivity Monitoring of Accelerator-Driven Nuclear Reactor Systems

MONDAY JANUARY 4, 2016
Senaatszaal,
Aula of TU Delft,
Mekelweg 5,
Delft - The Netherlands

14:30 Introductory talk
15:00 Thesis defense

Wim Uyttenhove

More information on
www.thebindingenergy.com/phd

3E - Doctoraat uitnodiging.indd 1 15/12/15 20:01

Reactivity Monitoring of Accelerator-Driven Nuclear Reactor Systems

Reactivity Monitoring of Accelerator-Driven Nuclear Reactor Systems

Proefschrift

ter verkrijging van de graad van doctor
aan de Technische Universiteit Delft,
op gezag van de Rector Magnificus Prof. ir. K.C.A.M. Luyben,
voorzitter van het College voor Promoties,
in het openbaar te verdedigen
op maandag 4 januari 2016 om 15:00 uur
door

Wim UYTTENHOVE

Nucleair en werktuigkundig-elektrotechnisch ingenieur, Universiteit Gent, België

geboren te Gent op 9 december 1980

Dit proefschrift is goedgekeurd door de promotor:

Prof. dr. ir. T.H.J.J van der Hagen

Samenstelling promotiecommissie:

Rector Magnificus,	voorzitter
Prof. dr. ir. T.H.J.J van der Hagen,	Technische Universiteit Delft, promotor
dr. ir. D. Lathouwers,	Technische Universiteit Delft, copromotor
Prof. dr. H. van der Graaf,	Technische Universiteit Delft
Prof. dr. S. Roeser,	Technische Universiteit Delft
Prof. dr. P. Désesquelles,	Université Paris-Sud
Prof. dr. ir. W. D'Haeseleer,	KU Leuven
dr. ir. P. Baeten,	SCK•CEN, Vrije Universiteit Brussel

Prof. dr. ir. J.-L. Kloosterman (Technische Universiteit Delft) en dr. ir. G. Van den Eynde (SCK•CEN, Universiteit Hasselt) hebben een belangrijke bijdrage geleverd in de begeleiding en ondersteuning van deze thesis.

© 2016, Wim Uyttenhove

All rights reserved. No part of this book may be reproduced, stored in a retrieval system, or transmitted, in any form or by any means, without prior permission from the copyright owner.

ISBN 978-94-6295-440-3

Keywords: nuclear, accelerator-driven systems, reactivity, reactor physics, experiments, modal analysis, VENUS, MYRRHA

The research described in this thesis was performed in the section Physics of Nuclear Reactors (PNR), of the department Radiation, Radionuclides & Reactors (R^3), of the Delft University of Technology, Delft, The Netherlands.

The research described in this thesis was (financially) supported by the Belgian Nuclear Research Centre (SCK•CEN) and by the GUINEVERE and FREYA projects within the 6th and 7th Framework Program of the European Commission.

Printed by Proefschriftmaken.nl || Uitgeverij BOXPress, 's-Hertogenbosch, The Netherlands

Contents

1 Introduction **1**
1.1 ADS Physics and Technology 2
1.2 Motivation for Accelerator-Driven Systems 5
1.3 Subcriticality Monitoring Techniques 7
1.4 Ongoing ADS Projects 17
1.5 The EFIT, MYRRHA and VENUS-F Reactor Designs 21
1.6 Research Outline 29

2 Spatial Effects in Subcriticality Monitoring **33**
2.1 Modal Analysis Approach 34
2.2 Start-up Reactivity Monitoring Techniques 38
2.3 The Current-To-Flux Reactivity Monitor 48
2.4 The Source Jerk Interim Reactivity Cross-Checking Method 51
2.5 Obtaining a Reference Subcriticality Level 55
2.6 Experiment Simulation via the DALTON Diffusion Code 57
2.7 Summary 59

3 Validation by Experimental Results from Subcriticality Measurements **61**
3.1 The VENUS-F Subcritical 'Reference' State 62
3.2 Subcriticality Monitoring during Start-up 67
3.3 Subcriticality Monitoring during Operation 90
3.4 Interim Reactivity Cross-Checking Techniques 97
3.5 Conclusion and Outlook 101

4 Subcriticality Monitoring in a Power ADS **103**
4.1 Selected MYRRHA Subcritical Cores for Reactivity Monitoring . . . 104
4.2 Subcriticality Monitoring during Start-up 108

4.3 On-line Subcriticality Monitoring during Normal Operation 114
4.4 Robustness of the Reactivity Monitoring against Incident Scenarios 123
4.5 Discussion 129
4.6 Conclusion 130

5 Conclusions and Recommendations 133
5.1 Conclusions 133
5.2 Recommendations 137

A The VENUS-F Models in DALTON 139
A.1 Geometry Description 139
A.2 Cross Section Generation 143

B The MYRRHA Model in DALTON 145
B.1 Geometry Description 145
B.2 Cross Section Generation 147

C List of Abbreviations 149

References 151

Summary 165

Samenvatting 169

Acknowledgements 173

List of Publications 175

Curriculum Vitae 181

1

INTRODUCTION

For Christ's sake, Soddy, don't call it transmutation.
They'll have our heads off as alchemists.

Ernest Rutherford, to his colleague Frederick Soddy
on the discovery of transmutation of thorium, 1901.

Picture: Homer Simpson ©FOX Broadcasting Company

In an Accelerator-Driven System (ADS) [Nifenecker et al., 2003; Kadi and Revol, 2002] accelerated particles create external source neutrons that drive a subcritical reactor. Thanks to the subcriticality of the reactor, fuels with a small delayed neutron fraction can be used in a safe way, i.e. in a reactor with a larger margin to supercriticality. Therefore, on the long term, the incineration of long-lived radiotoxic minor actinides (MA) can be envisaged in ADS. Subcriticality monitoring is required for both operational as well as safety reasons.

In this first chapter, the conceptual design of ADS is presented and the motivation of ADS is discussed. The ongoing projects are discussed and candidate reactivity measurement techniques are presented. The MYRRHA and VENUS-F reactors will be investigated in this thesis, being the major ongoing demonstrator project and zero power operational facility, respectively. Finally, the research topic is explained and coupled to the structure of this PhD thesis text.

1.1 ADS Physics and Technology

In an ADS, a particle accelerator, a spallation target and a nuclear reactor with a subcritical core are coupled, as shown in Fig. 1.1 [Nifenecker et al., 2001]. The accelerated particles, usually protons in power ADS designs, impinge on a spallation target, where they produce external source neutrons that drive the subcritical reactor. This section discusses the general neutron physics and main components of a full-scale ADS.

The fission power of an ADS is directly proportional to its beam current by [Gandini and Salvatores, 2002; Salvatores et al., 1994]

$$P = \frac{k_{eff}}{1-k_{eff}} \frac{i_p \overline{E_f}}{\overline{\nu}} Z \phi^* \tag{1.1}$$

with P the total power (W), k_{eff} the effective multiplication factor of the reactor, i_p the number of incident protons per second (1/s), $\overline{E_f}$ the average energy per fission (J), $\overline{\nu}$ the average neutron yield per fission, Z the number of source neutrons per incident source proton and ϕ^* the neutron source efficiency [Gandini and Salvatores, 2002; Mellier, 2005]. ϕ^* is defined by

$$\phi^* = -\rho \frac{\langle F\phi \rangle}{\langle S \rangle} \tag{1.2}$$

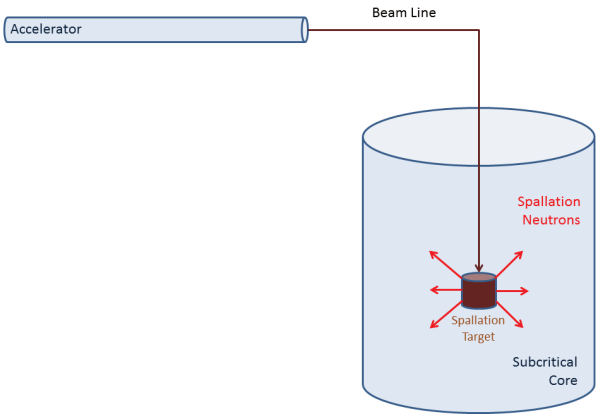

Figure 1.1: Concept of an Accelerator-Driven System.

with $\rho = \frac{k_{eff}-1}{k_{eff}}$ the reactivity of the reactor. The term $\langle F\phi \rangle$ represents the total production of neutrons by fission, $\langle S \rangle$ is the total production of neutrons by the external source and the brackets indicate integration over volume, solid angle and energy.

The flux ϕ (in n/cm^2/s) is the solution of the inhomogeneous transport equation [Bell and Glasstone, 1985]

$$(F-L)\phi + S = 0 \tag{1.3}$$

with F the fission operator, L the transport operator comprising neutron leakage, neutron collisions and neutron scattering, and S the source strength (n/cm^3/s):

$$F\phi = \frac{\chi(E)}{4\pi} \int_0^\infty dE' \int_{4\pi} d\widehat{\Omega}' \, \nu(E')\Sigma_f(\vec{r},E')\phi(\vec{r},\widehat{\Omega}',E') \tag{1.4}$$

$$L\phi = \widehat{\Omega}.\nabla\phi(\vec{r},\widehat{\Omega},E) + \Sigma_t(\vec{r},E)\phi(\vec{r},\widehat{\Omega},E) - \int_0^\infty dE' \int_{4\pi} d\widehat{\Omega}'\Sigma_s(\vec{r},\widehat{\Omega}' \to \widehat{\Omega}, E' \to E)\phi(\vec{r},\widehat{\Omega},E) \tag{1.5}$$

$$S = S(\vec{r},\widehat{\Omega},E) \tag{1.6}$$

The neutron source efficiency can also be defined as

$$\phi^* = \frac{\frac{1-k_{\text{eff}}}{k_{\text{eff}}}}{\frac{1-k_s}{k_s}} \tag{1.7}$$

with k_s the source multiplication factor

$$k_s = \frac{\langle F\phi \rangle}{\langle F\phi \rangle + \langle S \rangle} \tag{1.8}$$

The neutron source efficiency plays an important role in the ADS performance assessment. It expresses the importance of the external source generated neutrons relative to the neutrons generated by fission in the subcritical reactor. A value higher than 1 can reduce proportionally the proton beam current requirement for a given subcriticality level. Typical values vary around unity, e.g. between 0.9 (for a source positioned at the core-reflector interface) and 1.1 (for a source positioned at the centre height) [Gandini and Salvatores, 2002].

The **accelerator** provides high energy charged particles that drive the subcritical core. The choice between a linear accelerator or a cyclotron is application dependent. In order to reduce thermal stresses, a power ADS should be extremely reliable with regard to beam interruptions.

The **spallation target** provides the source neutrons that feed the fission process in the core. In case of a power ADS, they are produced by the spallation reaction of charged particles on a heavy metal target. An optimal target creates a maximum amount of neutrons per incident particle and per unit energy of the beam, and is able to remove the heat generated by the spallation process. Therefore, the target must be cooled. In case of power ADS, liquid (metal) targets are candidate to fulfill these requirements. Both lead and lead-bismuth eutectic are two primary candidates for the production of spallation targets in a power ADS. For the separation between the coolant and the beam guide (in vacuum), a beam window is foreseen [Keyers, 2010] in the ongoing designs. The period for replacement of the window due to radiation damage (by protons) is therefore an important parameter in the operation of a power ADS.

The **coolants** considered for fast reactors are also candidates to serve for ADS. Given the high power densities, liquid metals such as sodium, lead and lead-

bismuth are suitable candidates. Also gases, such as helium and CO_2, are possible candidates. A comparative overview of both liquid metals as well as gases as coolant is provided in [NEA, 2003], Chapter 4. For an ADS, lead and lead-bismuth have the additional advantage to serve as coolant as well as spallation target.

The **subcritical reactor** of an ADS acts as an amplifier for the source neutrons. The neutron energy spectrum of the subcritical reactor depends on its composition. A fast neutron spectrum leads to a better energetic yield for the transmutation of Minor Actinides (MA)[1], as well as a lower MA production. Power control in an ADS reactor can be performed by control rod movements or by beam current variations.

1.2 Motivation for Accelerator-Driven Systems

1.2.1 History

A comprehensive overview of the history of ADS is provided by [Gudowski, 1999; Kadi and Revol, 2002]. Already in 1940, E.O. Lawrence (USA) and W.N. Semenov (USSR) studied the use of accelerators to provide neutrons. In 1941, Glenn Seaborg was the first to produce Plutonium by using a 6 MeV deuteron accelerator impinging on U-238. In 1950, Lawrence proposed the Material Testing Accelerator (MTA) at the Lawrence Livermore Radiation Lab to produce Pu-239 from depleted uranium [Van Atta, 1977]. In 1952, W.B. Lewis (Canada) recommended to use an accelerator for the production of U-233 from thorium, for the CANDU reactors [Bartholomew and Tunnicliffe, 1966]. Both projects were slowed down or stopped by the discovery of rich uranium deposits in the USA and the reliability and cost of accelerator beams. The concept of accelerator breeding was also studied by Russian scientists. R.G. Vassylkov [Vassylkov et al., 1978] made a neutron yield experiment in depleted uranium blocks using the Dubna accelerator.

Renewed interest in ADS was gained in the 1980s at Brookhaven National Lab (USA) [Brookhaven National Laboratory, 2013], when the USA decided to slow

[1] Nuclear transmutation is the conversion of one chemical element or isotope into another through nuclear reactions or through radioactive decay. Transmutation technology has the potential to greatly reduce the long-term negative effects of radioactive wastes on human populations by reducing its radioactive half-life. This is the case for the MAs, i.e. the actinide elements (with atom number 89 until 103) other than uranium and plutonium, which are called major actinides. Minor actinides concerned in nuclear fuel are neptunium-237, americium-241, americium-243, curium-242 through -248, and californium-249 through -252.

down the development of critical fast reactors, and in the 1990s at CERN (Switzerland), when C. Rubbia became convinced that accelerator technology is mature enough for an exploitation of the ADS idea. He proposed a proton accelerator driven subcritical system with fast neutrons, based on thorium fuel and lead as spallation target, moderator and coolant [Rubbia et al., 1995]. Later on the scientific feasibility and the verification of the principle of energy amplification by a high energy cascade were proven in experiments such as FEAT [Andriamonje et al., 1995] and TARC [Arnould et al., 1999].

1.2.2 Motivation

Incineration and Transmutation

Today, multiple ADS projects are ongoing at different continents. They are presented in § 1.4. The principal goal, which makes an industrial scale ADS unique, is the incineration of large quantities of nuclear waste. A subtle difference should be made between transmutation and incineration.

During *transmutation*, a neutron capture causes the transformation of a radioactive nucleus. However, as stable nuclei could be transformed in radioactive ones, the method may require an initial separation of the isotopes that should be transmuted. *Incineration* is related to nuclear fission following neutron capture. This method goes on with transuranic elements and is already applied on plutonium, causing energy and neutron production.

Concerning safety, when inserting a considerable fraction of transuranic elements (in particular minor actinides) in a reactor fuel, its delayed neutron fraction decreases. This effect makes a critical reactor more difficult to control and limits the concentration of MA in fast reactor (FR) MOX fuel to 2.5 % ([IAEA, 2009a], Section 6.2.1). An alternative approach is to burn MA in an ADS, guaranteeing that in all conditions of operation, a sufficient margin to criticality is foreseen (see § 1.6.1).

Concerning the decay heat removal issue (the second important safety issue of a typical critical nuclear installation), no fundamental changes appear by using an ADS. The power density remains an important factor to study, and is design dependent.

Thorium ADS

A second motivation for an ADS is related to the use of thorium (Th). Th-232 is a fertile material. It is not fissionable by thermal neutrons, but can be converted into a fissile material by neutron absorption and subsequent nuclei conversions. Th-232 can be used for the production of fissile U-233 material. The fission of this isotope causes less radiotoxic waste (due to minor actinides) than the fission of U-235 or Pu-239 ([Nifenecker et al., 2003], Chapter 11). If a low reactivity variation is required during operation, a reactor with plutonium and minor actinides fuel is recommended rather than a thorium reactor, in order to reduce the required beam power in an industrial ADS.

1.2.3 Challenges

Compared to the incineration of minor actinides in (critical) fast reactors, challenges of industrial ADSs will be related to the fabrication of the fuel with a high concentration of minor actinides, towards the reliability of the accelerator and to other design-dependent technological issues.

Moreover, before studying *incineration* of minor actinides, *partitioning* is the first step to pass when studying the feasibility of transmutation of spent fuel minor actinides. A good overview of advanced fuel cycle partitioning is given in [IAEA, 2009b], Section IV, [Baetslé, 2001], Chapter 3 or [Chauvin et al., 2011]. Today, separation of minor actinides has only been demonstrated in small quantities, and needs to be simplified in order to allow upscaling to technological levels. Heterogeneous recycling of minor actinides is a way to avoid the dilution by troublesome nuclides, such as Cm-244 (as a major source of α-radiation), throughout the fuel fabrication step. Current research is only in an early stage of development.

1.3 Subcriticality Monitoring Techniques

Different techniques for subcriticality monitoring exist, based on manipulations with the ADS source. For each technique, multiple evaluation methods are possible, as both static and dynamic reactor physics can be applied in order to determine the reactivity value. The static approach relies on an integration of the detector response over a certain time period, whereas dynamic methods study the time dependent profile of the detector response. An overview of the existing techniques and related evaluation methods is provided in Table 1.1. In this

section, each evaluation method is presented, focusing on the applicability to subcriticality monitoring.

Technique	Evaluation Method	Static (S) Dynamic (D)	
Pulsed neutron source	Area	S	§ 1.3.1
	α	D	§ 1.3.1
	k_p	D	§ 1.3.1
	Noise	D	§ 1.3.6
Source jerk	Integrated (ISJ)	S	§ 1.3.2
	Standard (SJ)	S	§ 1.3.2
	α	D	§ 1.3.2
	k_p	D	§ 1.3.2
Source modulation	Prompt jump	S	§ 1.3.3
Continuous beam	Current-to-flux (CTF)	S-D	§ 1.3.4
	Source multiplication	S	§ 1.3.5
	Noise	D	§ 1.3.6

Table 1.1: Overview of the different reactivity monitoring techniques for ADS and their related evaluation methods.

1.3.1 The Pulsed Neutron Source (PNS) Technique

During the Pulsed Neutron Source (PNS) experiment [Sjöstrand, 1956], (Dirac shaped) neutron pulses are introduced in a subcritical reactor. The required period of the pulse (in general in the order of 0.1-1 ms) depends on the reactor design. In order to obtain a repetitive detector output, the prompt decay of the detector response on a neutron pulse should have died out before the next pulse is noticed in the detector response. Secondly, many (about 200000) pulses should be given to establish a stable 'delayed' level in the detector output of a pulse train [Baeten et al., 2006].

The PNS technique will be studied in this work as a candidate to determine the initial reactivity level before (power) operation of the ADS, as this technique requires the neutron to work in pulsed mode. From the pulse shape detector output, different evaluation techniques exist that provide the reactivity of the

reactor in dollars [2].

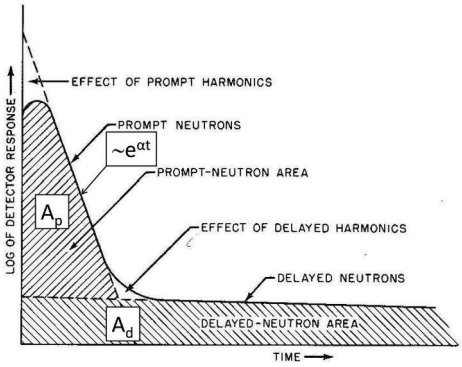

Figure 1.2: Graphical representation of the evaluation methods applicable on the PNS technique. [Bell and Glasstone, 1970]

The static evaluation of the PNS technique by the area (also called Sjöstrand) method [Sjöstrand, 1956] provides the subcriticality level of the reactor by the ratio of two areas in the decay of the neutron density after a pulse, as shown in Fig. 1.2:

$$\frac{-\rho}{\beta} = \frac{A_p}{A_d} \tag{1.9}$$

with ρ the reactivity, β the delayed neutron fraction, A_p the area related to the prompt decay of the neutron density and A_d the area related to the delayed decay of the neutron density.

The area method is a well-known robust method. Robust means that the reactivity (in dollars) can be derived directly from the ratio of the integrated prompt and delayed neutron fissions, without other reactor physics parameters intervening.

Dynamic evaluation techniques, such as the prompt decay α-method [Simmons and King, 1958; Garelis and Russell, 1963; Bell and Glasstone, 1970], are based on the prompt decay of the neutron density to determine the reactivity level. The prompt decay method allows to determine the reactivity via

$$\rho = \alpha\Lambda + \beta_{eff} \tag{1.10}$$

[2] ρ=1 \$ corresponds to $\rho=\beta_{eff}$, the effective delayed neutron fraction of the fuel.

with α the fundamental time eigenvalue of the subcritical system (1/s), i.e. the slope of the prompt neutron decay indicated in Fig. 1.2, and Λ the generation time (s).

Dynamic methods however are sensitive to some kinetic integral parameters values (e.g. the neutron generation time Λ) that are cumbersome to measure precisely and lose their physical significance [Dulla et al., 2011]. Therefore, these methods are less robust [Jammes et al., 2006] than the static ones.

Another dynamic method, the k_p method [Perdu et al., 2003], provides the reactivity by fitting the recorded pulse response to an interpretation model that makes use of a calculated fission time distribution. This method requires a significant calculational effort and a precise model description. This makes the method less robust than e.g. the area method.

1.3.2 The ADS Source Jerk Techniques

The source jerk technique [Ott and Neuhold, 1985] comprises the rapid removal of a neutron source out of an ADS. Both the physical removal of a (continuous) external neutron source or an interruption of the accelerator neutron source can represent the source jerk. Two types of source jerks exist.

The Integrated Source Jerk (ISJ) method consists in the evaluation of the neutron population over the complete dying-out time of the signal (in the order of hundreds of seconds), see [Ott and Neuhold, 1985], section 9-4:

$$\frac{-\rho}{\beta} = \frac{n(0)\sum_{i=1}^{q}\frac{a_i}{\lambda_i}}{\int_0^\infty n(t)dt} \tag{1.11}$$

with $n(0)$ the neutron density before beam stop, $a_i = \frac{\beta_i}{\beta}$ the delayed neutron fraction in precursor group i, λ_i the precursor decay constant of group i, and $\int_0^\infty n(t)dt$ the time integral from t=0 s (after beam interruption) until the dying out of the final precursor neutrons.

The (beam interruption) Source Jerk (SJ) method consists in determining the ratio of the prompt to the slowly decaying delayed neutron population directly in the first hundreds of µs after beam interruption, as shown in Fig. 1.3:

$$\frac{-\rho}{\beta} = \frac{n_0 - n_1}{n_1} \tag{1.12}$$

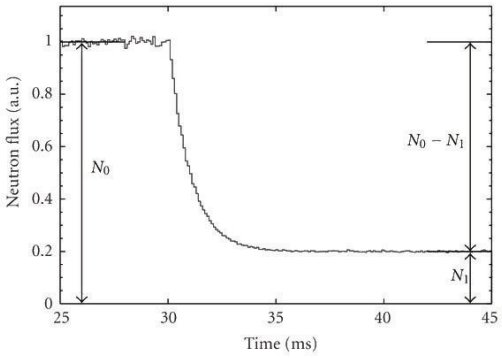

Figure 1.3: Graphical representation of the beam interruption Source Jerk (SJ) method. [Becares and Blazquez, 2012]

Both methods provide the reactivity of the subcritical reactor in dollars. For good statistics, the source jerk technique requires repetition (as for the PNS technique), whereas the integrated source jerk technique requires a high initial flux level and cannot be repeated.

During operation of an ADS, only the (beam interruption) source jerk mode is a candidate for subcriticality measurements. By briefly interrupting the continuous beam at regular times, a cross checking of reactivity is performed. Then the equivalent continuous beam current is the average value over the period of the beam interruption. The limiting factor to apply this technique is the beam interruption time, which should not be too long in order to avoid thermal stresses in the ADS, and which may not be too short in order to allow to determine with sufficient statistics the delayed neutron level.

The (beam interruption) source jerk technique allows also dynamic evaluation methods such as the α-methods and the k_p method, described in § 1.3.1 and [Billebaud et al., 2009]. In case the standard method (eq. (1.12)) cannot be used, e.g. because of a too long beam interruption time, these methods can serve as alternative.

1.3.3 The Source Modulation Technique

The source modulation technique [Baeten et al., 2006; Carta and D'Angelo, 1999; Ott and Neuhold, 1985] consists in changing the frequency of a pulsed source, as shown in Fig. 1.4. When looking on a macroscopic time scale, one can determine

the reactivity level, as for the source jerk technique, based on prompt and delayed neutron densities:

$$\frac{-\rho}{\beta} = \frac{n_H - n_C}{n_C - n_L} \tag{1.13}$$

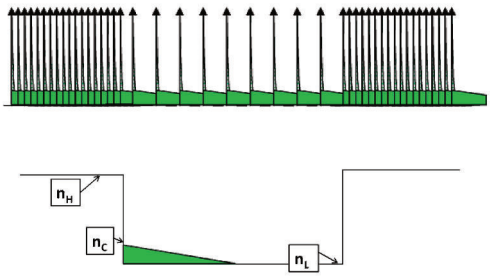

Figure 1.4: Graphical representation of the source modulation method on a microscopic (top) and macroscopic (bottom) level. [Baeten et al., 2006]

The technique can be used as a calibration technique during start-up, but easier evaluation methods for techniques with fixed frequency (e.g. the PNS technique) exist. In theory, this method is an alternative for the standard source jerk technique. In reality, it is technologically complicated to change from continuous beam to a source modulation mode.

1.3.4 The Current-to-Flux (CTF) Technique

The Current-to-Flux (CTF) technique ([Mellier, 2005], § 9.1, and [Becares et al., 2013]) relates the reactivity level of a subcritical reactor with continuous neutron source to the ratio between beam current (or source neutrons) and flux (or neutron density, or fission neutrons, or power):

$$\rho = -c\frac{S}{\phi} \tag{1.14}$$

with ϕ the neutron flux (n/cm^2/s), S the accelerator beam current (A) and c the Current-to-Flux (CTF) proportionality coefficient (n/cm^2/s/A). The proportiona-

lity coefficient c can be calibrated if a reference reactivity is known. No other parameters are involved in the expression for the reactivity, this makes the CTF method robust as on-line reactivity monitoring technique during operation.

The CTF technique is only a relative monitor. Therefore, the behaviour of the proportionality coefficient, which takes into account the spatial dependent evolution of the dynamic behaviour of the neutron flux, can vary during operation of the ADS. Cross-checking with an absolute reactivity measurement technique is required at a regular base.

1.3.5 Source Multiplication Method

The source multiplication method [Ott and Neuhold, 1985; Blaise et al., 2011] allows to determine the subcriticality level of a new reactor state ('2') starting from another reactor state ('1') with a known subcriticality level, by keeping the neutron source constant and measuring the differences in neutron density (or detector count rates):

$$\frac{\rho_2}{\rho_1} = \frac{n_1}{n_2} \tag{1.15}$$

The source multiplication technique is static, so statistics on the count rates (and the derived reactivity level) can be improved by increasing the measurement time. This method is robust, as no other parameters than count rates and reactivity levels are applied. It can be applied to determine a reference subcritical level against which the techniques mentioned in this paragraph can be validated. To do so, a slightly subcritical state is obtained from a critical reactor by the rod drop technique [Ott and Neuhold, 1985]. From this state, the subcriticality level of deeper subcritical reactors can be determined by the source multiplication method (see § 2.5).

1.3.6 Noise Measurement Techniques

Noise methods are based on the study of the neutron fluctuations in a reactor. Several noise measurement techniques are available to determine reactivity levels, such as the Rossi-alpha, Feynman-alpha and the Cross Power Spectral Density (CPSD) techniques [Uhrig, 1956; J.A. Thie, 1963]. These reactivity measurement methods rely on the determination of the prompt neutron fundamental time decay constant α.

The noise techniques have the advantage to determine the reactivity level on an absolute scale. However, the methods are quite complicated to analyse, as no simple reactivity value can be determined by point kinetics evaluation techniques. Moreover, for an acceptable signal-to-noise ratio for ADS reactivity measurements, it is recommended to add a pulsed neutron source to the existing continuous beam [Baeten, 2003]. This is only possible at zero power operation. By doing this, evaluation techniques approach the dynamic PNS evaluation technique, which is not such a robust evaluation technique as its static alternative (see §1.3.1).

1.3.7 Experience with Zero Power Facilities

The main experiments related to subcriticality monitoring were performed during the FP5 MUSE project experiments [Soule et al., 2004; Mellier, 2005], at the MASURCA zero power facility at CEA Cadarache, France, and during measurements at the YALINA booster in Sosny, Belarus [Persson et al., 2005; Becares et al., 2013]. During both experiments, there was no possibility to obtain a reference subcriticality level via the alternative methodology presented in § 1.3.5.

A conclusion of this research programme is that an on-line reactivity monitoring methodology should consist of a combination of several techniques, for each stage of operation of an ADS. As a continuous monitor, the current-to-flux method seems a promising candidate, but needs to be tested extensively [Soule et al., 2004].

The reactivity was calibrated during MUSE with a relative accuracy of 10 % via the PNS technique [Soule et al., 2004; Cao and Lee, 2010]. The area method for the analysis of the PNS calibration experiment came out as a promising method, not depending on kinetic parameters [Mellier, 2005]. Particular attention should be paid to the careful determination of a 'reference' reactivity level (for validation purposes) and to perform measurements with sufficient statistics.

The area method seems the most robust evaluation method for the PNS technique. Fitting techniques [Soule et al., 2004] require the knowledge of kinetic parameters, and the k_p technique is sensitive to calculations and their related models [Chabod et al., 2014].

Beam interruption evaluation techniques could offer an additional reactivity cross-check, but could not be tested during the MUSE project. A so-called reflector effect (slow beam decay in the reflector after beam interruption) could hamper the efficient determination of reactivity levels via pulsed or beam interruption

techniques in that region. This effect should be investigated [Becares et al., 2013]. The Integrated Source Jerk (ISJ) method was not tested during MUSE, but can only be used during start-up, as the beam needs to be stopped for a while. The source strength should be high enough to assure good statistics of the ISJ method [Mellier, 2005].

Noise measurements seem to be interesting only close to criticality. In more deep subcritical reactors, long measurement times are required and the accuracy is limited [Berglof et al., 2011]. In order to improve the accuracy, noise measurements with a pulsed neutron source are investigated [Mellier, 2005], however they can serve only as start-up method. For that purpose, more robust techniques are available without the need to know the neutron generation time Λ.

1.3.8 Selected Monitoring Techniques

Based on the nature of the subcriticality measurement techniques and experience feedback presented in this section, an overview of the candidate monitoring techniques is presented in Table 1.2. One can conclude that one single technique is not sufficient to monitor the subcriticality of an ADS during all stages of operation. For a power ADS such as MYRRHA (see § 1.4), the start-up mode ends by moving the control rods to reach the desired reactivity level. Afterwards, the beam level is raised until 1 % of nominal power (Cold Zero Power - CZP). From that moment on, the beam power will rise and only short interruptions of the beam are allowed, to limit thermal stresses in the reactor.

In this work, the PNS area method is studied as a robust start-up reactivity measurement method (with the ISJ technique as alternative). The current-to-flux monitor, combined with the source jerk interim cross-checking technique is proposed for analysis as on-line reactivity monitor during operation. The selection is based on the robustness of the method and the technological ability to perform the experiment on (a full power) ADS.

The rod drop - source multiplication method will be applied in order to provide a subcriticality level via an alternative pathway against which the different selected techniques can be tested.

Evaluation Method	R/A	Selected? (Y/N)	Operational Mode	Discussion
PNS Area	A	Y	Start-up	Integral method, no other parameters involved, reproducible.
PNS α	A	N	Start-up	Dependent on Λ, more robust alternative by PNS area.
PNS k_p	A	N	Start-up	Requires calculational effort, dependent on input model, more robust alternative by PNS area.
ISJ	A	Y	Start-up	Integral method, depends on delayed neutron coefficients, not reproducible.
SJ (standard)	A	Y	Operation	No other parameters involved, reproducible, provides absolute value of the reactivity.
SJ α	A	N	Operation	Same as PNS equivalent, alternative method if (standard) SJ cannot be applied.
SJ k_p	A	N	Operation	Same as PNS equivalent, alternative method if (standard) SJ cannot be applied.
Source Modulation	A	N	Start-up and operation	Interesting method, but technical complexity to vary beam frequency.
CTF	R	N	Operation	Simple technique with no other parameters involved, which provides continuous monitor. Statistics depend on time interval for monitoring
Source Multiplication	R	Y	Reference	Simplified CTF technique used for determining reference subcriticality level starting from critical state.
Noise Techniques	A	N	Start-up and Operation	Dependent on Λ. PNS superposition needed for acceptable statistics, which limits application to start-up. For that mode more robust techniques are available.

Table 1.2: Overview of the different reactivity monitoring techniques for ADS, based on the nature of the method and the experience feedback from previous zero-power experiments. R = Relative technique, A = Absolute technique.

1.4 Ongoing ADS Projects

A recent overview on the international ongoing ADS programmes is given in [Gohar, 2012]. The latest status report from the OECD Nuclear Energy Agency (NEA) dates from 2003 [NEA, 2003]. In this section, an overview of the major ongoing ADS programmes is given, ranging from zero power experiments to power ADS.

1.4.1 Europe

Zero-Power Experiments

Subcritical reactor physics and reactivity measurement techniques were investigated between 2000 and 2004 within the European Framework Programme (FP5) project MUSE (MUltiplication avec Source Externe) [Soule et al., 2004; Mellier, 2005]. Sodium and lead reactors with 30 wt% MOX fuel were implemented at the MASURCA facility at CEA Cadarache, driven by the GENEPI deuteron accelerator.

On an international level, research went on at the YALINA facility in Belarus [Gohar and Smith, 2010], coordinated by the IAEA and International Science and Technology Centre (ISTC), between 1997-2008. The YALINA-Booster is a subcritical fast-thermal reactor. The reactor consists of a fast central lead zone with 36 wt% enriched U (booster), a thermal PolyEthylene (PE) zone with natural U, a radial graphite reflector and a front and back biological shielding of borated PE.

In 2006 the GUINEVERE (Generator of UnInterrupted NEutrons at the VEnus REactor) project was launched within the European FP6 IP-EUROTRANS collaboration [Knebel, 2006; Baeten et al., 2008] (2005-2010), in order to develop a methodology for reactivity monitoring in ADS. The existing zero-power VENUS facility at SCK•CEN, Belgium, was modified towards VENUS-F: a fast spectrum lead reflected system that can be operated in both critical and subcritical mode. In the latter mode, the reactor is coupled to the GENEPI-3C accelerator [Baylac et al., 2010], an updated version of the GENEPI-2 machine previously used for the MUSE experiments.

In February 2011, VENUS-F passed its first criticality. The first coupling with the accelerator was realised in October 2011. Today experiments go on in the framework of the FP7 Project FREYA (Fast Reactor Experiments for hYbrid Applications) [Kochetkov, 2010; Kochetkov et al., 2013].

The MYRRHA Demonstrator Project

Today, the main European ADS research is grouped into European Framework Programmes (FP). The Belgian nuclear research centre SCK•CEN inspired the European ADS research with its national ADONIS (Accelerator Driven Operated New Irradiation System, 1995-1997) and MYRRHA (Multi-purpose hYbrid Research Reactor for High-tech Applications, 1998-2005) projects [Aït Abderrahim et al., 2012; Van den Eynde et al., 2012, 2014]. While ADONIS was a water cooled 1.5 MWth ADS design with a U-235 fuel target to produce Mo-99 for medical applications, MYRRHA aims to serve as a fast neutron material test facility, as well as to prove the feasibility of transmutation in a demonstrator ADS. The target and coolant is eutectic Pb-Bi, foreseen to be driven by 350 MeV protons in a MOX fuel core. The MYRRHA design power evolved from 30 MWth (2002) towards 52 MWth (2005).

Later on, the MYRRHA knowledge base was shared for the European FP6 project IP-EUROTRANS [Knebel, 2006] (2005-2009), a successor of the FP5 PDS-XADS project (2001-2004) [Bianchi et al., 2006]. Detailed design studies were carried out in the so-called XT-ADS version of MYRRHA. Then the FP7 CDT (Central Design Team) project (2009-2012) [De Bruyn and Fernandez, 2012] was launched to obtain a more advanced design of a flexible irradiation facility FASTEF (FAst Spectrum Transmutation Experimental Facility) with a maximum power of 100 MWth, able to work in both subcritical and critical mode.

In 2010, the Belgium government expressed its support to realise the MYRRHA project after a positive evaluation of the project proposal by the MYRRHA International Review Team (MIRT) [Aït Abderrahim et al., 2008; OECD/NEA, 2009], coordinated by the OECD on request of the Belgian government. During the 2010-2014 period SCK•CEN has to finalise the Front End Engineering Design (FEED) to secure the licensing, and to set-up an international consortium for the financial and technical support to the project.

Today MYRRHA is presented as a multi-purpose facility to perform research for Generation IV fission reactors, fusion, fundamental physics and transmutation studies, meanwhile producing radio-isotopes. Since 2010, MYRRHA is recognised on the priority list of the European Strategy Forum on Research Infrastructures (ESFRI) [ESFRI, 2010], as well as by the Strategic Research and Innovation Agenda of the Sustainable Nuclear Energy Technology Platform (SNETP) [SNETP, 2013]. The complete installation should be operational by 2024, making it today the

most concrete ADS demonstrator design in the world.

The European Facility for Industrial Transmutation (EFIT)

In the framework of the IP-EUROTRANS FP6 project, a design study was made for an industrial transmutation machine, called EFIT [Artioli et al., 2008; Mansani et al., 2011]. EFIT consists of a 800 MeV proton accelerator, providing spallation neutrons inside a Pu-MA fueled core, cooled by Pb, with a 400 MWth power.

1.4.2 Japan

Japan's ADS programme envisages the transmutation of transuranics and the generation of nuclear energy [Pyeon, 2013]. On the long term, a 800 MWth design is proposed with a 1.5 GeV∼20 MW proton beam, Pb-Bi spallation target and coolant, and (Pu+MA)N+ZrN fuel with a 2.5 ton MA initial inventory. Experiments today are ongoing with regard to the target window and Lead-Bismuth Eutectic (LBE) loops (JLBL1-3).

The Kyoto University runs the KUCA subcritical assembly [KUCA, 2013], which is driven by a 14 MeV D-T neutron source in a highly enriched uranium core with a PE reflector. Recently, KUCA has been combined with a proton beam accelerator to supply spallation neutrons to its subcritical reactor.

In the near future, Japan aims to construct the Japan Proton Accelerator Research Complex (J-PARC), which will host TEF-T (an ADS target test facility), foreseen to be operational by 2017, and TEF-P (a transmutation physics zero power critical assembly), foreseen to be operational by 2022.

1.4.3 China

The Chinese ADS programme [Pyeon, 2013] is related to fissile material breeding. Measurements are being performed on VENUS-1, operated by the Chinese Institute of Atomic Energy (CIAE). VENUS-1 is a subcritical physics experiment, driven by a 14 MeV pulsed neutron source in a reactor with a fast (natural U in an Al grid) and thermal (enriched U in PE) zone.

In 2011, the Chinese Academy of Science (CAS) announced to build an ADS system, including the development of the China LEad Alloy cooled Reactor (CLEAR). Four phases of development are foreseen: a lead based zero-power facility (CLEAR-0), a 10MWth lead-bismuth cooled research reactor (CLEAR-I) to be built in the

2010s, a 100MWth lead alloy cooled experimental reactor (CLEAR-II) to be built in the 2020s, and a 1000MWth lead alloy cooled demonstration reactor (CLEAR-III) to be built in the 2030s.

1.4.4 India

India's ADS programme [Degweker et al., 2013] aims to support the thorium fuel cycle by producing U-233. Also the transmutation of nuclear waste is considered on the long term. The first phase of research covers the different ADS research domains such as a windowless spallation target and Heavy Liquid Metal (HLM) experiments with mercury and lead-bismuth. A physics experiment is available at the PURNIMA labs at the Bhaba Atomic Research Centre (BARC). In a further stage, the development of two demo ADS (of 1 and 40 MWth power) with a spallation neutron source of LBE (cooled by light water) are scheduled.

1.4.5 The United States of America (USA)

Although the USA have no national full ADS project, they are active in the construction of an electron accelerator driven system in Ukraine at the Kharkov Institute of Physics and Technology (KIPT), via an IAEA collaboration [Gohar, 2012] (see § 1.2). This ADS, which should be operational in 2014, will operate with low enriched uranium as fuel, water as coolant and beryllium as reflector.

Other US research deals with the development of an ADS concept for the national spent fuel inventory (by Argonne National Laboratory), material test stands (at Los Alamos National Laboratory) and the physics of ADS using zero power facilities. For the latter, experiments were carried out at the YALINA booster in Belarus [Gohar and Smith, 2010].

1.4.6 Other International Programmes

In 2013, the IAEA reports that 18 countries are performing R&D in one or more domains of the ADS research: Argentina and Brazil (physics programme), Poland and Belarus (experimental physics programme), Italy and Russia (physics and technology programme), South Korea and Spain (transmutation programme), Norway (energy and thorium fuel cycle studies) and Germany (complete ADS programme) [Gohar, 2012].

1.5 The EFIT, MYRRHA and VENUS-F Reactor Designs

In this section, the design of the industrial EFIT ADS, the MYRRHA demonstrator and the VENUS-F zero power facility are presented. First the EFIT study is presented to show the transmutation capacities of an industrial design, and to check the expected reactivity swing during operation of an industrial ADS. Then the MYRRHA project is discussed, being the most advanced demonstrator ADS project currently ongoing. On this design, the subcriticality monitoring methodology will be applied. Finally, VENUS-F will serve for the validation of the subcriticality monitoring concept for the MYRRHA demonstrator ADS.

Table 1.3 provides the main characteristics of the three systems. VENUS-F can, thanks to a (unique) critical reference state, validate the different subcriticality monitoring techniques for MYRRHA and perform benchmarking activities. For the MYRRHA project however, the research is focused on beam reliability, the study of power effects and the behaviour of the Pb-Bi coolant. For EFIT studies, the minor actinide fuel design, the fuel performance and the lead coolant are the main challenges.

	VENUS-F	MYRRHA	EFIT
Power	Max 500 W	65-100 MWth	400 MWth
Accelerator	D, 250 keV	P, 600 MeV	P, 800 MeV
Neutron Source	(D,T) fusion neutrons	spallation neutrons	spallation neutrons
Fuel	Metallic U (30 wt% enriched)	MOX (30 wt% enriched)	Pu-MA
Coolant	Pb simulated coolant	Pb-Bi	Pb

Table 1.3: Main Characteristics of VENUS-F, MYRRHA and EFIT. [Uyttenhove and Van den Eynde, 2012]

1.5.1 EFIT

As industrial transmuter, EFIT aims to burn about 42 kg/TWh minor actinides, up to 20-25 % of the initial heavy metal in the fuel within 4-6 years. These goals should be met in a U-free fuel, by obtaining a break-even Pu balance. A flat reactivity profile is envisaged around k_{eff}=0.97 ± 0.01, to limit the compensation by beam current variations or control rod movements. As electricity production with an

acceptable efficiency is foreseen, higher primary circuit temperatures are reached with Pb: 400 °C at reactor inlet and 480 °C at reactor outlet.

The design of the EFIT reactor is presented in figure 1.5. Inside the core, 3 (or 6) rings of fuel assemblies can be hosted, comprising 198 position for fuel assemblies and 19 positions for the spallation target. The core barrel is completed with 252 positions for Pb dummy assemblies and absorber elements. Two types of fuels are studied, one with ceramic MgO (CERCER) and the other with metallic Mo (CERMET) as matrix material. In order to optimise the goals with regard to burn-up and reactivity swing, the fuel assembly parameters are optimised [Uyttenhove et al., 2011b; Sobolev et al., 2011b]. The final reactor design foresees an active fuel height of about 90 cm.

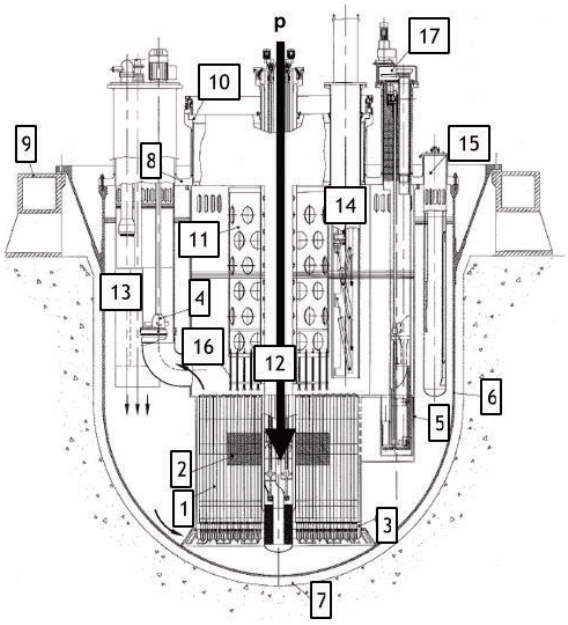

Figure 1.5: The EFIT reactor design from [Mansani et al., 2011] (1-core, 2-active zone, 3-diagrid, 4-primary pump, 5-cylindrical inner vessel, 6-reactor vessel, 7-reactor cavity, 8-reactor roof, 9-reactor vessel support, 10-rotating plug, 11-above core structure, 12-target unit, 13-steam generator unit, 14-fuel handling machine, 15-filter unit, 16-core instrumentation, 17-rotor lift machine).

1.5.2 MYRRHA

At the time of the writing of this text, the MYRRHA design is in continuous evolution. A general description of the MYRRHA project is found in [Aït Abderrahim et al., 2008], and the latest design status is presented in [Aït Abderrahim and Baeten, 2012; Aït Abderrahim et al., 2012; Van den Eynde et al., 2014]. In this work, the MYRRHA-FASTEF (FAst Spectrum Transmutation Experimental Facility) reactor will be studied [De Bruyn and Fernandez, 2012; Sarotto et al., 2013].

The layout of the MYRRHA-FASTEF reactor is shown in figure 1.6. While MYRRHA-FASTEF is a pool-type ADS, the reactor vessel houses all the primary systems. The reactor has a double stainless steel vessel with an outer diameter of about 8 m and a height of about 11 m. The inner vessel contains all the LBE and the outer vessel serves as secondary containment in case the inner reactor vessel breaks. The reactor cover closes the vessel and supports all the in-vessel components. In the MYRRHA-FASTEF design, the diaphragm divides the LBE into a hot (upper) and a cool (lower) pool. Two axial pumps circulate the LBE while two primary heat exchangers per pump will cool the LBE. The main parameters are listed in Table 1.4.

Fuel assembly length	200 cm
Nominal power	100 MWth
Reactor inlet temperature	270 °C
Reactor outlet temperature	410 °C
Coolant velocity inside the reactor	2 m/s
Coolant pressure drop	2.5 bar
Primary coolant	LBE
Secondary coolant	saturated water/steam
Tertiary coolant	air

Table 1.4: Main Characteristics of MYRRHA-FASTEF.

MYRRHA can be operated in both critical and subcritical mode. The MYRRHA-FASTEF reactor is cylindrical, with an active fuel height of 60 cm inside the assembly with length 200 cm, and a variable width (critical core radius of about 60 cm), depending on the subcriticality level of the reactor and the experimental assemblies inside. The core radius is limited by the barrel with internal radius 71.5 cm. The reactor consists of typical mixed U-Pu oxide (MOX) fuel assemblies, LBE dummy assemblies, dedicated reflector assemblies, control rods and safety rods. Different positions can be loaded with In-Pile Sections (IPS), foreseen for

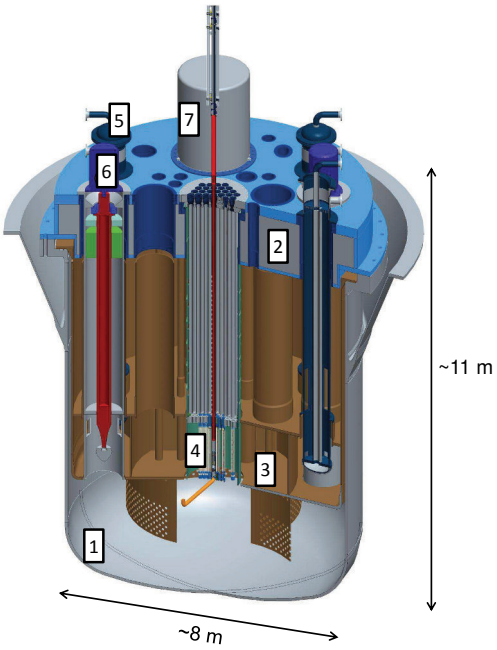

Figure 1.6: The MYRRHA-FASTEF reactor design from [De Bruyn and Fernandez, 2012] (1-reactor vessel, 2-cover, 3-diaphragm, 4-core, 5-primary pump, 6-primary heat exchanger, 7-in-vessel fuel handling machine).

experiments and isotope production units. The windowed beam-tube spallation target for operation in subcritical mode fits in the central fuel assembly position. As an example, Fig. 1.7 shows the FASTEF Beginning-Of-Life (BOL) subcritical core configuration.

The design of a MYRRHA fuel assembly (FA) is similar to the liquid sodium cooled fast reactors (SFR) [Sobolev et al., 2011a]. Each FA consists of a hexagonal bundle (hexagon pitch of 5.225 cm) of cylindrical fuel elements (also called rods or pins, 126 for the MYRRHA-FASTEF design) surrounded by a hexagonal shroud (wrapper), as shown in figure 1.8. The upper and lower ends of the shroud are connected to the inlet and outlet nozzles guiding a LBE coolant through the FA.

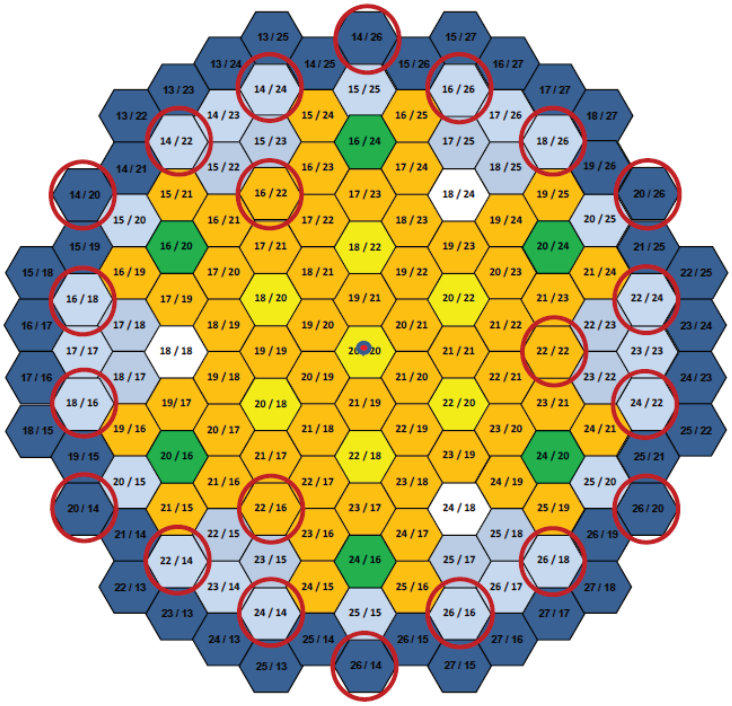

Figure 1.7: The MYRRHA-FASTEF BOL subcritical core design from [Sarotto, 2011] (orange: 57 FAs, yellow: 7 IPS including the spallation unit, green: 6 control rods, white: 3 safety rods, light blue: 36 inner dummy LBE assemblies, dark blue: 42 outer dummy YZrO assemblies, red circles: available positions for inserts from the top).

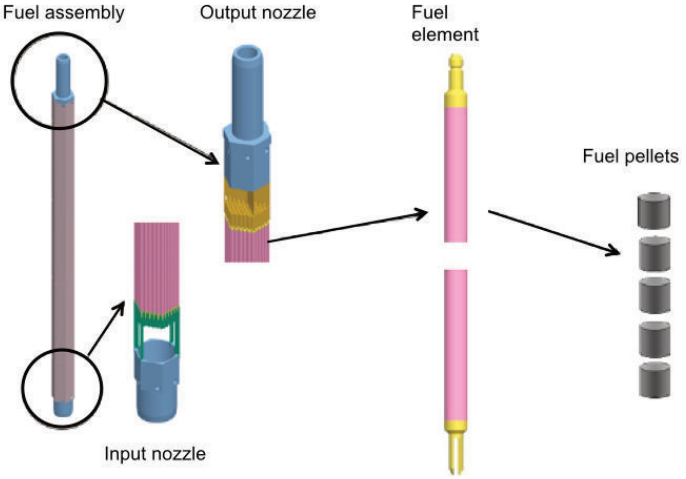

Figure 1.8: The MYRRHA-FASTEF fuel assembly design ©SCK•CEN.

1.5.3 VENUS-F

During the GUINEVERE project, the VENUS facility, hosted at the SCK•CEN site in Mol (Belgium) was modified from the existing zero-power thermal water-moderated VENUS reactor towards the fast VENUS-F reactor. The GENEPI-3C accelerator [Baylac et al., 2010], an updated version of the GENEPI-1 machine previously used for the MUSE experiments, was installed in a new accelerator hall on top of the existing VENUS bunker. Deuterons accelerated to an energy of 220 keV hit a Ti-Tritium target in the middle of the core, producing 14 MeV fusion neutrons. A picture of the updated VENUS facility (with additional accelerator room) is shown in Fig. 1.9 and 1.10.

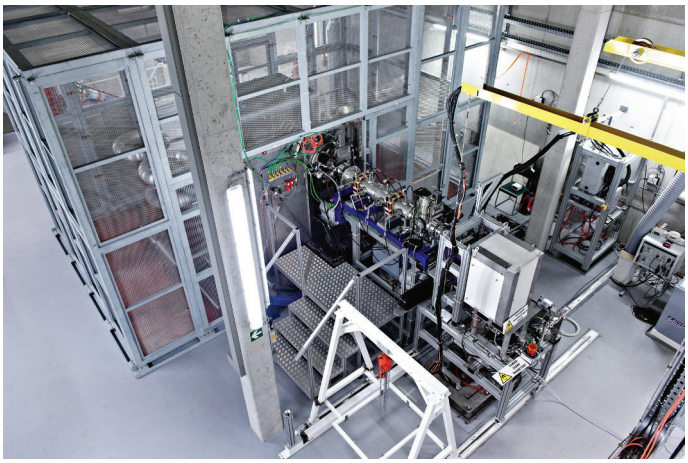

Figure 1.9: The VENUS-F accelerator hall.

As the zero power VENUS-F reactor should be representative for a full scale ADS like MYRRHA, solid lead blocks are chosen as reactor material within the existing VENUS vessel. The reactor design is almost symmetrical, as shown in figure 1.11. A detailed design of the VENUS-F reactor for the GUINEVERE project is given in [Uyttenhove et al., 2009]. In the centre of the cylindrical reactor (with radius 80 cm and height 160 cm), a 12x12 grid is introduced, in which square assemblies (width 8 cm) fit. This core grid will mainly be filled with lead and fuel assemblies (FAs), as well as with safety and control rods, and experimental assemblies. Around the fuel, a 40 cm lead top and bottom reflector is foreseen, as well as a radial reflector around the grid that fills the existing VENUS vessel.

The fuel assemblies for the first VENUS-F core, analysed in this thesis, are

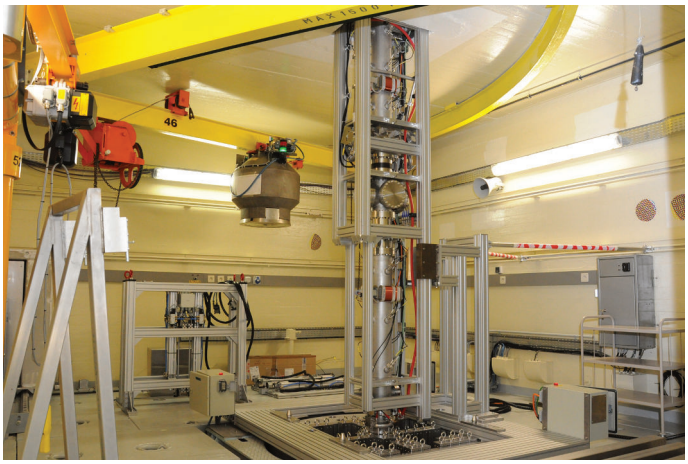

Figure 1.10: The VENUS-F reactor bunker.

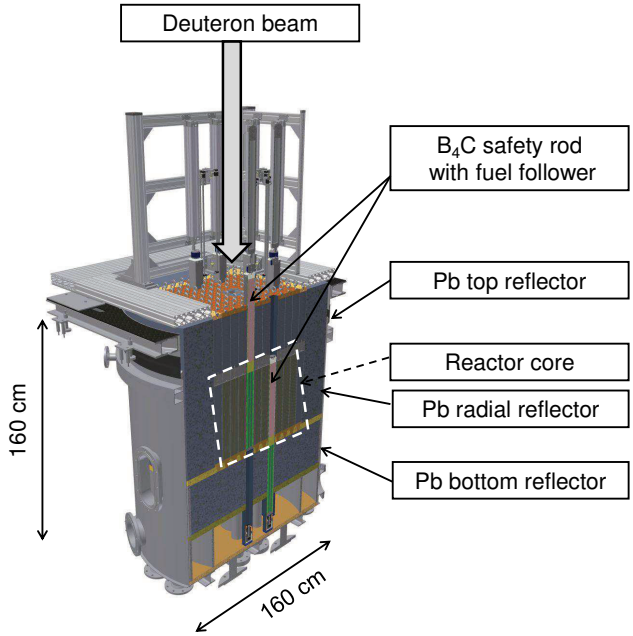

Figure 1.11: The VENUS-F reactor design ©SCK•CEN.

designed based on the experience from the MUSE project. The fuel rodlets are made of metallic uranium 30 wt. % enriched in U-235, with a diameter of 1.27 cm and a height of 20.32 cm. Three of them are piled up in a 5x5 lattice filled with lead blocks and fuel rodlets, as shown in figure 1.12, in order to obtain an active fuel height of 60.96 cm, representative for the MYRRHA reactor design. The fuel is arranged in a symmetrical way in the 5x5 grid of the FA, so possible types of FAs can comprise 4,9,13 or 25 positions in the 5x5 grid. Above the active fuel part, the top reflector is included in the fuel assembly in order to allow easy manipulations inside the grid.

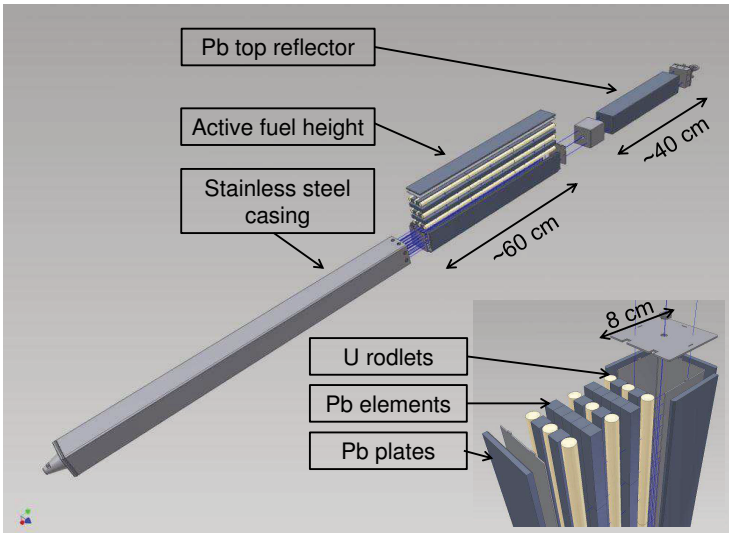

Figure 1.12: The VENUS-F fuel assembly design ©SCK•CEN.

The lead assemblies of the VENUS-F reactor are similar to the fuel assemblies, except for the active fuel part. In that zone, the complete 5x5 lattice is filled with lead elements.

6 safety rods are foreseen in a fixed position of the grid to cover any type of reactivity insertion in the reactor. They have the same design as a fuel assembly, except for the top reflector, which is replaced by boron carbide (B_4C). This design

leads to a double reactivity effect: inserting the safety rods implies not only an introduction of neutron poison but also a removal of the fuel. Two control rods with B_4C inside the 12x12 grid can be introduced in the reactor for fine-tuning the reactivity level.

Also different types of experimental assemblies can be loaded in the 12x12 grid. Thanks to this set-up a symmetrical and so-called 'clean' and 'modular' reactor is obtained, that is representative for a lead cooled ADS.

1.6 Research Outline

In this section, the PhD research question is motivated and described. Finally, the structure of the thesis is presented.

1.6.1 Motivation for an Accurate Reactivity Monitoring System

The main goal of on-line subcriticality monitoring in ADS is to **guarantee a sufficient margin against criticality** during all stages of operation of an ADS [NEA, 2003]. From the other side, for full-power ADS, one strives for the highest k_{eff} level for economical reasons, i.e. to limit the required beam power (in eq. (1.1)) of the accelerator.

In this view, the reactivity impact of different accidental scenarios is estimated. The maximum (positive) reactivity insertion limits the upper value for k_{eff} of an ADS. The maximum allowable k_{eff} level is also depending on the operational mode of the installation. Power feedback effects induce a decrease in reactivity for a temperature increase in the reactor. The elimination of this effect should be taken into account in the Cold Zero Power (CZP) operational phase.

Preliminary estimations of the maximum allowable subcriticality level were done in the framework of the XT-ADS [Van den Eynde, 2009] and EFIT [Artioli et al., 2008] project. The results are shown in Fig. 1.13. A safety limit of 1000 pcm (per cent mille, as in [Van den Eynde, 2009], value not motivated) is taken into account for the two designs. For XT-ADS an operational level for k_{eff}=0.95 is determined without margin for monitoring uncertainty, whereas for EFIT, k_{eff}=0.97 is foreseen with a 1000 pcm reactivity measurement uncertainty. The 1000 pcm remains a reference target for subcriticality monitoring at zero-power ADS [Baeten et al., 2008].

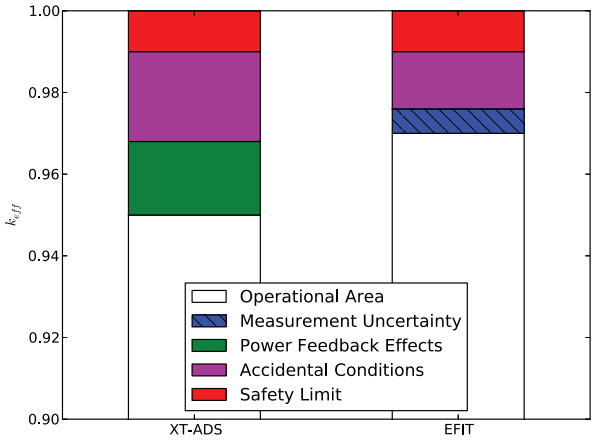

Figure 1.13: Determination of the maximum operational reactivity level in ADS for XT-ADS and EFIT.

In the framework of the licensing of the MYRRHA project, a detailed analysis of accident scenarios is performed to investigate carefully the maximum positive reactivity insertion [Ariën, 2014] for this ADS. In this note, the overcooling experiment appears to be the accident yielding the largest positive reactivity insertion in both critical and subcritical mode. For the subcritical mode, the maximum allowable k_{eff} value is 0.993 at Cold Zero Power (CZP) and 0.98 at Hot Full Power (HFP) (taking into account some limitations as present in § 4 of the note). From there, the measurement uncertainty should be subtracted to obtain the maximum operational k_{eff} level. No safety margin is discussed yet in [Ariën, 2014].

Besides the safety purpose, the reactivity of an ADS needs follow-up for operational reasons, in order to measure the burn-up of the fuel. Especially for EFIT, designed with a Pu and MA core, special attention should be paid to reactivity swing, starting from $k_{\text{eff}} = 0.95$, rising with 0.01 before decreasing [Uyttenhove et al., 2011b].

The specific goal of this work is to **investigate the uncertainty on the reactivity monitoring** itself. The uncertainties are related to the parameters involved in the evaluation method, to the detector type, its efficiency, and the location of the detectors. The role of the detector positioning is explained in the following

paragraphs.

1.6.2 Spatial Corrections on Subcriticality Measurement Results

All evaluation methods for the candidate reactivity measurement techniques presented in § 1.3 are based on point kinetics and therefore only valid close to criticality. Therefore, the reactivity values obtained by a measurement technique should be corrected by so-called spatial correction factors (SCFs). The common approach during previous and ongoing experimental programmes includes simulations of the experiment by deterministic and probabilistic codes (see [Chevret et al., 2014; Marie et al., 2013; Dulla et al., 2014] for VENUS-F). These calculations allow to obtain (precise) SCFs at specific detector locations. Moreover, some experimental techniques are difficult to simulate by using probabilistic codes.

This work aims to understand the SCFs of the selected experimental techniques for a complete ADS reactor, not only for specific detector positions. Rather than calculating SCFs precisely, it is important to know the behaviour of the SCFs during the different operational phases of an ADS. Therefore, the SCFs for the evaluation methods of candidate experimental techniques are derived analytically via static modal analysis. In this view, a static approach is chosen to simplify the determination of the SCF (see also § 1.3). By performing modal analysis of the SCF of the considered experimental techniques, the SCF behaviour can be understood by studying the eigenmodes characteristics in an ADS. The understanding is validated by 3D simulations of the SCF for the selected experimental techniques.

A reactivity monitoring system for ADS should be robust. As a first step, robust evaluation methods are selected in § 1.3.8. Secondly, the theory developed in this work aims to **identify robust detector positions by means of a thorough understanding of the SCF of the selected experimental techniques**. Robust positioning does not exclude spatial correction factors to be applied, but requires detector positions with a constant (or small change in) SCF during different phases of operation of an ADS.

1.6.3 Validation of a Subcriticality Monitoring Methodology on a Zero-Power ADS

In order to **confirm the analytical development and simulation methods of the SCFs for reactivity monitoring techniques**, the different candidate measurement techniques will be assessed on the VENUS-F ADS presented in § 1.5.3. Thanks to

the modular character of the installation, different cores can be loaded. Moreover, the critical reference state allows to determine a 'reference' subcriticality level via an alternative methodology (see § 2.5) to evaluate the selected measurement techniques.

Operational parameters are determined on VENUS-F for the different experimental techniques (e.g. pulse frequency, beam interruption time, detector specifications, ...). Measurement uncertainties on the point kinetic reactivity values are derived. SCFs obtained by modal analysis and experiment simulations (made by the same calculational tool) are validated by measurement results. Thanks to the development of the SCFs for the complete ADS reactor, **robust detector positions and types are determined for different phases of operation** of a zero-power ADS.

1.6.4 Robustness of Subcriticality Monitoring for a Power ADS

As a final step to set up a monitoring methodology, an extrapolation towards a demonstrator ADS (MYRRHA) is made. Different **aspects proper to a reactivity monitoring system for a demonstrator (power) ADS** like MYRRHA are studied based on the methodology validated in the previous section. The above mentioned parameters of the selected experimental techniques are checked for MYRRHA. The effect of burn-up, inhomogeneous core loadings and accidental conditions is investigated.

Finally, the outcome of this work presents an approach to a robust reactivity monitoring system for ADS. Detector types and positions are selected for a power ADS, able to limit the uncertainty on the reactivity during normal operation, and able to identify possible incident scenarios.

1.6.5 Thesis Structure

The related reactor physics behind each selected monitoring technique is studied by modal analysis in Chapter 2. In this chapter also the calculation tools are presented. In Chapter 3, the analytical SCFs for the selected monitoring techniques are validated by VENUS-F measurement results and completed by experiment simulations. Chapter 4 deals with the extrapolation of the techniques towards a demonstrator power ADS (MYRRHA).

2

SPATIAL EFFECTS IN SUBCRITICALITY MONITORING

Whenever anyone says, 'theoretically', they really mean, 'not really'.

Dave Parnass (1941-), Canadian computer scientist pioneer.

Picture: Lambda ©Sigfried Lundberg

The selected candidate methods (from § 1.3) for subcriticality monitoring (start-up, continuous monitoring, interim cross-checking) are under theoretical investigation in this chapter. Point kinetics evaluations of the monitoring techniques need to be corrected for the spatial variation of the flux in a subcritical core with an external neutron source. The physical understanding of the Spatial Correction Factor (SCF) for each experimental method is indispensable to study robust subcriticality monitoring.

In this chapter, the SCFs are determined analytically in terms of λ-modes, via static modal analysis by neutron diffusion theory. The motivation for static modal analysis is given in § 1.6.2. Moreover, the analytical approach allows a full understanding of SCFs, and the identification of the important contributing factors to the SCF for each selected monitoring method.

In addition to the analysis of the selected measurement methods, the advantage of a reference critical state for subcriticality monitoring is presented, in order to obtain an alternative 'reference' subcriticality level to validate the selected techniques. The spatial dependence of this alternative pathway is discussed. At the end of this chapter, the calculational tools are presented, which will be used to perform a modal analysis and to simulate experiments in the next chapters.

2.1 Modal Analysis Approach

2.1.1 λ-Eigenmodes

The behaviour of a nuclear reactor is determined by the distribution of the neutrons in the system as a function of time, space and energy. The prediction of this behaviour is obtained by solving the transport equation or Boltzmann equation [Bell and Glasstone, 1985]. In steady state and presented in operator form, this equation becomes

$$(F-L)\phi + S = 0 \tag{2.1}$$

with ϕ the neutron flux, S the source strength, F the fission operator and L the transport operator comprising neutron leakage, neutron collisions and neutron scattering as explained in § 1.1.

The λ-eigenvalue problem is set up by scaling the fission operator F with λ in the homogeneous Boltzmann equation, i.e. (2.1) with S=0. Each eigenmode l of

the flux is then associated with an eigenfunction ϕ_l [Bell and Glasstone, 1970]

$$L\phi_l = \lambda_l F \phi_l \tag{2.2}$$

The smallest eigenvalue λ_1 is equal to the inverse of the effective multiplication factor k_{eff}.

The application of λ-mode analysis has been used for the modal study of instabilities in reactors, e.g. for oscillations typical for Boiling Water Reactors (BWRs). When calculating λ-modes for a BWR case [Verdu et al., 1994], a typical shape of the harmonics is obtained, as shown in Fig. 2.1. The first higher modes are two azimuthal ones, followed by an axial mode and two azimuthal (so-called rotating) modes. In the following chapters, λ-mode analysis of he VENUS-F and MYRRHA subcritical cores are performed, as motivated in § 2.1.3, in order to check the pattern of the mode shapes.

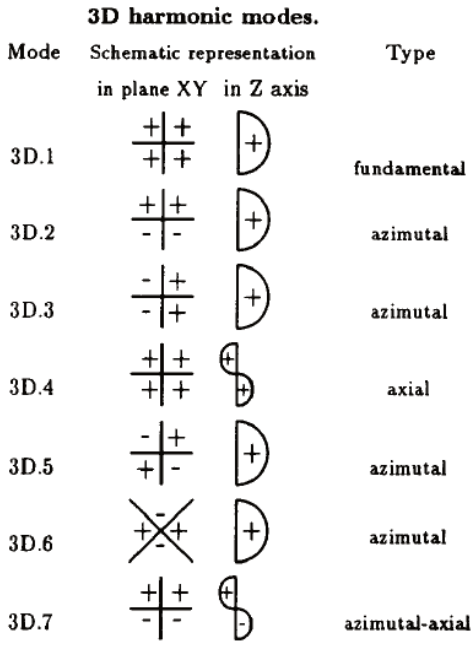

Figure 2.1: Typical 3-dimensional shapes of static spatial eigenfunctions for a critical BWR reactor. [Verdu et al., 1994]

2.1.2 Reconstruction of a Subcritical Fixed Source System by λ-Modes Amplification

Static modal analysis can be applied to determine the amplification coefficient of each eigenfunction in order to reconstruct the full flux solution of a static fixed source problem [Bell and Glasstone, 1970]. The outcome of this analysis allows determining the validity of a point kinetics approach, to distinguish important modes contributing to the full solution and to determine the number of modes required to reconstruct the fixed source problem with a sufficient degree of accuracy.

The general (i.e. time-dependent) modal expansion of the neutron flux is written as

$$\phi(\vec{r},\widehat{\Omega},E,t)=\sum_{l=1}^{\infty}P_l(t)\phi_l(\vec{r},\widehat{\Omega},E) \tag{2.3}$$

$P_l(t)$ is the amplification factor of mode l. An infinite number of modes is needed to reconstruct the full flux [Bell and Glasstone, 1970]. In its static form, P_l becomes a constant.

Between the modes there exists an orthogonality relationship, obtained by multiplying the λ-eigenvalue problem (2.2) for mode l with the adjoint mode m (indicated with the + sign):

$$(\lambda_l-\lambda_m^+)\left\langle\phi_m^+,F\phi_l\right\rangle=0 \tag{2.4}$$

with

$$\langle X,Y\rangle=\int_{4\pi}\int_E\int_V X(\vec{r},\widehat{\Omega},E)Y(\vec{r},\widehat{\Omega},E)dV\,dE\,d\widehat{\Omega} \tag{2.5}$$

By introducing eq. (2.3) in the static transport equation (2.1) and multiplying with the adjoint eigenfunction ϕ_m^+, one obtains the amplitude P_l for each mode:

$$P_l=-\frac{\left\langle\phi_l^+,S\right\rangle}{(1-\frac{1}{\lambda_l})\left\langle\phi_l^+,F\psi_l\right\rangle} \tag{2.6}$$

with S the steady state neutron source density (n/cm^3/s).

In problems that are geometrically symmetric, often degenerate eigenvalues show up (λ_l=λ_m for $l \neq m$). In that case, more than one (mostly two, rarely three) eigenfunction is associated to the same eigenmode. As a consequence, a set of equations needs to be solved to obtain the amplification factors. For two degenerate modes l and m the system of equations becomes

$$\begin{pmatrix} (1-\lambda_l)\left\langle \phi_m^+, F\phi_l \right\rangle & (1-\lambda_m)\left\langle \phi_m^+, F\phi_m \right\rangle \\ (1-\lambda_l)\left\langle \phi_l^+, F\phi_l \right\rangle & (1-\lambda_m)\left\langle \phi_l^+, F\phi_m \right\rangle \end{pmatrix} \begin{pmatrix} P_l \\ P_m \end{pmatrix} = \begin{pmatrix} -\left\langle \phi_m^+, S \right\rangle \\ -\left\langle \phi_l^+, S \right\rangle \end{pmatrix} \tag{2.7}$$

The development of this theory on a basic example is shown in [Uyttenhove et al., 2012b].

2.1.3 Diffusion Theory to understand Spatial Dependence of Reactivity Measurement Techniques

The evaluation methods of experimental techniques for subcriticality measurements make use of point kinetics theory to obtain an expression for the reactivity. Therefore, one assumes that the flux can be represented by a single, called fundamental, mode [Duderstadt and Hamilton, 1976]. In an ADS however, a local external neutron source is introduced in a subcritical core and many modes (so-called harmonics) are amplified to contribute to the total flux. When applying point kinetics evaluation techniques, Spatial Correction Factors (SCFs) are needed to correct the obtained results [Dulla et al., 2005].

The choice of static evaluation methods for the selected experimental techniques is motivated in § 1.6.2. Moreover, when performing static modal analysis, analytical expressions for SCFs are obtained in the following sections for the considered evaluation methods for the experimental techniques, by means of diffusion theory. This approach allows a better understanding of the behaviour of the SCFs throughout subcritical cores of ADS, compared to SCFs determined by experiment simulations. Diffusion calculations are chosen for the sake of computational cost and availability of an appropriate software code for the purpose of this work (see § 2.6).

The approximations related to diffusion theory ([Duderstadt and Hamilton, 1976], 4.IV) and eigenmode calculations [Saracco et al., 2012] need to be evaluated for each case study. In the case of fast ADS systems, only the limitation on the flux gradient could hamper a proper interpretation of calculational results close

to large flux gradients (control rods, neutron source,...). Several mean free paths away from any sources or boundaries (in a weakly absorbing medium), the flux is slowly varying in space and the diffusion theory is valid. In this work however, one aims to understand the spatial dependence in ADS cores to check robustness of detector positions, rather than determining precise correction factors. For the latter purpose, probabilistic software codes are more appropriate.

2.2 Start-up Reactivity Monitoring Techniques

2.2.1 The Area Method Evaluation of the Pulsed Neutron Source Technique

The area method (also called Sjöstrand method) [Sjöstrand, 1956] is a static evaluation for subcriticality measurements by means of a Pulsed Neutron Source (PNS), presented in § 1.3.1. It states that the reactivity of a subcritical system driven by a pulse train of external source neutrons, can be estimated by the ratio of two areas in the decay of the neutron density (or proportional detector signal) after a pulse, as shown in eq. (1.9) and Fig. 1.2.

In order to derive the area ratio by point kinetics, the time dependent behaviour of the homogeneous point kinetics equations for neutron density $n(t)$ and precursor density $C(t)$ is derived via basic reactor theory and Laplace transformation (assuming $\frac{|\rho-\beta|}{\Lambda} >> \lambda$):

$$n(t) = A_1 e^{s_1 t} + A_2 e^{s_2 t} \tag{2.8}$$

$$C(t) = A_1 \frac{\beta}{\Lambda(s_1+\lambda)} e^{s_1 t} + A_2 \frac{\beta}{\Lambda(s_2+\lambda)} e^{s_2 t} \tag{2.9}$$

with Λ the neutron generation time (s), λ the average decay constant of the precursors (1/s), and

$$s_1 = \frac{\rho-\beta}{\Lambda} \tag{2.10}$$

$$s_2 = \frac{\rho\lambda}{\rho-\beta} \tag{2.11}$$

The coefficients A_1 and A_2 are determined via the initial conditions at t=0. Suppose at t=0 a Dirac pulse from an external neutron source with strength S (n/s) in a subcritical medium with $C(0)$=0, then the neutron density is given by [Baeten et al., 2006][1]

$$n(t) = S\left(e^{\frac{\rho-\beta}{\Lambda}t} + \frac{\lambda\beta\Lambda}{(\rho-\beta)^2} e^{\frac{-\rho\lambda}{\rho-\beta}t} \right) \tag{2.12}$$

The theory can be easily expanded towards more groups of delayed neutrons. For clarity, only one family of delayed neutrons is shown in eq. (2.12). One can distinguish the prompt and delayed contribution to the neutron density via the different exponential constants.

The area method however is only valid when the asymptotic precursor concentration is reached, i.e. after (tens of) thousands of pulses with pulse period T. In that case

$$C(0) = -\frac{S\beta}{\rho\lambda T} \tag{2.13}$$

In [Baeten et al., 2006] the derivation of the neutron density is performed for an infinite pulse train $\sum_{n=0}^{\infty}\delta(t-nT)S$:

$$n(t) = S\left(e^{\frac{\rho-\beta}{\Lambda}t} + \frac{\beta\Lambda}{(\rho-\beta)\rho T} e^{\frac{-\rho\lambda}{\rho-\beta}t} \right) \tag{2.14}$$

At $t=0$ the neutron density is slightly higher than S due to the delayed neutron contribution from the second term in eq. (2.14). When integrating (2.14) over the period T and separating the prompt from the delayed contribution, (1.9) is obtained, as [Baeten et al., 2006]

$$A_p = \frac{\Lambda S}{(\rho-\beta)T} \tag{2.15}$$

$$A_d = \frac{S\beta\Lambda}{(\rho-\beta)\rho T} \tag{2.16}$$

[1] At t=0 the second term in eq. (2.12) can be neglected.

2.2.2 Modal Analysis of the SCF for the Area Method

Definition of SCF_{area}

In this work, SCFs will be applied on reactivity values obtained by point kinetics, in order to obtain a credible estimation of the reactivity at different locations in a subcritical core. They will depend on the reactivity level, the fuel burn-up, the detector type used for the measurements, etc. In this section, the SCF for the area evaluation of the PNS experiment is defined as

$$SCF_{area}(\vec{r}) = \frac{\frac{A_p(\vec{r})}{A_d(\vec{r})}}{\frac{\rho_{ref}}{\beta}} \tag{2.17}$$

with ρ_{ref} the reference 'true' reactivity value (in \$, see § 2.5), A_p and A_d the detector counts during a pulse at a detector location, associated to prompt and delayed neutrons, as in eq. (1.9).

Derivation of SCF_{area}

In Appendix III of [Sjöstrand, 1956] the modal analysis of SCF_{area} is determined via age theory for a one energy group case in a homogeneous core. In this paragraph, a general multigroup area (Sjöstrand) correction factor is derived via modal analysis and diffusion theory, with one lumped family of precursors.

The diffusion equation for total flux and precursor density is written as (notation as in [Duderstadt and Hamilton, 1976])

$$\begin{aligned}
&\frac{1}{\mathrm{v}}\frac{\partial \phi(\vec{r},E,t)}{\partial t} = \\
&\nabla.D(\vec{r},E)\nabla\phi(\vec{r},E,t) - \Sigma_t(\vec{r},E)\phi(\vec{r},E,t) + \int_0^\infty \Sigma_s(\vec{r},E'\rightarrow E)\phi(\vec{r},E',t)dE' \\
&+ \chi_p(E)\int_0^\infty (1-\beta)\nu(E')\Sigma_f(\vec{r},E')\phi(\vec{r},E',t)dE' + \chi_d(E)\lambda C(\vec{r},t) + S(\vec{r},E,t)
\end{aligned} \tag{2.18}$$

$$\frac{\partial C(\vec{r},t)}{\partial t} = \beta\int_0^\infty \nu(E)\Sigma_f(\vec{r},E)\phi(\vec{r},E,t)dE - \lambda C(\vec{r},t) \tag{2.19}$$

Assuming the precursor density constant during the pulse, $C(\vec{r})$ corresponds to a fixed source problem with constant neutron source strength $\frac{S}{T}$:

$$C(\vec{r}) = \frac{\beta}{\lambda} \int_0^\infty \nu(E)\Sigma_f(\vec{r},E)\phi(\vec{r},E,t)dE \tag{2.20}$$

As the integral of the flux over the pulse is required to determine the prompt and delayed areas, we introduce eq. (2.20) in eq. (2.18) and integrate over a time interval T. Moreover, as for the PNS experiment evaluation, $\phi(t=T) \equiv \phi(t=0)$,

$$\begin{aligned}\int_0^T \frac{1}{\mathrm{v}} \frac{\partial \phi(\vec{r},E,t)}{\partial t} dt &= \frac{1}{\mathrm{v}}\big(\phi(t=T)-\phi(t=0)\big) = 0 = \int_0^T \nabla.D(\vec{r},E)\nabla\phi(\vec{r},E,t)dt \\ &- \Sigma_t(\vec{r},E)\int_0^T \phi(\vec{r},E,t)dt + \int_0^T\int_0^\infty \Sigma_s(\vec{r},E'\to E)\phi(\vec{r},E',t)dE'dt \\ &+ \chi(E)\int_0^T\int_0^\infty \nu(E')\Sigma_f(\vec{r},E')\phi(\vec{r},E',t)dE'dt + \int_0^T S(\vec{r},E,t)dt \end{aligned} \tag{2.21}$$

with $\chi(E) = \chi_p(E)(1-\beta) + \chi_d(E)\beta$.

When performing a modal expansion of the neutron flux:

$$\phi(\vec{r},E,t) = \sum_{n=1}^{\infty} P_n(t)\phi_n(\vec{r},E) \tag{2.22}$$

the k-eigenmodes ($k_n = \frac{1}{\lambda_n}$) are the solution of the homogeneous steady state solution of eq. (2.18):

$$\begin{aligned}\nabla.D(\vec{r},E)\nabla\phi_n(\vec{r},E) - \Sigma_t(\vec{r},E)\phi_n(\vec{r},E) + \int_0^\infty \Sigma_s(\vec{r},E'\to E)\phi_n(\vec{r},E')dE' \\ + \frac{\chi(E)}{k_n}\int_0^\infty \nu(E')\Sigma_f(\vec{r},E')\phi_n(\vec{r},E')dE' = 0\end{aligned} \tag{2.23}$$

Substituting the eigenmode expression for $\nabla.D(\vec{r},E)\nabla\phi_n(\vec{r},E)$ in eq. (2.21) yields:

$$\sum_{n=1}^{\infty}\int_0^T P_n(t)dt\,\chi(E)\frac{1-k_n}{k_n}\int_0^{\infty}\nu(E')\Sigma_f(E')\phi_n(\vec{r},E')dE' = \int_0^T S(\vec{r},E,t)dt \tag{2.24}$$

In order to obtain an expression for $\int_0^T P_n(t)dt$, we multiply both sides by the adjoint function $\phi_m^+(\vec{r},E)$ and apply the orthogonality relationship (2.4). Then, supposing no degenerate eigenvalues,

$$\int_0^T P_n(t)dt = \frac{k_n}{1-k_n}\frac{\left\langle \phi_n^+(\vec{r},E), \int_0^T S(\vec{r},E,t)dt \right\rangle}{\left\langle \phi_n^+(\vec{r},E), \chi(E)\int_0^{\infty}\nu(E')\Sigma_f(E')\phi_n(\vec{r},E')dE' \right\rangle} \tag{2.25}$$

with the meaning of the brackets $\langle\rangle$ as explained in eq. (2.5).

The total area under the pulse can then be written as

$$A_t(\vec{r}) = \sum_{n=1}^{\infty}\int_0^T P_n(t)dt\int_0^{\infty}\Sigma_d(E)\phi_n(\vec{r},E)dE = \sum_{n=1}^{\infty}\frac{k_n}{1-k_n}\frac{\left\langle \phi_n^+(\vec{r},E), \int_0^T S(\vec{r},E,t)dt \right\rangle}{\left\langle \phi_n^+(\vec{r},E), \chi(E)\int_0^{\infty}\nu(E')\Sigma_f(E')\phi_n(\vec{r},E')dE' \right\rangle}\int_0^{\infty}\Sigma_d(E)\phi_n(\vec{r},E)dE \tag{2.26}$$

with Σ_d the macroscopic cross section for the detector of interest. In order to investigate the spatial dependence of the complete core for the area method, Σ_d is independent of its position.

In a similar way, the expansion coefficient $\int_0^T P_{n,p}(t)dt$ related to the prompt eigenvalue problem can be calculated. Therefore, the fission operator F in (2.1) is modified towards its prompt equivalent F_p. This corresponds to a replacement of $\chi(E)$ by $(1-\beta)\chi_p(E)$ in eq. (2.21). Then

$$A_p(\vec{r}) = \sum_{n=1}^{\infty} \frac{k_{n,p}}{1-(1-\beta)k_{n,p}} \frac{\left\langle \phi^+_{n,p}(\vec{r},E), \int_0^T S(\vec{r},E,t)dt \right\rangle}{\left\langle \phi^+_{n,p}(\vec{r},E), \chi_p(E)\int_0^\infty \nu(E')\Sigma_f(E')\phi_{n,p}(\vec{r},E')dE' \right\rangle} \int_0^\infty \Sigma_d(E)\phi_{n,p}(\vec{r},E)dE \quad (2.27)$$

The area ratio can now be determined via

$$\frac{A_p(\vec{r})}{A_d(\vec{r})} = \frac{A_p(\vec{r})}{A_t(\vec{r}) - A_p(\vec{r})} \quad (2.28)$$

$\phi_n(\vec{r},E)$ is the solution of eq. (2.23), and $\phi_{n,p}(\vec{r},E)$ is the solution of the same equation with $\chi(E)$ replaced by $\chi_p(E)$. Therefore, one can suppose

$$\frac{\left\langle \phi^+_n(\vec{r},E), \int_0^T S(\vec{r},E,t)dt \right\rangle}{\left\langle \phi^+_n(\vec{r},E), \chi(E)\int_0^\infty \nu(E')\Sigma_f(E')\phi_n(\vec{r},E')dE' \right\rangle} \cong \frac{\left\langle \phi^+_{n,p}(\vec{r},E), \int_0^T S(\vec{r},E,t)dt \right\rangle}{\left\langle \phi^+_{n,p}(\vec{r},E), \chi_p(E)\int_0^\infty \nu(E')\Sigma_f(E')\phi_{n,p}(\vec{r},E')dE' \right\rangle} \quad (2.29)$$

as both eigenfunctions appear as a ratio in this formula. By a similar reasoning, $k_{n,p}$=(1-β)k_n can be replaced by k_n when introducing eq. (2.26) and (2.27) in eq. (2.28), as for mode n

$$\frac{\frac{k_{n,p}}{1-(1-\beta)k_{n,p}}}{\frac{k_n}{1-k_n} - \frac{k_{n,p}}{1-(1-\beta)k_{n,p}}} \cong \frac{\frac{k_n}{1-(1-\beta)k_n}}{\frac{k_n}{1-k_n} - \frac{k_n}{1-(1-\beta)k_n}} \quad (2.30)$$

Then

$$\frac{A_p(\vec{r})}{A_d(\vec{r})} = \frac{\sum_{n=1}^{\infty} \frac{k_n}{1-(1-\beta)k_n} I_n \int_0^\infty \Sigma_d(E)\phi_n(\vec{r},E)dE}{\sum_{n=1}^{\infty} \frac{k_n}{(1-(1-\beta)k_n)} \frac{\beta k_n}{1-k_n} I_n \int_0^\infty \Sigma_d(E)\phi_n(\vec{r},E)dE} \quad (2.31)$$

via eq. (2.28), with

$$I_n = \frac{\left\langle \phi_n^+(\vec{r},E), \int_0^T S(\vec{r},E,t)dt \right\rangle}{\left\langle \phi_n^+(\vec{r},E), \chi(E)\int_0^\infty \nu(E')\Sigma_f(E')\phi_n(\vec{r},E')dE' \right\rangle} \tag{2.32}$$

In order to identify the SCF for the area method, $n=1$ is separated from the summation in eq. (2.31) and, according to eq. (2.17)

$$\frac{A_p(\vec{r})}{A_d(\vec{r})} = \frac{-\rho}{\beta} SCF_{area} = \frac{-\rho}{\beta} \frac{1+\sum_{n=2}^\infty \frac{I_n(1-(1-\beta)k_1)k_n \int_0^\infty \Sigma_d(E)\phi_n(\vec{r},E)dE}{I_1(1-(1-\beta)k_n)k_1 \int_0^\infty \Sigma_d(E)\phi_1(\vec{r},E)dE}}{1+\sum_{n=2}^\infty \frac{I_n k_n^2(1-(1-\beta)k_1)(1-k_1)\int_0^\infty \Sigma_d(E)\phi_n(\vec{r},E)dE}{I_1 k_1^2(1-(1-\beta)k_n)(1-k_n)\int_0^\infty \Sigma_d(E)\phi_1(\vec{r},E)dE}} \tag{2.33}$$

with $\rho = \frac{k_1-1}{k_1}$ the reactivity. Then

$$SCF_{area}(\vec{r}) = \frac{1+\sum_{n=2}^\infty \frac{I_n(1-(1-\beta)k_1)k_n \int_0^\infty \Sigma_d(E)\phi_n(\vec{r},E)dE}{I_1(1-(1-\beta)k_n)k_1 \int_0^\infty \Sigma_d(E)\phi_1(\vec{r},E)dE}}{1+\sum_{n=2}^\infty \frac{I_n k_n^2(1-(1-\beta)k_1)(1-k_1)\int_0^\infty \Sigma_d(E)\phi_n(\vec{r},E)dE}{I_1 k_1^2(1-(1-\beta)k_n)(1-k_n)\int_0^\infty \Sigma_d(E)\phi_1(\vec{r},E)dE}} \tag{2.34}$$

Analysis

In order to understand the behaviour of SCF_{area} in an ADS core, the parameters that contribute to the area method SCF in eq. (2.34) require further attention. First of all, it is important to note the similarity between numerator and denominator in eq. (2.34). The only difference is inside the k-eigenvalue ratio. As $\beta << 1$, one can reduce this factor to $\frac{k_n(1-k_1)}{k_1(1-k_n)}$ in the numerator and $(\frac{k_n(1-k_1)}{k_1(1-k_n)})^2$ in the denominator. This ratio is positive in both numerator and denominator, however the influence of this factor on the SCF is dominated by the term in the denominator.

If the neutron source of the ADS is positioned in the centre of the core, modes that obtain a maximum in the centre of the core are highly amplified (represented by a high numerator in eq. (2.32)). Moreover, the factor $\frac{k_n(1-k_1)}{k_1(1-k_n)}$ is exponentially decreasing for ADS (e.g. see Fig. 3.16), so higher order modes are reduced by this factor. Therefore, one could assume that close to the zeros of the first higher order modes with a maximum in the centre, the spatial correction factor should be close to unity. At these locations the contribution of the most important modes (except from the fundamental one) to the SCF is extinguished.

This location is not necessarily a suitable detector location, but provides valuable information about the boundary between SCF < 1 (safe overestimation of the k_{eff} level) and SCF > 1 (unsafe underestimation of the k_{eff} level). Criteria for robust detector positioning are developed in the next chapters of this thesis.

2.2.3 The Integrated Source Jerk Method

An alternative calibration method for the initial subcriticality level determination in ADS could be the Integrated Source Jerk (ISJ) method, presented in § 1.3.2. The ISJ method allows determining the reactivity value (in \$) of a subcritical core by analysing the neutron decay after stopping the external neutron source (i.e. the accelerator beam in an ADS) until complete dying out of the neutron population, according to eq. (1.11).

The ISJ evaluation method makes use of inverse point kinetics theory to obtain the expression (1.11) for the reactivity. Therefore, as for the area method, spatial corrections need to be investigated to improve the point kinetic estimation. Given the nature of the method, the spatial correction for the ISJ method can be different from the one for the PNS area method, influencing the applicability of the ISJ method for calibration purposes.

2.2.4 Modal Analysis of the SCF for the ISJ Method

Definition of SCF_{ISJ}

The definition of SCF_{ISJ} is similar to the one of SCF_{area}:

$$SCF_{ISJ}(\vec{r}) = \frac{\beta}{\rho_{ref}} \frac{\int_0^\infty \Sigma_d(E)\phi(\vec{r},E,0)dE \sum_{i=1}^{q} \frac{a_i}{\lambda_i}}{\int_0^\infty \int_0^\infty \Sigma_d(E)\phi(\vec{r},E,t)dE\,dt} \tag{2.35}$$

with ρ_{ref} the reference 'true' reactivity value (in \$, see § 2.5), $\phi(\vec{r},E,0)$ the flux at time '0' (corresponding to the stable state before interruption of the beam) and q the number of precursor groups.

Derivation of SCF_{ISJ}

The steady state flux $\phi(\vec{r},E,0)$ and precursor density $C(\vec{r},0)$ before beam interruption are derived from the diffusion equation (2.18) and (2.19). By integrating over the time period after the beam stop, i.e. from t=0 s to t=∞, with $\phi(\vec{r},E,\infty)$=$C(\vec{r},\infty)$=0

$$-\frac{\phi(\vec{r},E,0)}{\mathrm{v}}=\int_0^\infty\Big[\nabla.D(\vec{r},E)\nabla\phi(\vec{r},E,t)-\Sigma_t(\vec{r},E)\phi(\vec{r},E,t)+\int_0^\infty\Sigma_s(\vec{r},E'\to E)\phi(\vec{r},E',t)dE'+\chi_p(E)\int_0^\infty(1-\beta)\nu(E')\Sigma_f(\vec{r},E')\phi(\vec{r},E',t)dE'\Big]dt+\chi_d(E)\lambda\int_0^\infty C(\vec{r},t)dt \tag{2.36}$$

$$-C(\vec{r},0)=\beta\int_0^\infty\int_0^\infty\nu(E)\Sigma_f(\vec{r},E)\phi(\vec{r},E,t)dE\,dt-\lambda\int_0^\infty C(\vec{r},t)dt \tag{2.37}$$

The initial flux just at beam interruption time becomes

$$\frac{\phi(\vec{r},E,0)}{\mathrm{v}}=n(\vec{r},E,0)=\int_0^\infty-\Big[\nabla.D(\vec{r},E)\nabla\phi(\vec{r},E,t)-\Sigma_t(\vec{r},E)\phi(\vec{r},E,t)+\int_0^\infty\Sigma_s(\vec{r},E'\to E)\phi(\vec{r},E',t)dE'+\chi(E)\int_0^\infty\nu(E')\Sigma_f(\vec{r},E')\phi(\vec{r},E',t)dE'\Big]dt-\chi_d(E)C(\vec{r},0) \tag{2.38}$$

with $n(\vec{r},E,0)$ the steady state neutron density before beam interruption. Equation (2.38) is expanded to

$$n(\vec{r},E,0)=-\sum_{n=1}^\infty\int_0^\infty P_n(t)dt\Big[\nabla.D(\vec{r},E)\nabla\phi_n(\vec{r},E)-\Sigma_t(\vec{r},E)\phi_n(\vec{r},E)+\int_0^\infty\Sigma_s(\vec{r},E'\to E)\phi_n(\vec{r},E')dE'+\chi(E)\int_0^\infty\nu(E')\Sigma_f(\vec{r},E')\phi_n(\vec{r},E')dE'\Big]-\chi_d(E)C(\vec{r},0) \tag{2.39}$$

Now, the homogeneous steady state diffusion equation (2.23) is used to introduce the eigenmodes of the system in equation (2.39). In order to determine

$\int_0^\infty P_n(t)dt$, the summation is eliminated by making use of the orthogonality relationship (2.4) between the eigenfunctions. Therefore, from the previous equation,

$$\int_0^\infty P_n(t)dt = \frac{1}{\rho_n} \frac{-\left\langle \phi_n^+(\vec{r},E), n(\vec{r},E,0)+\chi_d(E)C(\vec{r},0)\right\rangle}{\left\langle \phi_n^+(\vec{r},E), \chi(E)\int_0^\infty \nu(E')\Sigma_f(E')\phi_n(\vec{r},E')dE'\right\rangle} = \frac{R_n}{\rho_n} \quad (2.40)$$

with

$$R_n = -\frac{\left\langle \phi_n^+(\vec{r},E), n(\vec{r},E,0)+\chi_d(E)C(\vec{r},0)\right\rangle}{\left\langle \phi_n^+(\vec{r},E), \chi(E)\int_0^\infty \nu(E')\Sigma_f(E')\phi_n(\vec{r},E')dE'\right\rangle} \quad (2.41)$$

Using the definition eq. (2.35), SCF_{ISJ} becomes

$$SCF_{ISJ} = \frac{\beta}{\rho}\sum_{i=1}^{q}\frac{a_i}{\lambda_i}\frac{\sum_{n=1}^\infty P_n(0)\int_0^\infty \Sigma_d(E)\phi_n(\vec{r},E)dE}{\sum_{n=1}^\infty \int_0^\infty P_n(t)dt\int_0^\infty \Sigma_d(E)\phi_n(\vec{r},E)dE} \quad (2.42)$$

Via (2.40) one gets

$$SCF_{ISJ} = \beta\sum_{i=1}^{q}\frac{a_i}{\lambda_i}\left(\frac{P_1(0)\int_0^\infty \Sigma_d(E)\phi_1(\vec{r},E)dE + \sum_{n=2}^\infty P_n(0)\int_0^\infty \Sigma_d(E)\phi_n(\vec{r},E)dE}{R_1\int_0^\infty \Sigma_d(E)\phi_1(\vec{r},E)dE + \sum_{n=2}^\infty R_n\frac{\rho_1}{\rho_n}\int_0^\infty \Sigma_d(E)\phi_n(\vec{r},E)dE}\right) \quad (2.43)$$

or finally

$$SCF_{ISJ} = \beta\sum_{i=1}^{q}\frac{a_i}{\lambda_i}\frac{P_1(0)+\sum_{n=2}^\infty P_n(0)\frac{\int_0^\infty \Sigma_d(E)\phi_n(\vec{r},E)dE}{\int_0^\infty \Sigma_d(E)\phi_1(\vec{r},E)dE}}{R_1+\sum_{n=2}^\infty R_n\frac{\rho_1}{\rho_n}\frac{\int_0^\infty \Sigma_d(E)\phi_n(\vec{r},E)dE}{\int_0^\infty \Sigma_d(E)\phi_1(\vec{r},E)dE}} \quad (2.44)$$

When simplifying this equation to point kinetics, one neglects the first term in the numerator of eq. (2.41). This is also done to obtain the point kinetics eq. (1.11). Indeed, as before interruption of the beam, via point kinetics,

$$C(0) = \frac{\beta n(0)}{\Lambda\lambda} \quad (2.45)$$

one notices that $C(0)$ exceeds many times $n(0)$. Therefore, by making the same assumption in eq. (2.41) using point kinetics

$$R_1 = \frac{C(0)}{\nu\Sigma_f \phi_1} = \frac{1}{\nu\Sigma_f} \frac{k_{eff}\beta}{\lambda l} \frac{P_1(0)\phi_1}{\mathrm{v}} \tag{2.46}$$

and with one group of precursors for simplification, one gets, as the summations disappears in equation (2.44)

$$SCF_{ISJ} = \frac{\beta}{\lambda} \frac{P_1(0)}{R_1} = 1 \tag{2.47}$$

as expected.

Analysis

SCF_{ISJ} is more complex to analyse than SCF_{area}. The factor is determined by two terms ($P_1(0)$ and R_1) linked to the fundamental mode, and two summations with higher modes that are related to the spatial correction. Terms with a high amplification $P_n(0)$, i.e. with a maximum in the centre of the ADS core, will contribute significantly to SCF_{ISJ}. Therefore, the spatial correction factor will be closer to unity at positions where these modes have zero crossings, as for SCF_{area}. Secondly, the denominator summation will be reduced for higher modes, as $\frac{\rho_1}{\rho_n}$ decreases with increasing mode number.

2.3 The Current-To-Flux Reactivity Monitor

2.3.1 Point Kinetics Analysis

By monitoring the ratio of the beam current and the flux level of an ADS using a continuous accelerator current, one can evaluate the reactivity by using the relation (1.14). This formula can easily be derived from point kinetics [Duderstadt and Hamilton, 1976]. The proportionality coefficient c can be defined in a different way, taking into account the measurement methods for S and ϕ. The relationship between current and flux only remains valid when c does not vary as a function of time, i.e. when there is no variation of spatial dependence in time, when the source neutron production does not vary, etc. This section provides a deeper insight into the proportionality between beam current and neutron flux, taking into account the spatial dependence by modal analysis.

2.3.2 Modal Analysis of the SCF for the CTF Method

Definition of SCF_{CTF}

As alternative to the CTF coefficient in point kinetics, the SCF for the CTF reactivity ratio between the two states in the monitoring process is defined as

$$SCF_{CTF} = \frac{\frac{\rho'_{CTF}}{\rho_{CTF}}}{\frac{\rho'_{ref}}{\rho_{ref}}} \tag{2.48}$$

with the original known (calibrated) state indicated without prime, and the actual state with prime. $\rho(')_{CTF}$ is the reactivity obtained via the CTF monitor in (see eq. (1.14)), and $\rho(')_{ref}$ is the 'true' reactivity obtained via another reference technique such as the PNS method at the original state, or an interim cross-checking technique such as the beam trip method at the actual state. In point kinetics equivalent, SCF_{CTF} corresponds to $\frac{c}{c'}$.

Derivation of SCF_{CTF}

In order to identify the spatial dependence in the CTF relationship, we start - similar to the PNS SCF determination - from the stationary homogeneous diffusion equation in which the eigenmodes are introduced, i.e. eq. (2.23). By replacing the flux Laplacian in the stationary diffusion equation with eliminated precursor term (from eq. (2.18) and (2.19)) by the stationary eigenfunction expansion from eq. (2.22) one finds

$$\begin{aligned}
&\sum_{n=1}^{\infty} P_n \Big(\Sigma_t(\vec{r},E)\phi_n(\vec{r},E) - \int_0^{\infty} \Sigma_s(\vec{r},E'\to E)\phi_n(\vec{r},E')dE' \\
&\qquad - \frac{\chi(E)}{k_n} \int_0^{\infty} \nu(E')\Sigma_f(\vec{r},E')\phi_n(\vec{r},E')dE' \Big) - \Sigma_t(\vec{r},E) \sum_{n=1}^{\infty} P_n \phi_n(\vec{r},E) \\
&+ \sum_{n=1}^{\infty} \int_0^{\infty} \Sigma_s(\vec{r},E'\to E)\phi_n(\vec{r},E')dE' + \chi(E) \sum_{n=1}^{\infty} P_n \int_0^{\infty} \nu(E')\Sigma_f(\vec{r},E')\phi_n(\vec{r},E')dE' \\
&\qquad + S(\vec{r},E) = 0
\end{aligned}$$

or

$$\sum_{n=1}^{\infty} P_n \frac{1-k_n}{k_n} \chi(E) \int_0^{\infty} \nu(E')\Sigma_f(\vec{r},E')\phi_n(\vec{r},E')dE' = S(\vec{r},E) \tag{2.49}$$

Similar to the derivation of the SCF for the area method, an expression for P_n is derived via a multiplication with the adjoint function $\phi_n^+(\vec{r},E)$ and application of the orthogonality relationship (2.4). Therefore, from (2.49)

$$S_n = -\rho_n I_{f,n} P_n \tag{2.50}$$

with

$$S_n = \left\langle \phi_n^*(\vec{r},E), S(r,E) \right\rangle \tag{2.51}$$

$$I_{f,n} = \left\langle \phi_n^*(\vec{r},E), \chi(E) \int_0^{\infty} \nu(E')\Sigma_f(E')\phi_n(\vec{r},E')dE' \right\rangle \tag{2.52}$$

Therefore, the ratio for the change in flux between the two monitoring states is written as

$$\frac{\sum_{n=1}^{\infty} P_n' \phi_n'(\vec{r},E)}{\sum_{n=1}^{\infty} P_n \phi_n(\vec{r},E)} = \frac{\sum_{n=1}^{\infty} \frac{S_n' \phi_n'(\vec{r},E)}{\rho_n' I_{f,n}'}}{\sum_{n=1}^{\infty} \frac{S_n \phi_n(\vec{r},E)}{\rho_n I_{f,n}}} = \frac{\rho_1}{\rho_1'} \frac{1+\sum_{n=2}^{\infty} \frac{S_n' I_{f,1}' \rho_1' \phi_n'(\vec{r},E)}{S_1' I_{f,n}' \rho_n' \phi_1'(\vec{r},E)}}{\frac{S_1 I_{f,1}' \phi_1(\vec{r},E)}{S_1' I_{f,1} \phi_1'(\vec{r},E)} + \sum_{n=2}^{\infty} \frac{S_n I_{f,1}' \rho_1 \phi_n(\vec{r},E)}{S_1' I_{f,n} \rho_n \phi_1'(\vec{r},E)}} \tag{2.53}$$

The modal SCF_{CTF} becomes, via eq. (2.48),

$$\begin{aligned} SCF_{CTF} &= \frac{S'}{S} \frac{\frac{\sum_{n=1}^{\infty} P_n \int_0^{\infty} \Sigma_d(E)\phi_n(\vec{r},E)dE}{\sum_{n=1}^{\infty} P_n' \int_0^{\infty} \Sigma_d(E)\phi_n'(\vec{r},E)dE}}{\frac{\rho_{(1)}'}{\rho_{(1)}}} \\ &= \frac{S'}{S} \frac{\frac{S_1 I_{f,1}' \int_0^{\infty} \Sigma_d(E)\phi_1(\vec{r},E)dE}{S_1' I_{f,1} \int_0^{\infty} \Sigma_d(E)\phi_1'(\vec{r},E)dE} + \sum_{n=2}^{\infty} \frac{S_n I_{f,1}' \rho_1 \int_0^{\infty} \Sigma_d(E)\phi_n(\vec{r},E)dE}{S_1' I_{f,n} \rho_n \int_0^{\infty} \Sigma_d(E)\phi_1'(\vec{r},E)dE}}{1+\sum_{n=2}^{\infty} \frac{S_n' I_{f,1}' \rho_1' \int_0^{\infty} \Sigma_d(E)\phi_n'(\vec{r},E)dE}{S_1' I_{f,n}' \rho_n' \int_0^{\infty} \Sigma_d(E)\phi_1'(\vec{r},E)dE}} \end{aligned} \tag{2.54}$$

When the beam current is not changed between the two states, S=S' and eq. (2.54) becomes

$$SCF_{CTF} = \frac{\frac{\sum_{n=1}^{\infty} P_n \int_0^{\infty} \Sigma_d(E)\phi_n(\vec{r},E)dE}{\sum_{n=1}^{\infty} P_n' \int_0^{\infty} \Sigma_d(E)\phi_n'(\vec{r},E)dE}}{\frac{\rho_{(1)}'}{\rho_{(1)}}}$$
$$= \frac{\frac{S_1 I_{f,1}' \int_0^{\infty} \Sigma_d(E)\phi_1(\vec{r},E)dE}{S_1' I_{f,1} \int_0^{\infty} \Sigma_d(E)\phi_1'(\vec{r},E)dE} + \sum_{n=2}^{\infty} \frac{S_n I_{f,1}' \rho_1 \int_0^{\infty} \Sigma_d(E)\phi_n(\vec{r},E)dE}{S_1' I_{f,n} \rho_n \int_0^{\infty} \Sigma_d(E)\phi_1'(\vec{r},E)dE}}{1 + \sum_{n=2}^{\infty} \frac{S_n' I_{f,1}' \rho_1' \int_0^{\infty} \Sigma_d(E)\phi_n'(\vec{r},E)dE}{S_1' I_{f,n}' \rho_n' \int_0^{\infty} \Sigma_d(E)\phi_1'(\vec{r},E)dE}} \quad (2.55)$$

Please note that S_n can differ from S_n' for S=S' if e.g. the beam position changes between the actual (indicated with prime) state and the original (indicated without prime) state.

Analysis

When comparing SCF_{CTF} to SCF_{area} from eq. (2.34), one notices a dedicated term in the nominator, different from 1, due to the difference in fundamental mode between the original and the perturbed case. Only a slight difference in fundamental mode shape between the original and perturbed case can cause a SCF different from 1 as starting point. Moreover, similar to SCF_{PNS}, modes that obtain a maximum in the centre of the core will be amplified (high $\frac{S(')_n}{S(')_1}$ factor). One also notices the decreasing contribution of higher modes due to the decreasing factor $\frac{\rho_1}{\rho_n}$.

2.4 The Source Jerk Interim Reactivity Cross-Checking Method

2.4.1 Point Kinetics Evaluation

The standard Source Jerk (SJ) method ([Ott and Neuhold, 1985], section 9.3) evaluates the repetitive fast removal of a neutron source out of an initially stationary subcritical medium. In the case of ADS operation, the accelerator beam is interrupted. Contrary to the Integrated Source Jerk (ISJ) method from § 2.2.3, the beam is restored quickly in order to avoid thermal stresses in the ADS. The beam

interruption should however be long enough to identify the prompt neutron decay (order of microseconds). The period of the source jerk comprises also the time needed for the beam to obtain its original level (in the order of milliseconds).

Before the removal of the source (state '0' at t=0 s), the neutron and precursor population are given by

$$n_0 = \frac{\Lambda S}{-\rho} \tag{2.56}$$

$$C_0 = \frac{\beta n_0}{\Lambda \lambda} \tag{2.57}$$

with S the average source strength in equilibrium conditions, and λ the one-group precursor decay constant.

In order to obtain an expression for the absolute reactivity level, the evolution of the neutron density $n(t)$ directly after a beam stop (supposing a constant precursor level) is given by

$$n(t) = \left(\frac{\Lambda S}{-\rho} + \frac{\beta}{\rho - \beta} n_0 \right) e^{\frac{\rho - \beta}{\Lambda} t} - \frac{\beta}{\rho - \beta} n_0 \tag{2.58}$$

After the dying out of the prompt neutrons (state '1') the neutron density is given by

$$n_1 = -\frac{\beta}{\rho - \beta} n_0 \tag{2.59}$$

Therefore, by using the detector count rates at the two states '0' and '1', expression (1.12) for the reactivity is found

$$\frac{\rho}{\beta} = \frac{n_1 - n_0}{n_1} \tag{2.60}$$

2.4.2 Modal Analysis

Definition of SCF_{SJ}

Similar to the definition of the other reactivity measurement SCFs, the definition of SCF_{SJ} is given by the difference between the measured reactivity via (1.12) and

the reference reactivity (in \$)

$$SCF_{SJ}(\vec{r}) = \frac{1}{\rho_{ref}} \frac{\int_0^\infty \Sigma_d(E)\phi_0(\vec{r},E)dE - \int_0^\infty \Sigma_d(E)\phi_1(\vec{r},E)dE}{\int_0^\infty \Sigma_d(E)\phi_1(\vec{r},E)dE} \tag{2.61}$$

Determination SCF_{SJ}

For the determination of SCF_{SJ}, the precursor concentration will be kept constant, as only the first microseconds after a beam stop are considered. Therefore, using equations (2.18) and (2.19) after elimination of the neutron source one gets

$$\begin{aligned}\frac{1}{\mathrm{v}}\frac{\partial\phi(\vec{r},E,t)}{\partial t} &= \nabla.D(\vec{r},E)\nabla\phi(\vec{r},E,t) - \Sigma_t(\vec{r},E)\phi(\vec{r},E,t) \\ &+ \int_0^\infty \Sigma_s(\vec{r},E'\to E)\phi(\vec{r},E',t)dE' + \chi_p(E)(1-\beta)\int_0^\infty \nu(E')\Sigma_f(\vec{r},E')\phi(\vec{r},E',t)dE' \\ &+ \chi_d(E)\beta\int_0^\infty \nu(E')\Sigma_f(\vec{r},E')\phi(\vec{r},E',0)dE'\end{aligned} \tag{2.62}$$

By expanding the flux in eigenfunctions, and introducing the eigenmodes via (2.23)

$$\begin{aligned}\frac{1}{v}\sum_{n=1}^\infty \frac{dP_n(t)}{dt}\phi_n(\vec{r},E) &= \sum_{n=1}^\infty P_n(t)\left(\chi_p(E)(1-\beta) - \frac{\chi(E)}{k_n}\right)\int_0^\infty \nu(E')\Sigma_f(\vec{r},E')\phi_n(\vec{r},E')dE' \\ &+ \sum_{n=1}^\infty P_n(0)\chi_d(E)\beta\int_0^\infty \nu(E')\Sigma_f(\vec{r},E')\phi_n(\vec{r},E')dE'\end{aligned} \tag{2.63}$$

By multiplying with the adjoint eigenfunction and applying the biorthogonal relationship (2.4) one can write

$$\frac{dP_n(t)}{dt} = A_n P_n(t) + B_n \tag{2.64}$$

with

$$A_n = \frac{\left\langle \phi_n^+(\vec{r},E), \left(\chi_p(E)(1-\beta) - \frac{\chi(E)}{k_n}\right) \int_0^\infty \nu(E')\Sigma_f(E')\phi_n(\vec{r},E')dE' \right\rangle}{\left\langle \phi_n^+(\vec{r},E), \frac{1}{v}\phi_n(\vec{r},E) \right\rangle} \tag{2.65}$$

$$B_n = \frac{\left\langle \phi_n^+(\vec{r},E), \chi_d(E)\beta P_n(0) \int_0^\infty \nu(E')\Sigma_f(E')\phi_n(\vec{r},E')dE' \right\rangle}{\left\langle \phi_n^+(\vec{r},E)\frac{1}{v}\phi_n(\vec{r},E) \right\rangle} \tag{2.66}$$

Then the initial flux conditions are used to determine the behaviour of the amplification coefficient $P_n(t)$ as a function of time

$$P_n(t) = (P_n(0) + \frac{B_n}{A_n})e^{A_n t} - \frac{B_n}{A_n} \tag{2.67}$$

Finally, for the definition of state '1' in the SCF, the exponential in eq. (2.67) disappears. Expanding the point kinetics evaluation (1.12) of the dollar reactivity towards full fluxes, one gets

$$\frac{\sum_{n=1}^\infty (P_n(0) + \frac{B_n}{A_n}) \int_0^\infty \Sigma_d(E)\phi_n(\vec{r},E)dE}{\sum_{n=1}^\infty \frac{B_n}{A_n} \int_0^\infty \Sigma_d(E)\phi_n(\vec{r},E)dE} \tag{2.68}$$

and, with

$$\chi(E) = (1-\beta)\chi_p(E) + \beta\chi_d(E) \tag{2.69}$$

the separation of n=1 and isolation of $\frac{\beta}{\rho_{(1)}}$ leads to

$$SCF_{SJ} = \frac{1 + \sum_{n=2}^\infty \frac{\rho_n}{\rho_1} \frac{P_n(0)}{P_1(0)} \frac{I_n}{I_1} \frac{J_1}{J_n} \frac{\int_0^\infty \Sigma_d(E)\phi_n(\vec{r},E)dE}{\int_0^\infty \Sigma_d(E)\phi_1(\vec{r},E)dE}}{\frac{L_1}{J_1} + \sum_{n=2}^\infty \frac{P_n(0)}{P_1(0)} \frac{K_n}{I_1} \frac{J_1}{J_n} \frac{\int_0^\infty \Sigma_d(E)\phi_n(\vec{r},E)dE}{\int_0^\infty \Sigma_d(E)\phi_1(\vec{r},E)dE}} \tag{2.70}$$

with

$$I_n = \left\langle \phi_n^+(\vec{r},E), \chi(E) \int_0^\infty \nu(E')\Sigma_f(E')\phi_n(\vec{r},E')dE' \right\rangle \tag{2.71}$$

$$J_n = \left\langle \phi_n^+(\vec{r},E), (\chi_p(E)(1-\beta) - \frac{\chi(E)}{k_n}) \int_0^\infty \nu(E')\Sigma_f(E')\phi_n(\vec{r},E')dE' \right\rangle \tag{2.72}$$

$$K_n = \left\langle \phi_n^+(\vec{r},E), \chi_d(E) \int_0^\infty \nu(E')\Sigma_f(E')\phi_n(\vec{r},E')dE' \right\rangle \tag{2.73}$$

Analysis

The SCF_{SJ} has a similar form as the SCF_{area} in (eq. 2.34), although the scaling integrals are a little more complicated. The same tendency can be seen in both the numerator and the denominator. When assuming $\chi_p(E) \approx \chi(E)$, the term $\frac{\rho_n}{\rho_1}$ and all related integrals disappear in the second term of the numerator, and $\frac{\rho_1}{\rho_n}$ is created in the second term of the denominator. Therefore, the contribution of higher modes to the SCF is reduced by the increasing denominator term for higher modes.

For an ADS with a neutron source in the centre of the core, one could (as for the PNS area method) again assume that close to the zeros of the higher order modes with n low and a maximum in the centre, the SCF should be close to unity.

2.5 Obtaining a Reference Subcriticality Level

In order to validate the candidate experimental techniques for subcriticality measurements, it is recommended to have a (zero-power) test facility at a well-known reference subcriticality level. The methodology to obtain a reference subcriticality level is explained in § 2 of [Uyttenhove et al., 2011a].

First a critical reference state is required. In this state the so-called rod drop experiment ([Ott and Neuhold, 1985], section 9-3C) is performed to obtain a slight subcritical state. Then the Modified Source Multiplication (MSM) method [Blaise et al., 2011] is applied to link the slightly subcritical state to any other subcritical level.

2.5.1 Rod Drop Technique

The rod drop technique is based on the rapid insertion of a control rod (in this case from a critical state). The subsequent time evolution of the neutron population is recorded and the reactivity is derived by the inverse point-kinetics method [Soule et al., 2004; Mellier, 2005]:

$$\rho(t) = \beta + \Lambda \frac{d}{dt}\big(\ln(n(t)\big) - \lambda\beta \int_0^t \frac{n(t')}{n(t)} e^{-\lambda(t-t')} dt' - \Lambda \frac{s(t)}{n(t)} \tag{2.74}$$

with $n(t)$ the neutron density (n/cm^3), $s(t)$ the source strength (n/s), β and λ the effective delayed neutron fraction and the corresponding decay constant (1/s), and Λ the neutron generation time (s).

For fast reactors with a very short generation time, the expression above can be simplified using micro kinetics (i.e. the study of the time dependencies of the average fission chains, see [Ott and Neuhold, 1985], Chapter 7). The result for the reactivity in \$, for clarity shown for one group of precursors, becomes [Kloosterman et al., 2002]

$$\frac{\rho(t)}{\beta} = \frac{1}{n(t)} \left(n(t) + n_0 \left(e^{-\lambda t} - \lambda \int_0^t n(t') e^{-\lambda(t-t')} dt' \right) \right) \tag{2.75}$$

Using this expression, the reactivity value can be evaluated at whatever time after the rod drop experiment. For statistics, it is recommended to fit the value by calculating $\rho(t) x N(t)$ at every timestep after the rod drop ([Lecouey et al., 2015b] for VENUS-F). By fitting this equation to the results of a set of repeated experimental data, an accurate reactivity value of the slightly subcritical state is obtained. For small antireactivity insertions (up to 0.5 \$), no spatial correction is needed.

2.5.2 Modified Source Multiplication Method

The MSM method relates the reactivity levels of two subcritical states (1 and 2) to the detector count rates in the two states (assuming a constant neutron source) via a spatial correction factor. Using the common parameters as in [Blaise et al., 2011] one gets

$$\frac{\rho_2}{\rho_1} = SCF_{MSM} \frac{\int_0^\infty \Sigma_d(E)\phi_1(\vec{r},E)dE}{\int_0^\infty \Sigma_d(E)\phi_2(\vec{r},E)dE} \tag{2.76}$$

with SCF_{MSM} being equal to the SCF_{CTF} from eq. (2.55) with a constant source (S=S').

2.5.3 Analysis

This methodology to obtain a reference subcriticality level is also subject to spatial correction factors. The same analysis as for the CTF method (see § 2.3.2) is applicable. As for the other candidate measurement techniques, an intelligent choice of the neutron source and the detector position can reduce the necessity of a spatial correction.

It is not foreseen that demonstrator or power ADS will be able to work in critical mode. The different approach to obtain the reference reactivity level however allows a validation of the proposed experimental techniques mentioned in this chapter, e.g. on a zero-power experimental facility.

2.6 Experiment Simulation via the DALTON Diffusion Code

2.6.1 Description

DALTON [Boer et al., 2008, 2010] is a 3D diffusion code developed by TUDelft. The code can solve fixed source problems and calculate fundamental and higher order λ and α-modes through the Arnoldi method by linking with the ARPACK package [Lehoucq et al., 1998]. Forward and adjoint calculations are implemented. For spatial discretisation, a second order accurate finite volume method is applied.

Moreover, DALTON is also able to perform transient analyses with or without precursors. The implementation in the DALTON code is based on implicit time integration of the diffusion equation [Pautz and Birkhofer, 2003]. Thanks to these features, both experiment simulations and modal analysis can be performed by the same code in an efficient way. Thanks to the modular character of the code, subroutines can be added easily to process the simulation data needed for the evaluation of each experimental technique.

In the following chapters, static modal analysis will be compared to experiment simulations in DALTON. This approach allows to assess the capability of modal analysis to understand the SCFs for reactivity measurement methods (determined in the sections above). This section explains how the experiment simulations are performed in DALTON.

2.6.2 Start-up Reactivity Monitoring Methods

The **area method** (see § 2.2.1) is only valid when an equilibrium condition of precursors is obtained in the system, i.e. when $C(0) = C(T)$. This only happens after a few hundred thousand pulses [Baeten et al., 2006]. The precursor decay during the pulse is assumed to be negligible, given the short pulse period (hundreds of μs), compared to the precursor decay constants.

Contrary to probabilistic codes such as MCNP(X) [Pelowitz, 2008, 2011], one can bypass the time consuming simulation of the building-up of precursors by using an initial flux and precursor concentration estimation. As long as the pulse period T is much smaller than the decay of the precursors, constant precursor concentrations can be used as initial conditions. The precursor concentration can be linked to the steady state flux $\phi_{av}(\vec{r}, E)$ from a stationary fixed source problem. In that case, the source strength S_{av} is equal to the pulse source strength S averaged over the pulse period T. Then, using eq. (2.20):

$$C(\vec{r}) = \frac{\beta}{\lambda} \int_0^\infty \nu(E)\Sigma_f(\vec{r}, E)\phi_{av}(\vec{r}, E)dE \tag{2.77}$$

The average flux and the related precursor concentration are used as initial conditions for the simulation of a few pulses. Mostly 3 pulses are sufficient to obtain a stable reactivity value via the area method. Pulses for the PNS experiment are simulated as a Dirac pulse during one time step of 1 μs, used to simulate the complete experiment. The area values do not change when simulating the Dirac pulse during more than one time step, given the nature of the PNS area method. The introduced number of neutrons however should be correct.

For the **integrated source jerk method** first a fixed source calculation with full source strength S is performed. The output flux and precursor concentration of this calculation is used as input for the time dependent calculation, which is simply a decay simulation. The decay time is in the order of tens of seconds, as the longest-living precursor should die out. Therefore, an appropriate time step of

the time-dependent calculation is 0.1 s. There is no need for precise simulations of the prompt jump after beam interruption, seen the integrated character of the method.

2.6.3 Current-to-Flux Reactivity Monitor

The simulation of the CTF reactivity monitor is straightforward and based on fixed source calculations and calculations of k_{eff}, the fundamental lambda mode. In this way, the CTF parameter c can be determined via eq. (1.14). Different reactor states can be compared to study the evolution of the CTF parameter and to identify robust detector positions (e.g. places with a constant SCF_{CTF}, see next chapters of this work).

2.6.4 Source Jerk Interim Cross-Checking Method

For the source jerk interim cross-checking method, the same calculations as for the integrated source jerk method are used. The output of the fixed source calculation with source strength S is used as input of the time dependent decay simulation. For this method however, only a few tens of microseconds after beam interruption are sufficient to determine the required flux levels. Therefore, the time step of the time-dependent calculation is chosen equal to 1 μs.

The actual average source strength will be slightly lower than S, as the source jerk experiment is repeated for statistical reasons. Therefore, the real precursor concentration should correspond to the average source strength, taking into account the repeated small beam interruptions. As the beam interruption time is much smaller than the time to restore the flux level, this effect is assumed to be negligible.

2.7 Summary

As the available evaluation methods to determine the reactivity level rely on point kinetics theory, Spatial Correction Factors (SCFs) need to be applied on the measured reactivity values. Static modal analysis of each selected evaluation method for subcriticality measurements is outlined in this chapter.

Via modal analysis, the SCFs for the different methods are determined analytically. This approach allows a straightforward understanding of the spatial

dependence for the PNS area method, the Integrated SJ method and the CTF method. The modal SCF for the SJ method is more complex to interpret.

If an ADS core can be modified towards a critical reactor without major design changes (e.g. in some zero-power facilities), a so-called reference subcriticality level can be derived starting from criticality via the rod-drop technique and the Modified Source Multiplication (MSM) method. Although this procedure is also subject to spatial dependence, a subcriticality level to validate the candidate measurement techniques is derived via an alternative methodology.

The DALTON diffusion code is extended in order to simulate the selected experimental techniques. Thanks to its ability to calculate forward and adjoint modes, both modal analysis and experiment simulation can be performed with this code.

3

VALIDATION BY EXPERIMENTAL RESULTS FROM SUBCRITICALITY MEASUREMENTS

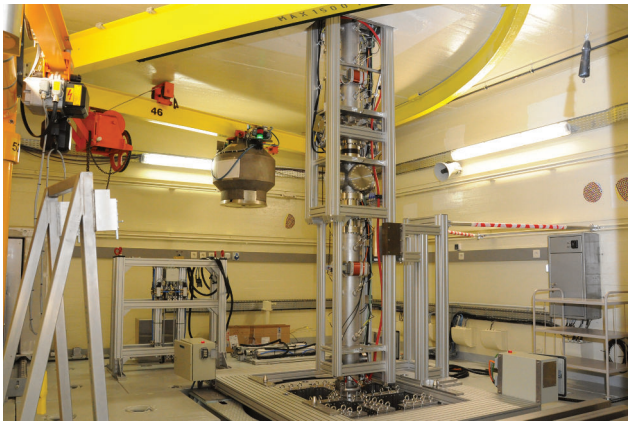

It doesn't matter how beautiful your theory is, it doesn't matter how smart you are.
If it doesn't agree with experiment, it's wrong.

Richard Feynman, The Character of Physical Law, 1965.

Picture: The VENUS-F facility at SCK•CEN, Mol (Belgium).

In this chapter, the modal analysis of the SCFs for the selected reactivity monitoring methods from Chapter 2, as well as the SCFs from experiment simulations are validated by experimental results from the zero-power VENUS-F ADS (described in § 1.5.3).

First the VENUS-F subcritical 'reference' state (SC1) is derived. Starting from this configuration, the PNS area and Integral Source Jerk (ISJ) candidate start-up reactivity measurement methods are tested. Then, a case study for subcriticality monitoring is analysed. Finally, the Source Jerk (SJ) candidate interim reactivity cross-checking technique is assessed. The validation of the various experiments are completed by simulations for different energy groups and reactor configurations, in order to derive detector type and positioning recommendations for the different phases of ADS operation.

The subcriticality measurements are carried out on VENUS-F by different European partners within the FREYA project [Kochetkov, 2010; Kochetkov et al., 2013]. The facility is described in § 1.5.3. The related calculational model used in this chapter is presented in Appendix A.

All experiments and simulations in this (and the next) chapter are performed in the centre plane of the VENUS-F reactor. As common ADS designs have their neutron source located in the centre of the core, the centre plane is the suitable location to reduce the SCFs for all selected experimental techniques. This choice is motivated in Chapter 2 and this chapter.

3.1 The VENUS-F Subcritical 'Reference' State

Thanks to the modular character of the VENUS-F reactor, it is possible to operate in critical or subcritical mode. Via the steps explained in § 2.5, a 'reference' subcriticality level is derived, for which the selected measurement methods are tested. The estimation of this level for the VENUS-F SC1 configuration is described in detail in [Lecouey et al., 2015b]. In this section, only a short overview is provided, focusing on the spatial correction factors (SCFs) related to this methodology.

3.1.1 The VENUS-F Critical Reactor

Before assessing subcriticality measurement techniques, the first configurations made in the VENUS facility were critical. The critical state CR0 considered in this work is shown in Fig. 3.1, consisting of 97 fuel assemblies (FAs), the control rods

positioned at 497.3 mm[1], with the PEAR (PEllet Absorber Rod) experimental rod in its upper position. The related detector characteristics are shown in Table 3.1.

The design choices (such as fuel assembly design and reflector dimensions) as well as the licensing requirements (e.g. a sufficient safety rod worth able to deal with reactivity incidents) for the first VENUS-F critical configurations are explained in [Uyttenhove et al., 2011a; Mercatali et al., 2010]. After obtaining the first criticality in VENUS-F, licensing [Uyttenhove et al., 2012a] and characterisation [Uyttenhove, 2013] experiments are performed, to understand the neutronics behaviour of this homogenous lead fast reactor. This analysis, out of the scope of this work, comprises the measurement of radial and axial flux profiles, spectral indices, peak flux factors, and control and safety rod performances.

No	Name	Deposit	Mass (mg)
1	CFUL659	^{235}U (≈ 92 wt%)	1000
2	CFUL658	^{235}U (≈ 92 wt%)	1000
3	CFUL653	^{235}U (≈ 92 wt%)	1000
4	RS10072	^{235}U (≈ 90 wt%)	100
5	RS10071	^{235}U (≈ 90 wt%)	100
6	RS10074	^{235}U (≈ 90 wt%)	100
7	RS10075	^{235}U (≈ 90 wt%)	100
8	CFUF34	^{235}U (≈ 100 wt%)	1
9	CFUM21-668(325)	^{235}U (≈ 90 wt%)	10
10	CFUM21-667(326)	^{235}U (≈ 90 wt%)	10

Table 3.1: Detectors (uranium fission chambers) in the VENUS-F reactor for the subcritical experiments analysed in this work.

3.1.2 The PEAR Drop Experiment

In order to derive a 'reference' subcritical state at a k_{eff} level about 0.96, first a slightly subcritical state needs to be derived, as explained in § 2.5. To do so, the experimental PEAR rod with a light antireactivity worth is dropped into the critical reactor, and via inverse point kinetics (see § 2.5.1), a slight subcritical state is determined.

[1]The control rods have an active length of 600 mm. At 0 mm the rods are completely introduced in the core, at 600 mm they are fully withdrawn.

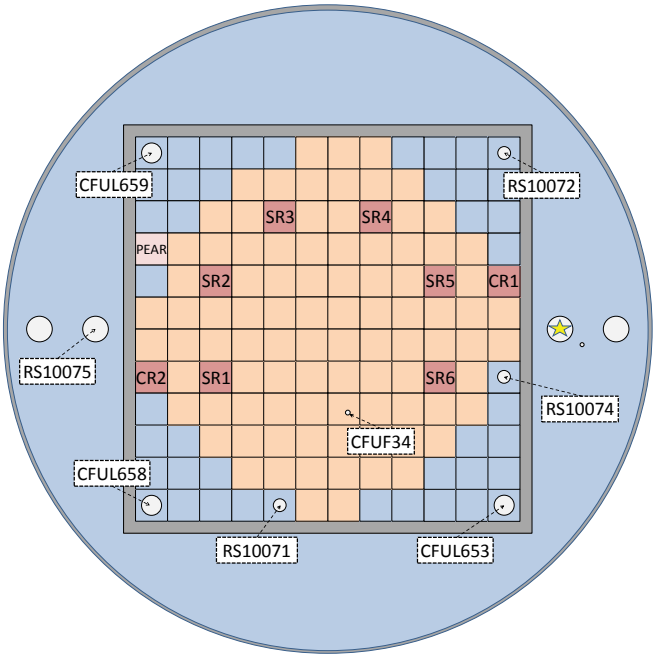

Figure 3.1: Setup of the VENUS-F critical CR0 reactor (97 FAs) at middle height with associated detector locations (orange - fuel, blue - lead, grey - stainless steel, SR - safety rod, CR - control rod, PEAR - experimental PEllet Absorber Rod). The yellow star indicates the position of the external Am-Be source.

After statistical analysis of the different detector outputs during this experiment, a reactivity value of -0.1881 ± 0.0024 $ is found for this reactor state [Lecouey et al., 2015b][2]. This reactivity value is obtained by fitting the experimental data for $\rho_{\$}(t).\overline{N(t)}$ against $\overline{N(t)}$ with a linear curve ($\overline{N(t)}$ being the average count rate from the different PEAR drop experiments), and by selecting the detectors that are not affected by spatial effects from the PEAR rod drop, as these effects are not taken into account in this methodology (close to critical). Using this methodology, the

[2] ρ=1 $ corresponds to $\rho=\beta_{eff}$. A value of 722 pcm is used in [Lecouey et al., 2015b] for the VENUS-F CR0 and SC1 configurations, based on deterministic calculations with the ERANOS code [Bianchini et al., 2010]. This value is applicable to all reactivities in dollar on VENUS-F in this work. MCNP(X) calculations lead to a value of β_{eff}=731 pcm. This value was determined before the construction of VENUS-F (see [Uyttenhove et al., 2011a], Table 1) and confirmed by calculations with the updated VENUS-F input file (see [Uyttenhove, 2012]) after commissioning of the reactor. Recently, experimental results confirmed calculations: β_{eff}=731 ± 12 pcm [Doligez et al., 2015].

uncertainty on the delayed neutron parameters (β_i and λ_i) is by far the dominant term in the final uncertainty of the reactivity estimate (see [Lecouey et al., 2015b]).

3.1.3 The MSM Experiment to obtain the VENUS-F SC1 Configuration

The Modified Source Multiplication (MSM) method (see § 2.5.2) relates the reactivity level of two subcritical states via the detector count rates of both states. In this case, the reactivity level of the slightly subcritical reactor (described above) is known via the rod drop experiment in the critical CR0 configuration.

Starting from this slight subcritical state, the 4 central assemblies are removed from the VENUS-F core and replaced by the GENEPI-3C beam line. In this way, the VENUS-F SC1 configuration is obtained (93 FAs, with the control rods still at 479.3 mm), shown in Fig. 3.2. The reactivity measurement techniques will be tested on this configuration in the next sections of this chapter.

An Am-Be neutron source in the reflector of the VENUS-F reactor is used to relate the detector count rates in the slightly subcritical state and the SC1 configuration to their reactivity levels. SCFs should be applied to the count rates to link them to the SC1 reactivity level. In [Lecouey et al., 2015b], the SCFs are calculated by means of detailed MCNP calculations with a detailed VENUS-F model [Uyttenhove and Steckmeyer, 2014]. By doing this, the variation in reactivity levels of the different detectors disappears, and the average absolute value of 5.28 ± 0.13 \$ is found as 'reference' subcriticality level for the SC1 configuration. A thorough sensitivity analysis (mainly related to MCNP calculation models and detector models) shows the accuracy of the SCF (see [Lecouey et al., 2015b]). From this state, other subcriticality levels can be derived again via the MSM method, e.g. for the SC1 state with control rods up and down (see [Lecouey, 2014; Lecouey et al., 2015a]).

3.1.4 Discussion

This section provides the derivation of a 'reference' subcritical level of the VENUS-F SC1 configuration, starting from the critical state. We call this a 'reference' level, as the reactivity values obtained by the selected subcriticality measurement techniques can be compared to this level, obtained via an alternative methodology. This approach is only applicable to modular zero-power ADS like VENUS-F, i.e. installations which allows an easy installation of the accelerator beam line, to go from critical to subcritical mode.

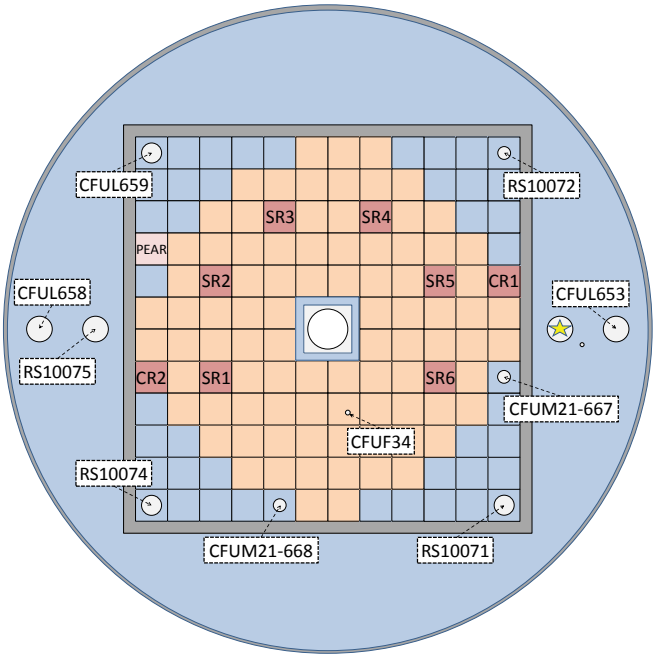

Figure 3.2: Set-up of the VENUS-F SC1 configuration (93 FAs) at middle height with associated detector locations (orange - fuel, blue - lead, grey - stainless steel, white - air or vacuum (in the central beam line), SR - safety rod, CR - control rod, PEAR - experimental PEllet Absorber Rod). The yellow star indicates the position of the external Am-Be source.

One should, however, take into account the spatial dependence of the MSM method. Therefore, this 'reference' subcritical level is also subject to calculated SCFs. Moreover, the uncertainty on the delayed neutron parameters of the rod drop technique is dominating the final uncertainty of the SC1 subcriticality level.

Thanks to the use of probabilistic code calculations, using detailed reactor models, the SCFs for the MSM method are accurately calculated at the detector locations. In the following sections, however, the spatial behaviour of the candidate reactivity measurement techniques will be tested throughout the complete VENUS-F reactor. Instead of calculating precisely SCFs at the detector locations, this work will focus on the physics of the SCFs in order to determine detector types and locations for ADS operation.

3.2 Subcriticality Monitoring during Start-up

In this section, experimental results are presented from the selected VENUS-F start-up monitoring techniques. As defined in § 1.3.8, the Pulsed Neutron Source (PNS) technique and the Integrated Source Jerk (ISJ) technique are candidates to measure the reactivity during start-up, i.e. at Cold Zero Power (CZP) until 1 % of nominal power.

The experimental results confirm the understanding of SCFs for both techniques, and show their usefulness in a zero-power ADS. SCFs are simulated for the complete VENUS-F core and compared to experimental results at different detector locations. The understanding of the spatial behaviour is assessed by modal analysis, and detector types and positions for robust reactivity monitoring during start-up are investigated.

3.2.1 Pulsed Neutron Source and Integrated Source Jerk Experiments in VENUS-F Subcritical Configurations

PNS (see § 1.3.1) and ISJ (see § 1.3.2) experiment results are analysed for two VENUS-F configurations with different subcriticality levels: SC1 and SC4. Their layouts are presented in Fig. 3.2 and Fig. 3.3. The characteristics of the detectors in these configurations are described in Table 3.1.

The 'reference' subcriticality levels for both SC1 and SC4 can be obtained via the alternative pathway (i.e. the rod drop and MSM experiments) as described in § 3.1. For SC1, $\left|\rho_{ref}\right|$=5.06 ± 0.13 \$, i.e. 3653 pcm (with CRs at 600mm, see [Lecouey et al., 2015b; Lecouey, 2014]) is obtained in this way. For SC4, $\left|\rho_{ref}\right|$= 17.70 ± 0.13 \$, i.e. 12779 pcm is obtained via precise MCNP calculations [Uyttenhove and Steckmeyer, 2014].

For the PNS experiments, (quasi) Dirac pulses are given every 500 μs in the centre of the core. The GENEPI-3C accelerator provides pulses of 1 μs with about 20 mA peak current. This corresponds to an injection of about 10^6 neutrons per pulse. After stabilisation of the delayed neutron levels, the experiment is repeated to obtain good statistics on the area method results. For the ISJ experiments, the continuous GENEPI-3C beam is interrupted and the decay of the neutron chains in the reactor is followed.

The available experimental reactivity values (from [Marie et al., 2013; Kochetkov et al., 2014; Kochetkov, 2014]) are given in Fig. 3.4 for both the PNS area method

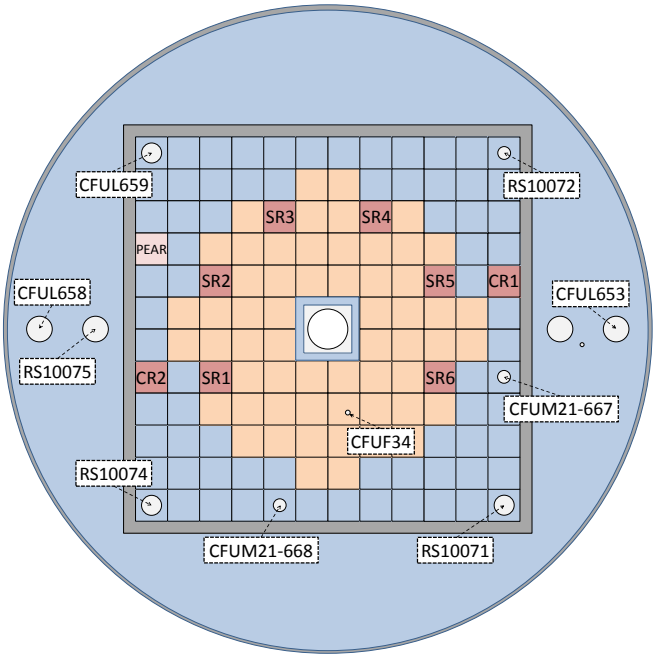

Figure 3.3: Set-up of the VENUS-F SC4 configuration (64 FAs) at middle height with associated detector locations (orange - fuel, blue - lead, grey - stainless steel, white - air or vacuum (in the central beam line), SR - safety rod, CR - control rod, PEAR - experimental PEllet Absorber Rod).

and the ISJ method for each detector. For the SC4 core, the experimental reactivity values and SCFs are shown in Fig. 3.5 for the ISJ method for each detector.

In order to understand the spatial corrections needed for both subcritical states, the experimental PNS area and ISJ reactivity values are compared to the 'reference' reactivity levels, according to the SCF definitions (2.17) and (2.35). The related SCFs, to be applied to the measurement values, are shown in Fig. 3.4 and Fig. 3.8 for the SC1 core, and in Fig. 3.5 for the SC4 core.

Except for the CFUF34 detector for the PNS SC1 experiment, both SCF_{area} and SCF_{ISJ} are smaller than unity in all detector positions, which indicates a safe underestimation of the absolute reactivity by both methods for almost all detectors. E.g. for the CFUL658 detector for the PNS SC1 experiment, SCF_{area}=0.883 corresponds to $|\rho|$=3226 pcm, an underestimation of the absolute reactivity value by

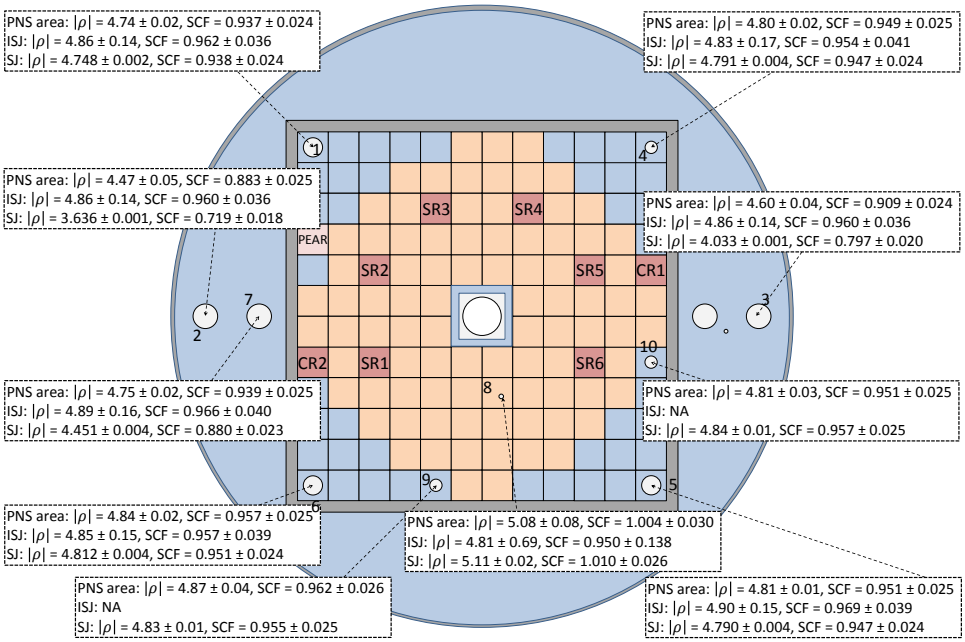

Figure 3.4: Absolute reactivities (in \$) and SCFs (and their absolute uncertainty) for the SC1 VENUS-F configuration (with CRs at 600 mm) at different detector locations obtained by the PNS area, the ISJ and the SJ method. $|\rho_{ref}|$=5.06 ± 0.13 \$. Detectors 9 and 10 were not available (NA) when the ISJ experiments were performed on SC1. From [Marie et al., 2013; Kochetkov, 2014; Kochetkov et al., 2014; Chevret et al., 2014].

427 pcm.

For the ISJ method, only results from detectors in the outer reflector are available for interpretation. The result for the detector in the fuel shows a too high uncertainty, due to the low detector count rates. The experiment can be performed only once, as the ADS is shut down, and therefore difficult to reproduce. In particular for the SC4 configuration, the results of the ISJ technique show a too high uncertainty (because of low count rates) to draw any conclusions about spatial dependence.

The applicability of the ISJ method on power ADS will thus depend on flux level, subcriticality level and detector type. As the uncertainty on the PNS method can be reduced by performing longer measurements, in theory, every level of subcriticality can be measured with a sufficient degree of accuracy.

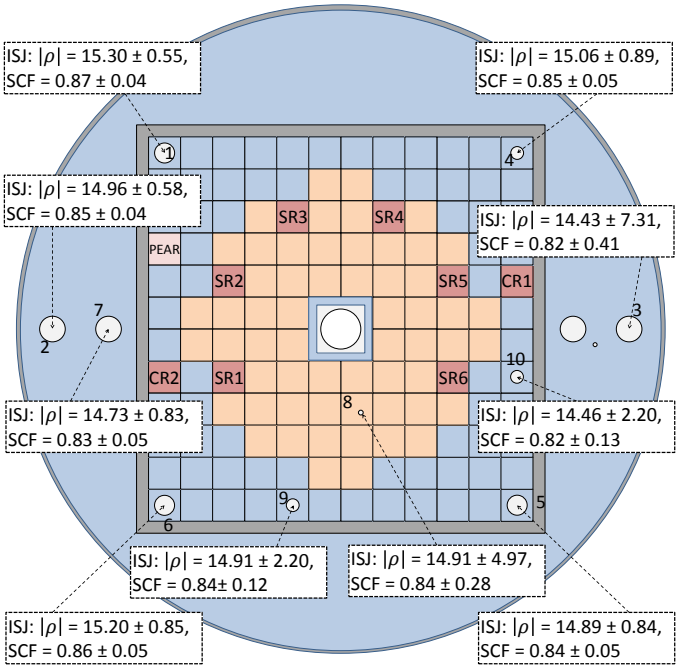

Figure 3.5: Absolute reactivities (in \$) and SCFs (and their absolute uncertainty) for the SC4 VENUS-F configuration (with CRs at 600 mm) at different detector locations obtained by the ISJ method. $|\rho_{ref}| = 17.70 \pm 0.13$ \$. From [Kochetkov, 2014; Kochetkov et al., 2014].

3.2.2 Validation of Experiment Simulations

In this section PNS and ISJ experiments in VENUS-F are simulated using the DALTON diffusion code (see § 2.6). Appendix A presents the VENUS-F XYZ model for the DALTON code simulations, as well as the related 6 energy groups (representative for the VENUS-F spectrum and applied detectors).

In order to validate the SCFs for the area method (defined by eq. (2.17) and the ISJ method (defined by eq. (2.35)), the incident is simulated via time-dependent calculations. The result from the experiment evaluation (e.g. the area ratio) is scaled on the 'reference' k_{eff}, obtained via an eigenmode calculation. Thanks to this approach, the SCF for both experiments is determined through the complete reactor and evaluated by experimental results (for the VENUS-F SC1 configuration). For all simulations the detector cross section, $\Sigma_d(E)$ equals unity.

PNS

For the PNS experiment simulations, a pulsed source of 1 μs is implemented in the highest (i.e. the first) energy group of the VENUS-F model in DALTON (with bunker $|\rho_{ref,DALTON}|$=3709 pcm, without bunker $|\rho_{ref,DALTON}|$=4082 pcm, see App. A). Different pulse shapes are found throughout the reactor for the lowest energy group (representative for the U-235 detectors), as shown in Fig. 3.6.

For the PNS method, special attention should be paid to thermalising effects. They considerably influence the pulse shapes and thus the experimental results, as U-235 detectors are used in the VENUS-F configurations for measurements (see Table 3.1). The VENUS-F bunker (made from barite concrete) is such an element. It thermalises and reflects neutrons, increases the absolute reactivity of the reactor (by 371 pcm for the DALTON calculations), and has a significant broadening effect on the pulse shapes. Therefore, an appropriate pulse period should be chosen (for VENUS-F i.e. 500 μs), in order to let the prompt neutron decay disappear by the end of the pulse period. The effect of thermalising elements is slightly noticeable in the other energy groups and other detector positions, but less pronounced.

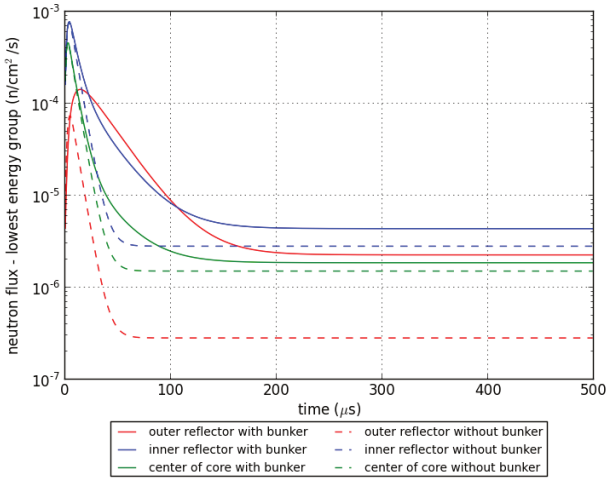

Figure 3.6: Simulated PNS responses in the lowest energy group (i.e. group 6) at different locations in the VENUS-F SC1 configurations across the X-axis at centre height (Y=Z=0). The flux level corresponds to a unit source strength implemented in the highest energy group 1 during the first time step of 1 μs.

Fig. 3.7 shows the behaviour of the simulated SCF of the lowest energy group for

the area method through the complete VENUS-F reactor by 2D plots at different heights above the centre of the core. The behaviour of the SCF is symmetrical to the centre plane of the VENUS-F SC1 configuration. SCF > 1, an (unsafe) overestimation of the absolute reactivity level, is found inside a sphere of about 20 cm from the centre of the core. In the reflector, the reactivity is (safely) underestimated by 3-4 % (SCF_{area}=0.96-0.97), $\left|\rho_{area}\right|$ is 111-148 pcm higher than $\left|\rho_{ref}\right|$= 3709 pcm .

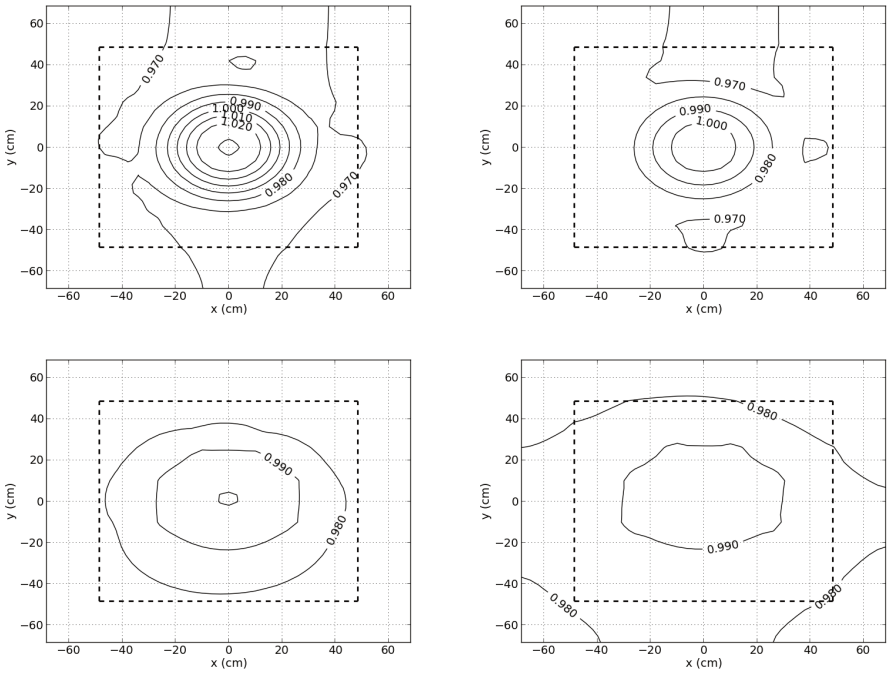

Figure 3.7: Simulated SCF_{area} for the lowest energy group (i.e. group 6) at different heights in the VENUS-F SC1 configuration (with bunker): 0 cm (center plane), 20 cm (fuel), 39 cm (top reflector) and 59 cm (top reflector). The dashed line corresponds to the boundary of the 12x12 grid in which the assemblies are loaded, indicated in grey in Fig. 3.2.

The simulated PNS area method results are slightly affected by the presence of the VENUS-F bunker. The top graph of Fig. 3.8 shows the experimental results and the difference in simulated SCF for the area method with and without bunker in the middle plane of the VENUS-F reactor, across the X-axis. For the clarity of

the figure, radial symmetry is supposed, justified by the SCF profiles at different heights in Fig. 3.7. Therefore, the location of the detectors on the X-axis on Fig. 3.8 corresponds to their radius to the centre of the core.

Good agreement between simulations and measurements is found for the area method in the fuel and inner reflector zone. In the outer reflector zone (in particular for detectors 2 and 3), local external thermalising elements that are not modeled in DALTON significantly affect the agreement between calculations and experiments (see e.g. [Chevret et al., 2014; Chevret, 2014a] for the same effect in the source jerk experiment, shown by MCNP(X) calculations with precise modelling).

PNS Area Conclusion

One concludes that the outer reflector zone of the VENUS-F reflector at centre height is the suitable location for start-up reactivity monitoring in VENUS-F via the PNS area method. In that region, the absolute reactivity is safely overestimated: SCF_{area}=0.96-0.97, which means that e.g. for the DALTON simulations, $\left|\rho_{area}\right|$ is 111-148 pcm higher than $\left|\rho_{ref}\right|$= 3709 pcm. The simulation results are confirmed by experimental values.

Although SCF_{area} is different from unity, the outer reflector is preferred as detector location because of the small gradient in SCF. Attention should be paid to (local) thermalising elements for U-235 detectors. This issue could be avoided by the use of threshold detectors, investigated further in this section.

ISJ

The simulation of the ISJ experiment in DALTON is analysed in this paragraph. The decay of the neutron population is simulated (see § 2.6, timestep dt=0.1 s) for the lowest energy group (representative for the U-235 detectors) in Fig. 3.9 for the first 200 s[3]. The contribution of the flux after 200 s to the integral in eq. (2.35) is negligible. The decay in the outer reflector is a little slower than in the inner reflector and fuel zone. The thermalising effect of the bunker is clear in the

[3]Because of the long calculation time, only the first 65 s of the decay are calculated for the configuration with bunker in Fig. 3.9. For the same reason no SCF_{ISJ} is available for the configuration with bunker in Fig. 3.8. The influence of the bunker on SCF_{ISJ} will be limited seen the integrated character of the method. Only the decay slope of the detector could be slower. During the first 65 s, this is, however, not the case.

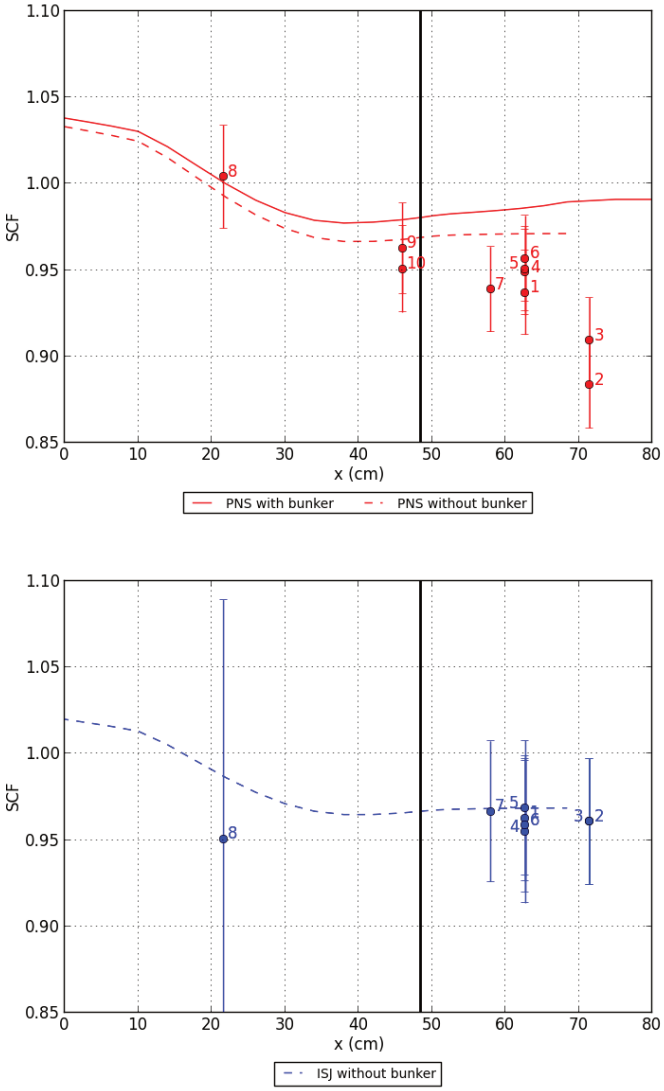

Figure 3.8: Simulated PNS (top) and ISJ (bottom) SCF (lines) and measurement results (dots) across the X-axis at centre height of the VENUS-F SC1 configuration (Y=Z=0). As the detector locations are not on the X-axis, the corresponding radius to the centre of the core is shown. The vertical line indicates the core-reflector interface.

outer reflector: a higher thermal flux component is found. The general slope of the decay, however, does not change significantly while taking into account the VENUS-F bunker.

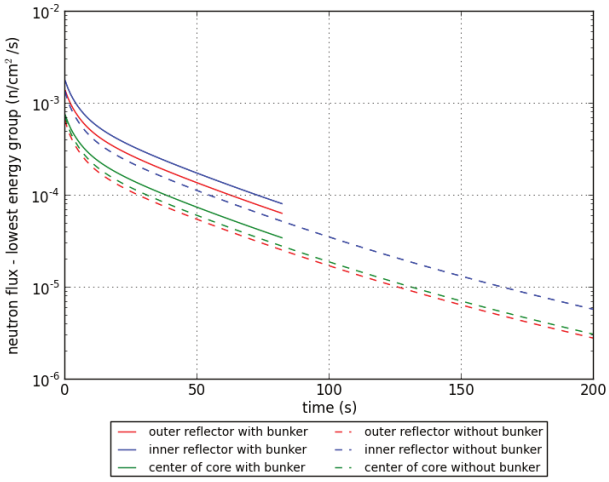

Figure 3.9: Simulated ISJ responses in the lowest energy group (i.e. group 6) at different locations in the VENUS-F SC1 configuration across the X-axis at centre height (Y=Z=0). The flux profile corresponds to the decay of a unit source strength implemented in the highest energy group 1, stopped at t=0 s.

Fig. 3.10 shows the simulated SCF_{ISJ} of the lowest energy group (defined by eq. (2.44)) for the ISJ method through the complete VENUS-F reactor, by 2D plots at different heights above the centre of the core. The behaviour of SCF_{ISJ} is symmetrical to the centre plane of the VENUS-F SC1 configuration. $SCF_{ISJ} > 1$, an (unsafe) overestimation of the absolute reactivity level, is found inside a sphere of about 20 cm from the centre of the core. In the midplane, a symmetrical SCF profile is found. In the reflector, the absolute reactivity is (safely) underestimated by 2-3 %. SCF profiles similar to the PNS ones are found.

The experimental ISJ results are presented in the Fig. 3.8 bottom graph and compared to the simulation results. For the clarity of the figure, radial symmetry is again supposed, justified by the SCF profiles at different heights in Fig. 3.10. Therefore, the location of the detectors on the X-axis on Fig. 3.8 corresponds to their radius to the centre of the core. Good agreement between simulations and measurements is found for the ISJ method in the outer reflector zone. Unfortu-

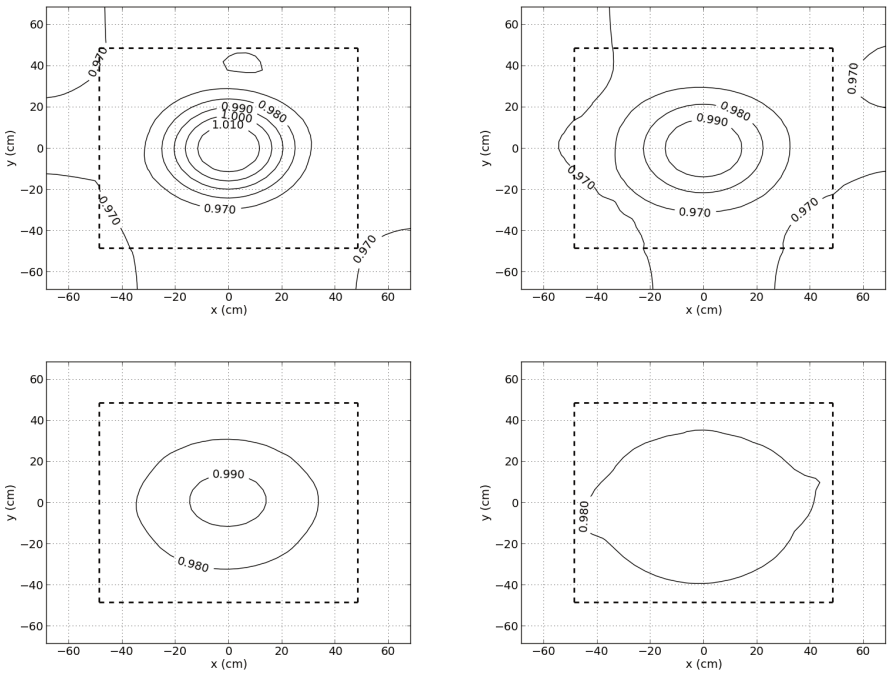

Figure 3.10: Simulated ISJ SCF for the lowest energy group (i.e. group 6) at different heights in the VENUS-F SC1 configuration: 0 cm (center of the core), 20 cm (fuel), 39 cm (top reflector) and 59 cm (top reflector). The dashed line corresponds to the boundary of the 12x12 grid in which the assemblies are loaded, indicated in grey in Fig. 3.2.

nately, this is the only zone where accurate measurement data are available.

ISJ Conclusion

The optimum zone for ISJ detector positioning is similar to the one of the PNS area method. Again the outer reflector zone of the VENUS-F reflector at centre height is the suitable location for start-up reactivity monitoring in VENUS-F via the ISJ method. In that region, the absolute reactivity is safely underestimated. The simulation results in that region are confirmed by experimental values.

Comparison between PNS area and ISJ method

The ISJ method shows the same spatial dependence trend as the PNS area method for the VENUS-F SC1 configuration. The PNS area method is however, due to its nature, more sensitive than the ISJ method to local thermalising elements that affect the detector results (see detectors 2 and 3 for the PNS area method in Fig. 3.8). Precise calculations (as shown in [Chevret et al., 2014; Chevret, 2014a]) are required to improve the agreement between experiments and simulations for these detectors. The issue of thermalising elements could be avoided by the use of threshold detectors, and will be checked in future experimental programmes on VENUS-F.

We conclude that although the spatial dependence of both methods is quasi similar, the PNS area method is more robust: it is reproducible and independent of the delayed neutron constants. Therefore, the ISJ method will be excluded as candidate for power ADS start-up reactivity monitoring in Chapter 4.

3.2.3 Modal Analysis Understanding of Spatial Correction Factors

In order to understand the behaviour of the SCF for the different experimental methods, modal analysis is applied in this thesis. For the PNS area method, SCF_{area} obtained by modal analysis is presented in eq. (2.34). For the ISJ method, the SCF_{ISJ} obtained by modal analysis is presented in eq. (2.44). Again $\Sigma_d(E)$=1 is supposed for the analysis.

VENUS-F Eigenfunctions

As a first step, we have a look at the VENUS-F eigenfunctions. They are calculated in DALTON and plotted for the VENUS-F SC1 configuration (with bunker) in Figures 3.11, 3.12 and 3.13 for the total flux. The total flux is the sum of the eigenfunctions for each energy group. The shape is similar for each group, e.g. for the 9th mode in Fig. 3.14. For a simple symmetric 2-zone VENUS-F model with 1 energy group cross sections (see Appendix A), the shape of the eigenfunctions follows a structured sequence of azimuthal and axial modes (as in Fig. 2.1), as shown in [Uyttenhove et al., 2012b]. In the VENUS-F case, the shapes of subsequent modes are combinations of the ones in Fig. 2.1. The general behaviour of the modes, however, remains unchanged.

Most (power) ADS have the source in the centre of the core [Nifenecker et al., 2003]. Therefore, the fundamental mode is significantly amplified and contributes

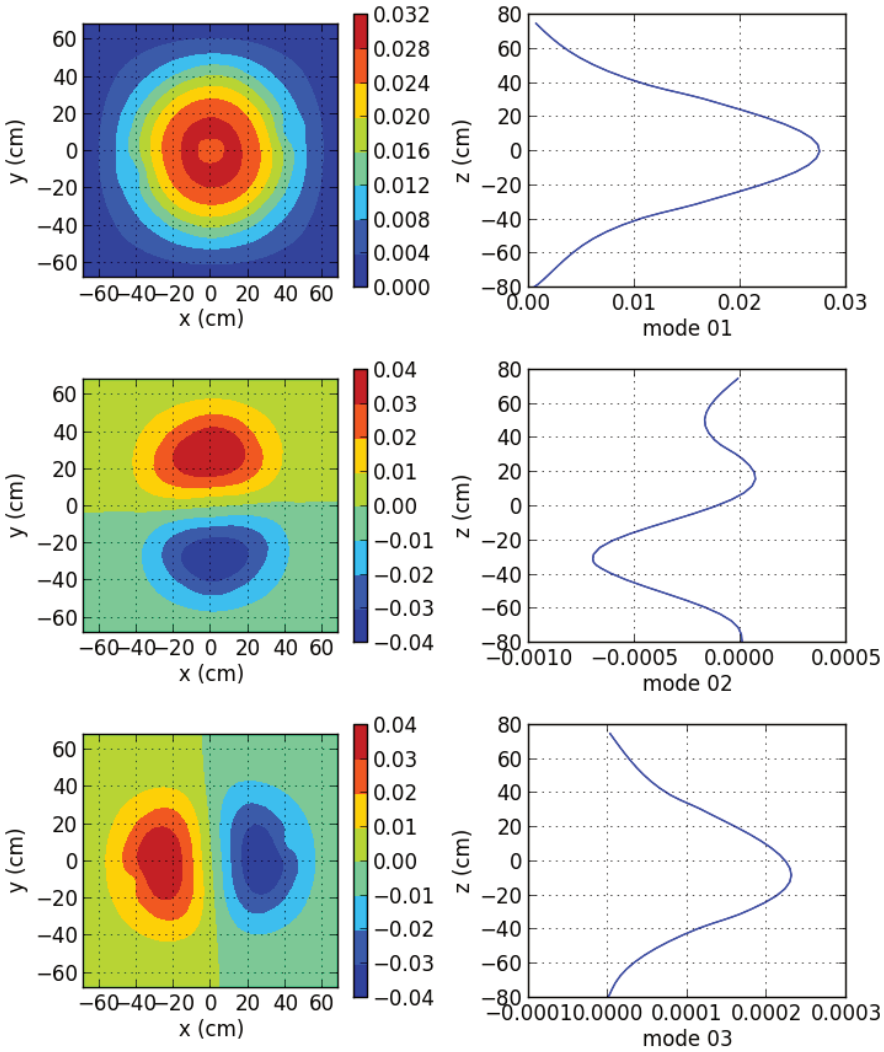

Figure 3.11: XY (Z=0) and Z (X=Y=0) plots of the 1st to the 3rd eigenfunction of the VENUS-F model of the SC1 (with CRs out) configuration. The sum over the 6 energy groups of each mode is shown.

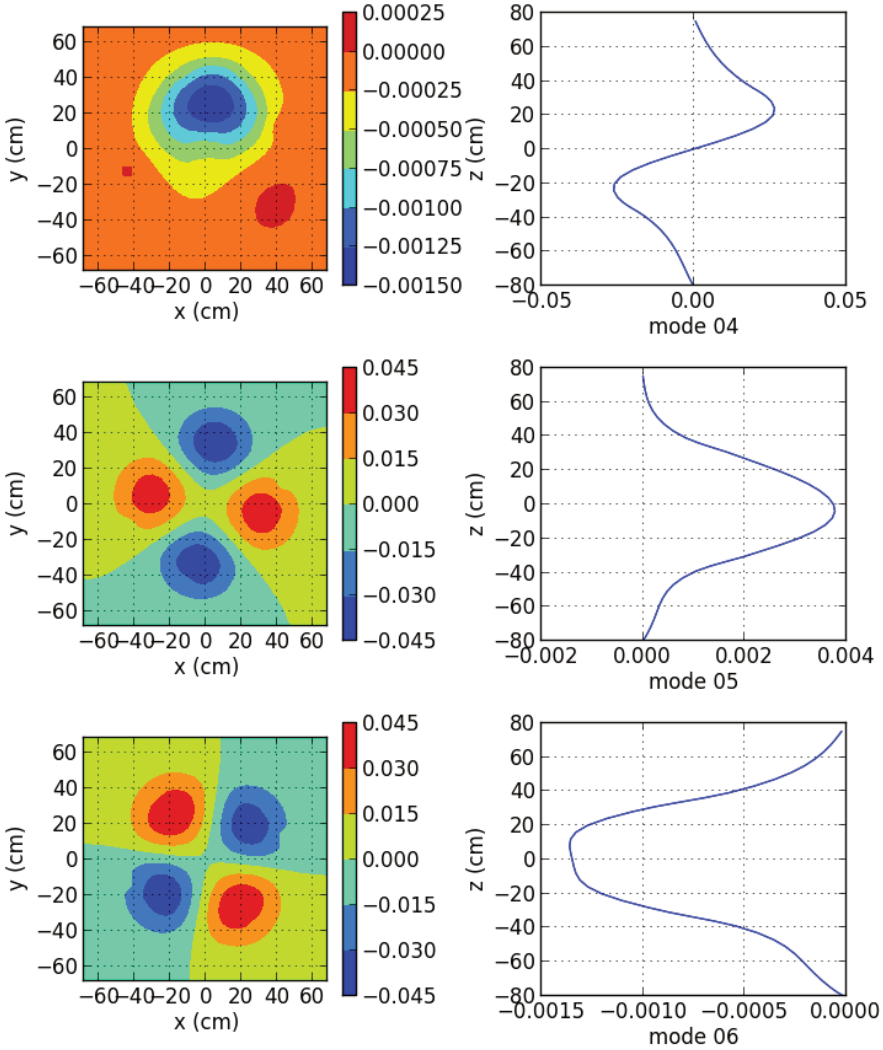

Figure 3.12: XY (Z=0) and Z (X=Y=0) plots of the 4th to the 6th eigenfunction of the VENUS-F model of the SC1 (with CRs out) configuration. The sum over the 6 energy groups of each mode is shown.

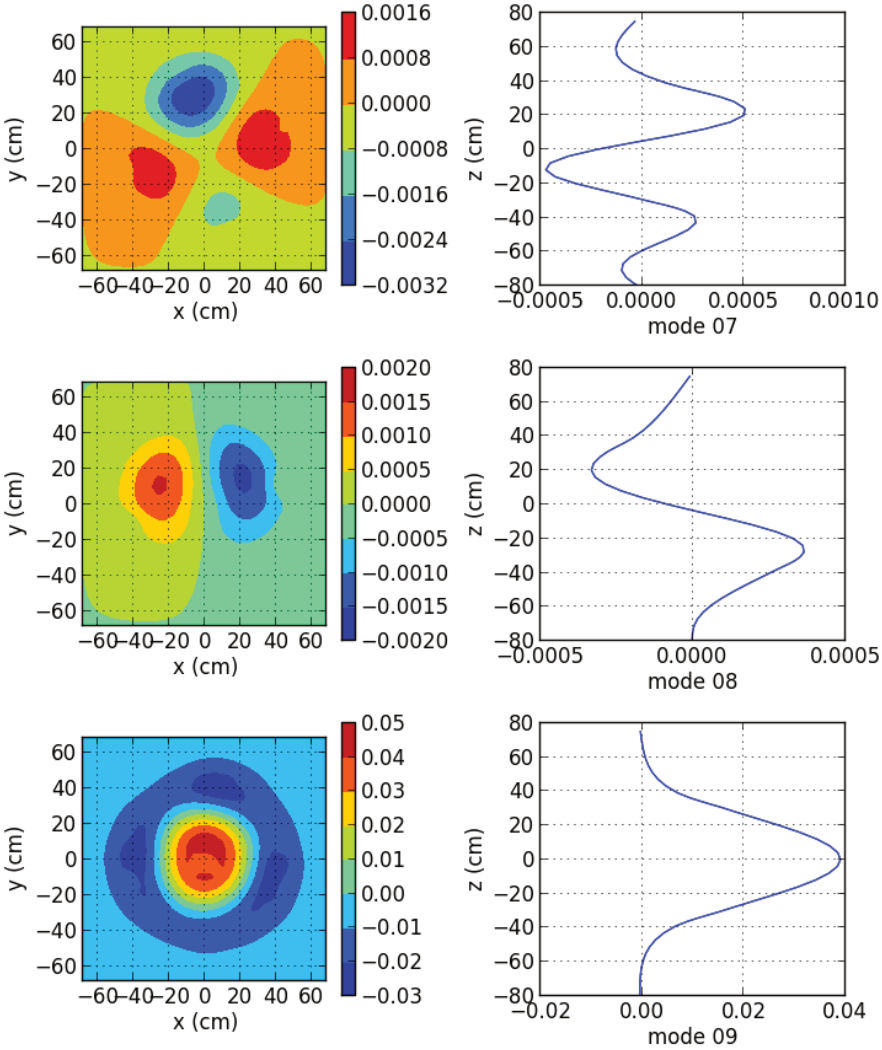

Figure 3.13: XY (Z=0) and Z (X=Y=0) plots of the 7th to the 9th eigenfunction of the VENUS-F model of the SC1 (with CRs out) configuration. The sum over the 6 energy groups of each mode is shown.

significantly to the full flux solution [Uyttenhove et al., 2014]. SCFs close to unity will therefore be found in the central plane. This conclusion can also be retrieved from the analytical expression of the SCFs for the selected experimental techniques, in eq. (2.34),(2.44),(2.54) and (2.70). For this reason detector positioning exercises focus on the reactor centre plane, also in this work.

The first (fundamental) mode has no zero crossings and a maximum in the centre of the core. The next modes (2-8) do not show maxima in the centre of the core. The 9th mode is the first higher mode with a maximum in the centre of the core, and has a zero crossing at a radius of about 25 cm from the centre of the core at centre plane height. Higher modes show a more complicated shape. For the first 50 modes, only few modes have their maximum in the neighbourhood of the centre of the core.

When looking into the different energy groups, one notices that the shape of a mode does (almost) not change through the different energy groups, although the amplitude of the mode varies per energy group. This is shown in Fig. 3.14, providing the 9th eigenfunction of each energy group for the VENUS-F SC1 configuration. The zero crossing remains for each energy group around 20-25 cm from the centre of the core at centre plane height.

Important modes for the VENUS-F ADS flux reconstruction

The full flux of the VENUS-F SC1 configuration with continuous source can be reconstructed by the summation of each amplified mode (see eq. (2.6) and § 2.1.2). The full solution is in principle obtained with an infinite number of modes. In practice, most of the experimental techniques for the determination of ADS reactivities [Soule et al., 2004; Mellier, 2005] rely on point kinetics, in which only the first (fundamental) mode of the flux is taken into account.

For the VENUS-F ADS, having the neutron source in the centre of the subcritical core, much more than 100 modes are needed to reconstruct the full solution accurately (see Fig. 10 in [Uyttenhove et al., 2014]). Indeed only few of these 100 modes have a maximum in the centre of the core, given the profile sequence of the modes in Fig. 2.1. The 9th mode contributes significantly to the full solution, being the first mode with a maximum in the centre of the core (different from the fundamental one), as shown in [Uyttenhove et al., 2014].

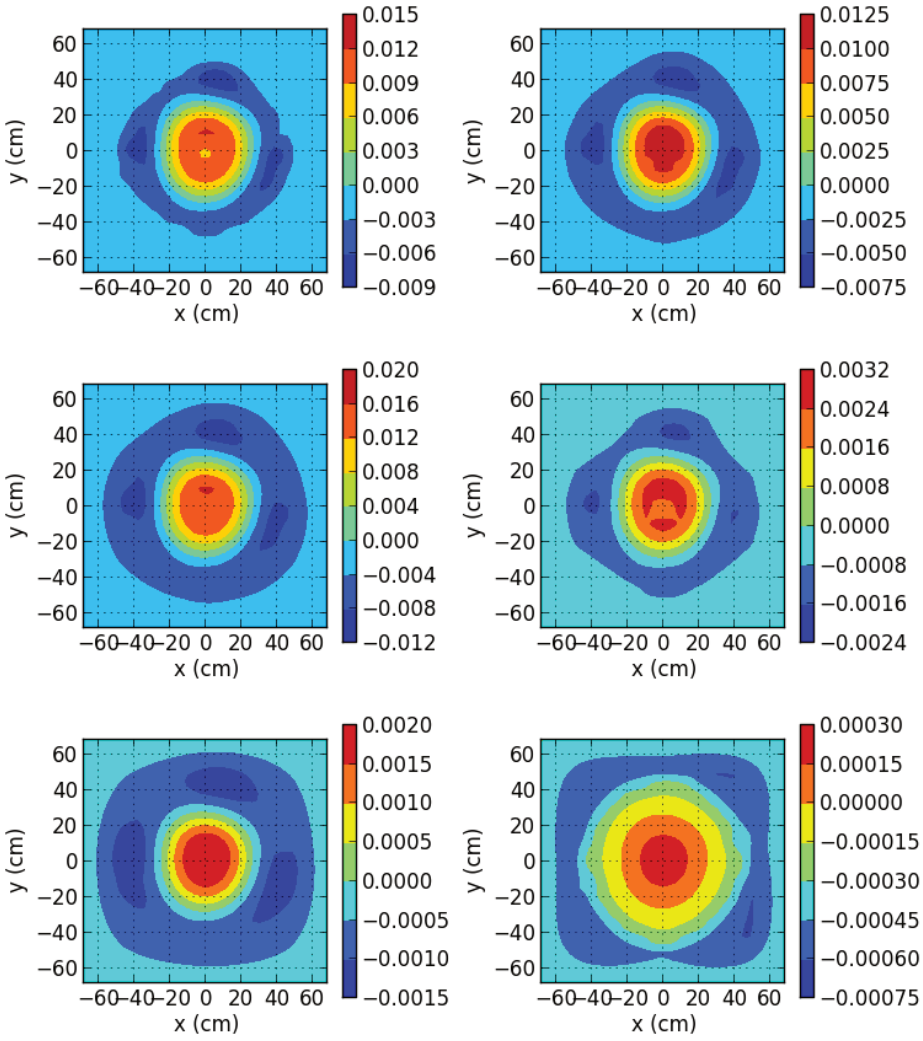

Figure 3.14: XY (Z=0) and Z (X=Y=0) plots of the 9th eigenfunction for each energy group of the VENUS-F model of the SC1 (with CRs out) configuration, from the highest (top left) to the lowest (bottom right) energy level.

Analysis of the SCF for the PNS area and ISJ technique

The modal analysis approach is interesting to understand the reactor physics behind important modes contributing to the SCFs for experimental techniques. In Fig. 3.15, the SCF for the PNS area method by modal analysis (see eq. (2.34)) is shown for the VENUS-F SC1 configuration for the lowest energy group.

One notices the important role of the 9th mode to SCF_{area}, which provides the shape of the SCF from this mode on. SCF remains unity along the X-axis for the first 8 modes: their amplification factors (see eq. (2.6)) are small. By taking into account only 9 modes, SCF_{area}=1 is found at about 20-25 cm from the centre of the core (depending on the energy group), i.e. the zero crossing of the latter mode for the concerned energy group.

Other higher modes obtaining their maximum at the centre of the core are also contributing significantly to the SCF shape. Also these modes have zero crossings at a radius of about 20-25 cm from the centre of the core. Therefore, the location with correction factor equal to unity remains almost unchanged at about a radius of 20-25 cm from the centre of the core with increasing number of modes contributing.

Moreover, the contribution of the higher modes to the SCF is reduced by the numerator correction factor $\frac{k_n(1-k_1)}{k_1(1-k_n)}$ and the denominator factor $(\frac{k_n(1-k_1)}{k_1(1-k_n)})^2$ in eq. (2.34), as shown for the VENUS-F reactor in Fig. 3.16) for the first 100 modes. Nevertheless, these higher modes are required to approximate the simulated SCF profile further away from the centre of the core, i.e. to adapt SCF_{area} to local perturbations (such as the VENUS-F control rods in this case).

For the ISJ method, almost the same conclusions from modal analysis as for the PNS area method can be made, as expected in § 2.2.4 and eq. (2.44). As for SCF_{area}, the strongly amplified modes - i.e. the modes with a high $P_n(0)$ - contribute significantly to the SCF_{ISJ}. The 9th mode is the first mode (different from the fundamental one) with a high $P_n(0)$ value.

Again, SCF_{ISJ}=1 is found at about 20-25 cm from the centre of the core (depending on the energy group), i.e. the zero crossing of the latter mode for the concerned energy group. Also higher modes with a maximum in the centre of the core exhibit a zero crossing at this location. Therefore, the same conclusions can be made as for the PNS area method. This is confirmed by the simulation results, shown in Fig. 3.8 (bottom).

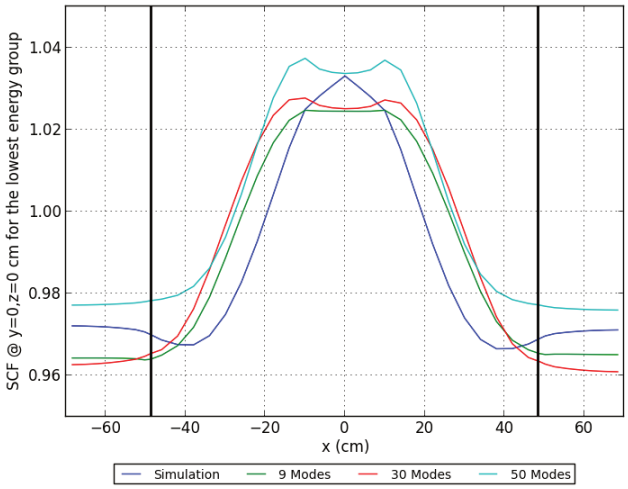

Figure 3.15: SCF for the PNS area method in the VENUS-F SC1 configuration along the X-axis (Y=Z=0), obtained by modal analysis and simulation. The vertical lines indicate the core-reflector interface.

Conclusion for Modal Analysis

For ADS with the neutron source in the centre of the core, the 9th eigenmode is contributing significantly to the full flux solution of ADS with a centre in the source, as it is the first higher mode (i.e. different from the fundamental mode) with a maximum in the centre of the core. Even more important is the contribution of the 9th mode to SCF_{area} (and similar, to SCF_{ISJ}), as the contribution of higher modes to the SCFs is reduced (e.g. by $\frac{k_n(1-k_1)}{k_1(1-k_n)}$ and $(\frac{k_n(1-k_1)}{k_1(1-k_n)})^2$ in eq. (2.34)).

Higher eigenmodes (i.e. higher than the 9th) with a maximum in the centre of the core show also a zero-crossing at about 20-25 cm from the centre of the core (depending on the energy group), i.e. the same location of the 9th eigenmode. Therefore, the boundary between SCF < 1 and SCF > 1 remains unchanged from the 9th eigenmode on (see Fig. 3.15), and can thus be determined by analysing this eigenmode only for VENUS-F. This conclusion is evaluated for less homogeneous configurations in § 4.2.2 (for the MYRRHA power ADS).

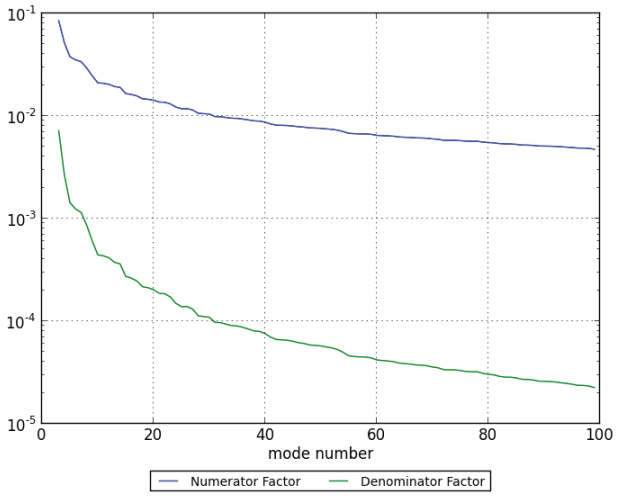

Figure 3.16: Evolution of the numerator and denominator k-factor of eq. (2.34) for the VENUS-F SC1 configuration for 100 modes.

3.2.4 Robustness Checks for the PNS Area Methods

In this section, two robustness checks for start-up reactivity monitoring are performed: the choice of detector type and the change in SCF_{area} during core loading.

Detector Type Choice

In § 3.2.1, the experimental PNS and ISJ results are shown for U-235 detectors on VENUS-F. The simulated SCFs are validated by experimental results in the lowest energy group. In order to study the effect of the detector type, the SCF for the PNS area method is shown in Fig. 3.17 for each energy group of the VENUS-F SC1 configuration model.

Due to the high energetic neutron source, the SCF_{area} is the highest in the first energy group for both methods. The shape of the 9th eigenfunction is similar for all energy groups (see Fig. 3.14), but the zero crossing radius of the mode differs. As a consequence, the position on the X-axis where SCF_{area}=1 shifts from 20 cm for group 6 to 37 cm for group 1. The absolute reactivity level in the reflector is quasi independent on the neutron energy group. The same energy dependence is found for SCF_{ISJ}.

It is important to notice that this model does not include local thermalising elements, which are present around the VENUS-F reactor. As shown in Fig. 3.8, the PNS results are affected by these effects. One may assume that these elements do not perturb SCF_{area} for higher energy groups (e.g. threshold detectors). This statement can only be evaluated by simulations of the PNS method in probabilistic codes that can take into account local perturbations. That research falls out of the scope of this work.

As a conclusion, the choice of the outer reflector is reconfirmed for reactivity monitoring during start-up. SCF_{area}<1 and does not differ from 0.96-0.97 depending on the detector type. Threshold detectors could be more robust against local thermalising elements. This issue is studied more in detail in chapter 4 for power ADS.

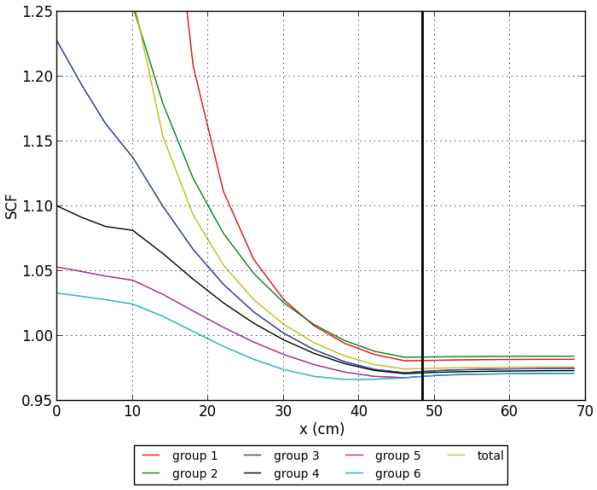

Figure 3.17: Simulated SCFs for the PNS area method across the X-axis (Y=Z=0) in the centre plane of the VENUS-F SC1 configuration for the different energy groups of the model. The vertical line indicates the core-reflector interface.

Subcriticality Level

In this paragraph SCF_{area} is studied for the SC1 (see Fig. 3.2), SC4 (see Fig. 3.3), SC5 and SC6 (see Fig. 3.18) VENUS-F configurations. These states have different subcriticality levels, varying from k_{eff}=0.751 to k_{eff}=0.961, as indicated in Table

3.2. Fuel assemblies are symmetrically placed around the middle of the VENUS-F core to obtain these configurations.

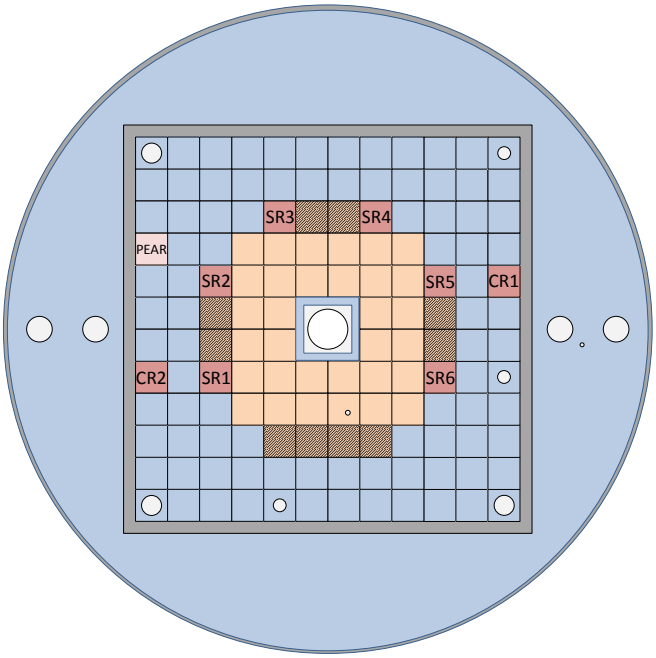

Figure 3.18: Set-up of the VENUS-F subcritical SC5 and SC6 configuration at middle height (orange - fuel, blue - lead, grey - stainless steel, SR - safety rod, CR - control rod, PEAR - experimental PEllet Absorber Rod). The shaded fuel assemblies should be replaced by lead assemblies in the SC5 configuration to obtain the SC6 state.

Fig. 3.19 shows the SCFs of the considered configurations along the X-axis of the VENUS-F reactor, for the thermal energy group (in case the same detectors are used as for the SC1 experiments), as well as for the integrated flux. The same SCF profiles are noticed for different subcriticality levels, although the SCF_{area}=1 crossing is getting closer to the reactor centre (for the integrated flux) with decreasing level of subcriticality. This effect originates from the difference in zero crossing of the 9th eigenmode (see § 3.2.3).

For the SC4-SC6 configurations, SCF_{area}<1 everywhere in the reactor for the thermal detector. In general, the SCFs approach unity with increasing subcriticality level: the higher k_{eff}, the less (safety) margin in underestimation of the

Name	k_{eff}	Number of FAs	Fig.
SC1	0.961	93	3.2
SC4	0.885	64	3.3
SC5	0.821	48	3.18
SC6	0.751	38	3.18

Table 3.2: Calculated subcriticality levels, number of FAs (including the ones in the SRs) and description reference for the different VENUS-F configurations used in the simulations for start-up reactivity monitoring.

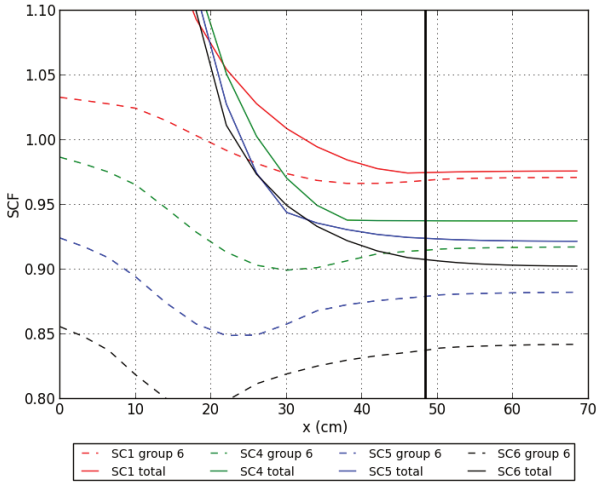

Figure 3.19: Simulated SCFs for the PNS area method across the X-axis (Y=Z=0) in the centre plane of the VENUS-F reactor for different subcritical configurations: SC1, SC4, SC5 and SC6. The vertical line indicates the core-reflector interface.

absolute reactivity level.

As a conclusion we notice a large variation in SCF_{area} in the outer reflector for the different levels of subcriticality. A maximum (safe) underestimation of the absolute reactivity level of 16 % is obtained by the thermal detector in the SC6 configuration (i.e. 5305 pcm on an absolute level of 33156 pcm). The closer to criticality, the smaller the underestimation. This overconservative effect should be taken into account for ADS core loading procedures.

3.2.5 Conclusion for Start-up Reactivity Monitoring

The two selected candidates for start-up reactivity monitoring, the PNS area and ISJ method, are investigated in this section on VENUS-F. Simulations are modally analysed to understand the behaviour of the SCFs, and validated by experimental data.

The ISJ experimental count rates suffer from low statistics and the experiment is difficult to reproduce, which makes it not applicable for low flux machines (such as VENUS-F) or deep subcritical states. Also the uncertainty on the delayed neutron data influences the uncertainty of the ISJ results. From this viewpoint, the PNS area method is more robust than the ISJ method, and will be selected as start-up reactivity monitoring method. Moreover, the experiment is reproducible, so statistics depend on the measurement time.

For the PNS area method, special attention should be paid to local thermalising elements affecting the VENUS-F experimental results (in the reflector). This disadvantage, however, is supposed to disappear when using threshold detectors.

The SCFs of the PNS area method and ISJ method are simulated by DALTON for different configurations. Simulations are in agreement with the experimental results, except for 2 detectors in the outer reflector, where the PNS area results are influenced by local thermalising elements. The simulated SCF behaviour is similar for both methods and confirmed by modal analysis.

The SCF for both methods equals unity around a radius varying from 20 to 25 cm from the centre of the core, depending on the detector type. This distance corresponds to the zero crossing of the first higher harmonics with a maximum in the centre of the core (i.e. the 9th mode). Studying the 9th eigenmode allows thus to identify the boundary for a safe SCF.

A safe overestimation of the absolute reactivity level is found in the reflector (SCF < 1), whereas getting closer to the centre of the core, an (unsafe) underestimation of the reactivity is found. In the reflector, SCF_{area}=0.96-0.97, which means that e.g. for the DALTON simulations, $|\rho_{area}|$ is 111-148 pcm higher than $|\rho_{ref}|$= 3709 pcm. Therefore, the reflector zone is considered as the recommended location for detector positioning, moreover the SCF gradient is small in this zone (except from the thermalising elements in this zone when using thermal detectors).

When decreasing the subcriticality level during start-up, the (safe) overestimation of the reactivity level in the VENUS-F reflector decreases. The SCF, however,

stays smaller than unity. This conservative effect is the highest in the lowest energy group, but also for the highest energy group, the SCF for the VENUS-F SC1 configuration remains smaller than unity.

3.3 Subcriticality Monitoring during Operation

For a power ADS such as MYRRHA (see § 1.5.2), no (long) beam interruptions are allowed during normal operation from the moment 1 % of nominal power is obtained. Therefore, the continuous Current-to-Flux (CTF) monitor is candidate to monitor (changes in) reactivity during operation of an ADS (see § 1.3.8).

By measuring the ratio of source neutrons to count rates from detectors in the reactor, the reactivity is monitored, according to equation (1.14). The evolution of c, the CTF proportionality coefficient, needs to be investigated during ADS operation, in order to identify the need for interim reactivity cross-checking (and re-calibration of c).

Changes in reactivity in ADS can be global (e.g. burn-up) or local (e.g. control rod ejection). As there is no significant burn-up of the VENUS-F fuel, a control rod variation case study is made in this chapter in order to understand the monitoring of local perturbations. More CTF applications during normal ADS operation and incident conditions are studied for power ADS in § 4.3 and 4.4.

In this section, the case study will be validated by experimental data from VENUS-F. Moreover, SCFs for this experiment will be simulated (with $\Sigma_d(E)$=1) for the complete VENUS-F core, and assessed by modal analysis. Detector types and positions for robust reactivity monitoring during this experiment are investigated.

3.3.1 Case Study Experimental Results - VENUS-F Control Rod Worth Estimation

For the rod worth experiment, the control rods CR1 and CR2 (with B_4C poison) are introduced in the VENUS-F SC1 configuration (as shown in Fig. 3.2, described in § 1.5.3), driven by a constant beam of about 400 μA (corresponding to a source of about 10^{10} n/s).

The source neutron monitoring on VENUS-F (for the CTF technique) is explained in [Billebaud et al., 2010] and [Uyttenhove and Krasa, 2013]. These neutrons should be measured for the CTF monitoring on VENUS-F, rather than

the beam current. Indeed, due to target consumption, beam positioning etc., the number of neutrons produced per unit of current is not constant.

The source neutron monitoring is performed by registration of the α-particles created during the D-T fusion reaction in addition to the 14 MeV source neutron. Also the parasitic D-D reaction should be taken into account. During this reaction there is a 50 % chance to make a 2-3 MeV neutron and a He-3 atom. The other half of the reactions leads to a proton and a T atom. Therefore, the parasitic source neutrons are measured by measuring the protons. The parasitic source neutrons have a (slightly) different angular distribution, therefore the ratio of D-T neutrons to D-D neutrons should be constant in order to assure consistent CTF monitoring.

The study of the source neutron monitoring is ongoing. For the case study performed in this work, the runs are performed under constant source neutron production. The absolute source neutron production is not precisely known, but not needed. More important is the need for a constant neutron source production to avoid changes in the CTF proportionality coefficient c in eq. (1.14) due to changing source neutron specifications.

The detectors in the reactor are shown in Table 3.1. The control rods are positioned at 600 mm (completely out of the core) and at 0 mm (fully inserted). The count rates are measured in both positions with a sampling time of 1 s.

$SCF_{CTF,exp}$, defined in eq. (2.54), is determined by scaling the ratio of the detector count rates in the two states to the ratio of the reference reactivities in both states. As reference (experimental) reactivity values, -5.06 ± 0.13 \$ is taken for the SC1 configuration with CRs up, and -6.25 ± 0.13 \$ for the SC1 configuration with fully inserted CRs [Lecouey et al., 2015b; Lecouey, 2014]. Therefore, $\frac{\rho'_{ref,exp}}{\rho_{ref,exp}}$=1.24 ± 0.04.

The $SCF_{CTF,exp}$ for the detectors in the VENUS-F reactor is shown in Fig. 3.20, varying from 0.987 to 1.132. If $SCF_{CTF,exp} < 1$, then $\frac{\rho'_{CTF,exp}}{\rho_{CTF,exp}} < \frac{\rho'_{ref,exp}}{\rho_{ref,exp}}$, and thus the control rod worth is (safely) underestimated. E.g. for $SCF_{CTF,exp}$=0.987 (detector 8), $\rho'_{CTF,exp}$=-6.19 ± 0.18 \$, a safe underestimation of the true value of -6.25 ± 0.13 \$[4].

Close to the perturbation (detectors 7, and in less extent 2 and 3) the control

[4]The major part of the uncertainty on both reactivity values is due to the reference reactivity uncertainty, applied to determine both $\rho'_{ref,exp}$ and $\rho'_{CTF,exp}$. This is a systematic error, therefore we can make the conclusion about underestimation.

rod worth is overestimated ($SCF_{CTF,exp} > 1$), whereas for detectors 1, 5, 8 and 9, less than 1 % discrepancy from the reference value is found. To understand these results, simulations and modal analysis will be applied in the next sections.

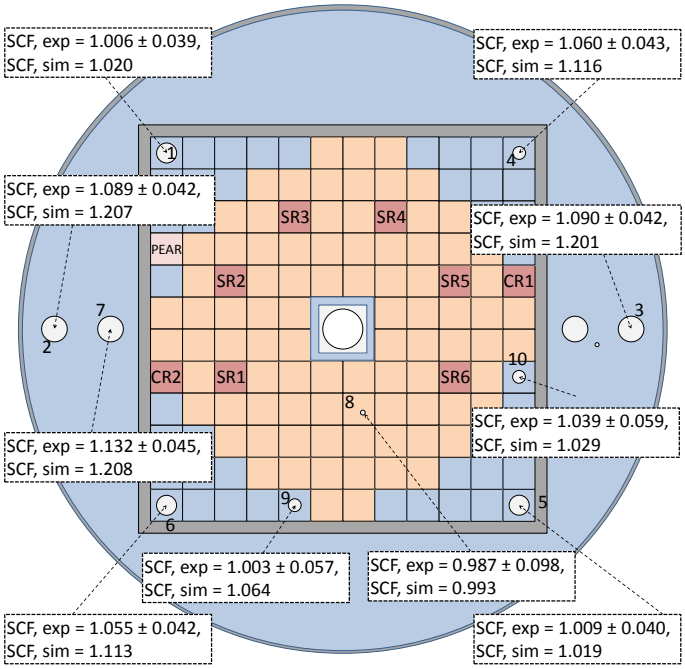

Figure 3.20: SCFs of the CTF monitoring of the CRs worth of the VENUS-F SC1 configuration at different detector locations.

3.3.2 Validation of the Experiment Simulations

In this section, the DALTON code (see § 2.6) is used to simulate the CTF case study above. The related XYZ model for the DALTON code is described in App. A, and 6 energy groups (representative for the VENUS-F spectrum and applied detectors) are chosen to perform the calculations. In order to determine SCF_{CTF} by simulation, the reference reactivities are obtained via the fundamental eigenmode calculation, whereas fixed source calculations are performed to determine the fluxes at the different detector positions.

The simulated SCF_{CTF} for the monitoring of the control rod drop experiment are presented in Fig. 3.21 through the complete VENUS-F reactor, by 2D plots

at different heights above the centre of the core. One notices almost everywhere inside the reactor $SCF_{CTF} > 1$, i.e. an (unsafe) overestimation of the control rod worth. Only inside a quasi-sphere of 20 cm around the centre of the core, the control rod worth is underestimated. Close to the perturbations (i.e. the control rods) high values of SCF_{CTF} are found. The effect of the VENUS-F bunker (see § 3.2.2) on this experiment is not relevant, as two static states of the VENUS-F reactor are compared, with the same systematic error from the bunker.

When comparing the experimental results to the ones obtained by simulations (see also Fig. 3.20), one notices the same tendencies in SCF_{CTF}. Absolute numbers, however, differ significantly. The SCFs obtained by simulations turn out to be systematically higher than the experimental values (except for detector 10), especially closer to the perturbation (detectors 2, 3, 6 and 7). This can be due to the limitations of diffusion theory to model local perturbations. The experimental control rod worth is 861 ± 28 pcm, whereas DALTON only finds 802 pcm.

3.3.3 Interpretation by Modal Analysis

Modal analysis is applied to understand the behaviour of SCF_{CTF}. The modal expression for SCF_{CTF}, provided by eq. (2.54), is shown in Fig. 3.22 and compared to the simulation results for the lowest energy group. The interpretation is more complex for this experiment than for absolute reactivity measurement techniques such as the PNS area method, as two reactivity states are compared.

In the centre of the core, the modal SCF_{CTF} is almost identical to the simulated one for the case of one mode. This effect appears due to the small difference in amplification of the fundamental mode between the original and the perturbed state to obtain the full flux (see eq. (2.6)), given the small change in k_{eff} between the two states.

A slightly asymmetrical profile of SCF_{CTF} is found at the core-reflector interface, because of the asymmetrical position of the control rods around the X-axis. Much more modes are needed to approach the simulated SCF_{CTF} in that region, as modes with local maxima at those zones will be amplified. These modes affect also the SCF_{CTF} in the centre of the core.

Being the first higher mode with a maximum in the centre of the core, the 9th mode is again important as lower order modes (high $\frac{\rho_1}{\rho_n}$) with centre in the core are strongly amplified (high $\frac{S_n}{S_1}$). $SCF_{CTF} = 1$ is found around the zero crossing of the 9th mode, which is almost identical for the original and perturbed state.

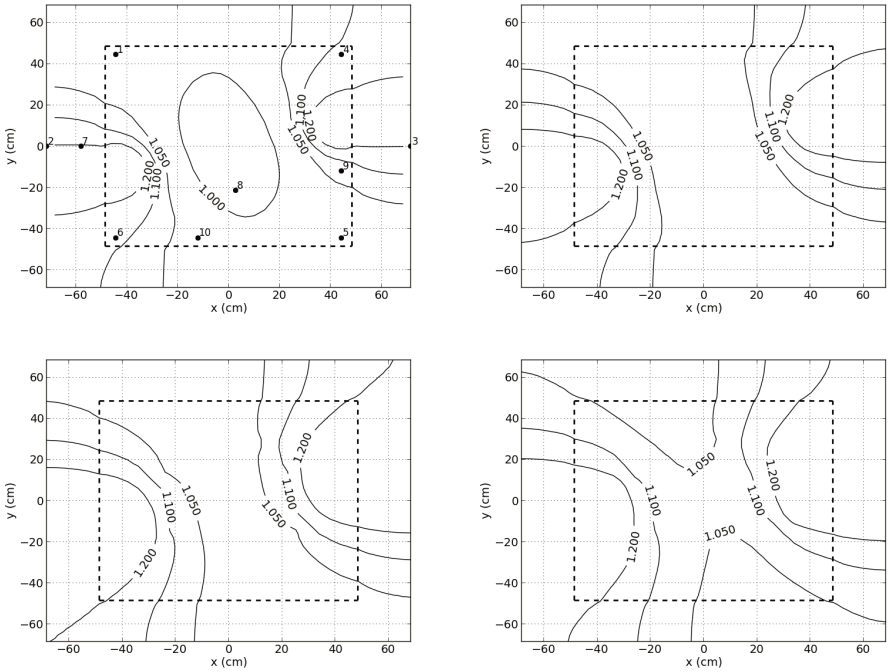

Figure 3.21: Simulated CTF SCF for the lowest energy group (i.e. group 6) at different heights in the VENUS-F SC1 configuration: 0 cm (center of the core), 20 cm (fuel), 39 cm (top reflector) and 59 cm (top reflector). Contour lines are indicated from 0.95 to 1.2. The dashed line corresponds to the boundary of the 12x12 grid in which the assemblies are loaded, indicated in grey in Fig. 3.2. The detector positions are indicated on the picture at centre height.

3.3.4 Robustness Check on Energy Dependence

In § 3.3.2, $SCF_{CTF,exp}$ results for the concerned case study are shown for U-235 detectors available in the VENUS-F reactor. The experimental results are therefore validated by simulations in the lowest energy group. In order to study the effect of the detector type, the simulated SCF_{CTF} is shown in Fig. 3.23 for each energy group (as defined in Appendix A) of the VENUS-F SC1 model.

Due to the presence of the source neutrons in the first energy group, SCF_{CTF} is smaller for the first energy group in the centre of the core than for the other energy groups. Indeed, given the lower k_{eff} level in the perturbed state (indicated

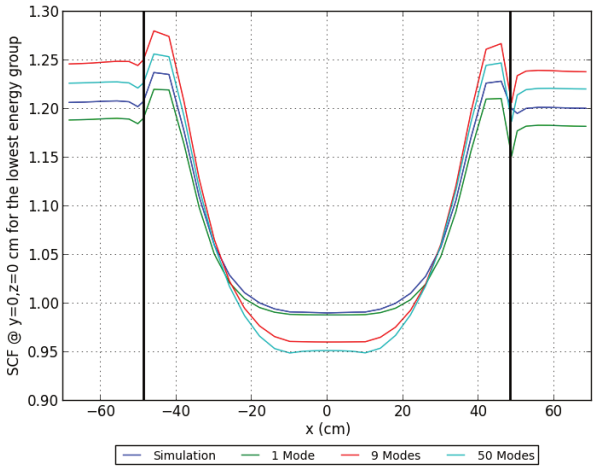

Figure 3.22: SCF for the CTF case study experiment in the VENUS-F SC1 configuration along the X-axis (Y=Z=0), obtained by modal analysis and simulation for the lowest energy group. The vertical lines indicate the core-reflector interface.

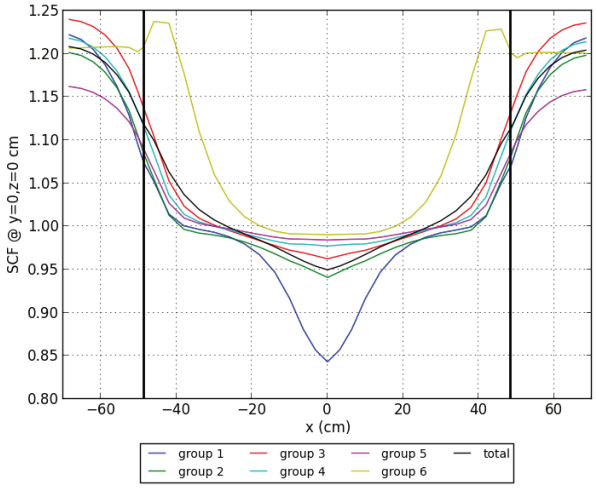

Figure 3.23: SCF for the CTF case study experiment in the VENUS-F SC1 configuration along the X-axis (Y=Z=0), for different energy groups, obtained by simulation. The vertical lines indicate the core-reflector interface.

with prime), the contribution of the source neutrons is more important in this state, leading to SCF_{CTF} differing from unity for the highest energy groups in the centre of the core.

The location where SCF_{CTF}=1 shifts from 20 cm for group 6 to almost 40 cm for group 1 on the X-axis. It is also important to notice the specific profile of the lowest energy group. This profile is due to local thermalising elements, such as the VENUS-F control rods (at the core-reflector interface on the X-axis). One can assume that these effects will less affect the SCFs with increasing energy groups. Therefore, the higher energy groups seem more robust, showing smaller gradients in SCF_{CTF}. This statement can only be evaluated by simulations in detailed models with probabilistic codes, which falls out of the scope of this work.

3.3.5 Conclusion and Outlook

In this section, the control rod drop case study experiment in the VENUS-F SC1 configuration is performed in order to understand the SCF_{CTF} for reactivity monitoring. For a decrease in reactivity (e.g. in this case a local rod drop), an (unsafe) overestimation of the decrease ($SCF_{CTF} > 1$) is obtained in the reflector zone and close to the perturbation. The SCF_{CTF} for this experiment is close to unity in the centre of the core. The U-235 detectors used in this experiment are more sensible for the concerned experiment because of the B_4C in the control rods, which causes a broader zone with $SCF_{CTF} > 1$.

Qualitative agreement is found between experimental results and simulations, although the DALTON diffusion code is not able to simulate SCF_{CTF} for this experiment quantitatively correct. The simulations overestimate the experimental results. For accurate SCF_{CTF} values, probabilistic transport codes are needed to assess local perturbations. Modal analysis enhances the understanding of the global behaviour of the SCF_{CTF} through the subcritical reactor.

The final aim of the current-to-flux monitor is to track global and local perturbations in the core, causing changes in reactivity, for operational and safety reasons. Only one case study with a local perturbation is examined in this section. More research in this field is performed in the next chapter, where reactivity monitoring will be assessed for a power ADS, with probabilistic codes. Therefore, in this chapter, no conclusions on reactivity monitoring are made.

3.4 Interim Reactivity Cross-Checking Techniques

During normal operation, an interim cross-checking of the CTF reactivity monitor can be required, as explained in § 3.3. The (beam interruption) source jerk (SJ) technique (presented in § 1.3.2) is selected in § 1.3.8 as interim reactivity cross-checking technique. Thanks to experimental results from the VENUS-F ADS, the choice of the beam interruption frequency and period is assessed in this chapter, simulated SCFs (as defined in eq. (2.61) with $\Sigma_d(E)$=1) are evaluated and analysed, and robust detector types and positions are determined.

3.4.1 Source Jerk Experiments in VENUS-F Subcritical Configurations

Several (beam interruption) SJ experiments are carried out in various VENUS-F configurations with different subcriticality levels and varying core heterogeneity, as presented in [Chevret et al., 2014; Chevret, 2014b], in order to test the robustness of this method. In this section, only the source jerk experiment results from the standard SC1 configuration (see Fig. 3.2) are evaluated, as this is the standard state at the foreseen operational k_{eff} level of an ADS. The detectors in this reactor are identical to the ones used for the PNS experiment (see Table 3.1).

For the SJ experiments described in this section, the continuous beam of 400 μA is interrupted for 2 ms every 25 ms (i.e. a frequency of 40 Hz), and corrected with a stability factor to compensate for the instability of the beam after the interruption (see [Chevret et al., 2014]). Due to the low flux of the VENUS-F ADS, about 10^5 beam interruptions are needed to obtain sufficient statistics on the count rates. Similar to the PNS experiments from § 3.2, the alternative pathway as described in § 3.1 provides a reference reactivity of -5.06 ± 0.13 $ [Lecouey et al., 2015b; Lecouey, 2014] (CRs at 600 mm). This reference level allows an evaluation of SCF_{SJ}, defined by eq. (2.61).

Experimental SCF_{SJ} in the VENUS-F SC1 configuration, from [Chevret et al., 2014], are shown in Fig. 3.4, and compared to the PNS method results from § 3.2. Similar to the PNS method, the reference reactivity uncertainty is contributing significantly to the total uncertainty on the SJ results. The results obtained by both techniques underestimate the absolute reactivity level (i.e. SCF < 1) in the (inner and outer) reflector zone, which is safe. For detector 8 inside the fuel, both PNS and SJ results match the reference reactivity value. The SCF_{SJ} for detector 2, 3 and 7 are the smallest, due to global and local thermalising elements [Chevret,

2014a]. This effect is even stronger for the SJ technique than for the PNS area method.

The obtained experimental SCF_{SJ} are successfully validated against precise MCNP simulations in [Chevret et al., 2014]). This work aims to simulate and understand the spatial behaviour of the SJ technique through the complete subcritical reactor. This analysis is performed in the next paragraph.

3.4.2 Validation of Experiment Simulations

In this section, the SJ experiment is again simulated with the DALTON diffusion code (see § 2.6). The related XYZ model for the DALTON code is described in and App. A, and 6 energy groups (representative for the VENUS-F spectrum and applied detectors) are chosen to perform the calculations. For a consistent evaluation of the SCF, the experiment simulation results from DALTON are scaled on a reference k_{eff} obtained via an eigenmode calculation in DALTON, using the same calculation model. Thanks to this approach, SCF_{SJ} for this experiment is determined through the complete reactor, and evaluated by experimental results from the VENUS-F SC1 configuration.

For the SJ experiment simulation, the decay of the full flux in the first 500 µs after beam stop is simulated. Different decay shapes are found throughout the reactor for the lowest energy group (representative for the U-235 detectors used for the VENUS-F experiments), as shown in Fig. 3.24 (with $\Sigma_d(E)$). For the SJ experiment the bunker has a clear influence on the decay shape of the lowest energy flux in the outer reflector.

Similar to the PNS area method, thermalising elements (not modeled in DALTON) can affect the SJ evaluation method for VENUS-F. As shown in Fig. 3 of [Chevret et al., 2014], not all prompt neutron chains have died out in one detector in the outer reflector at the end of the beam interruption, affecting the measurement results of the SJ technique (because of an erroneous determination of $n(1)$ in eq. (1.12)). Therefore, the use of threshold detectors (or a longer beam interruption time) can help solving this issue.

Fig. 3.25 shows the behaviour of the simulated SCF_{SJ} through the complete VENUS-F reactor (without bunker), by 2D plots at different heights above the centre of the core. The behaviour of SCF_{SJ} is almost symmetrical to the centre plane of the VENUS-F SC1 configuration. $SCF_{SJ} > 1$, an (unsafe) overestimation of the subcriticality level, is found inside a sphere of about 20 cm from the centre of

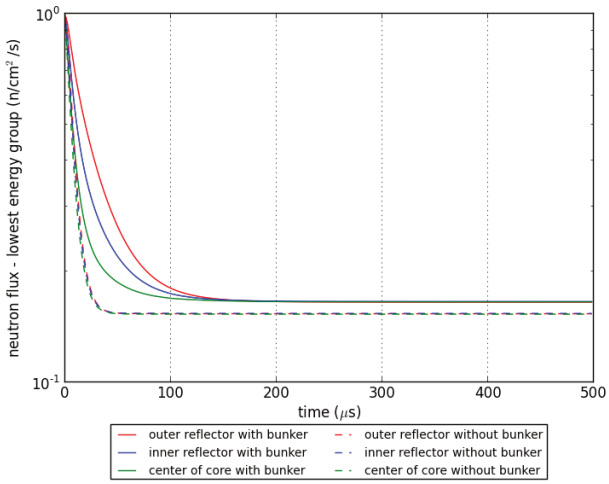

Figure 3.24: Simulated source jerk responses in the lowest energy group (i.e. group 6) at different locations in the centre plane of the VENUS-F SC1 configuration (Y=Z=0). The flux level is normalised to the full flux before the beam interruption in the concerned energy group.

the core. In the midplane, a symmetrical SCF profile is also found. In the reflector, the reactivity is (safely) underestimated by 3-4 %. The SCF results are similar to the ones of the PNS method (see Fig. 3.7). This is a logical effect, as the SJ technique is the inverse of the PNS technique.

SCF_{SJ} simulated and experimental values are shown in Fig. 3.26. For the clarity of the figure, radial symmetry is supposed, justified by the SCF profiles at different heights in Fig. 3.25. Therefore, the location of the detectors on the X-axis on Fig. 3.26 corresponds to their radial distance to the centre of the core. Similar to the PNS area experimental results, good agreement is found in the fuel and inner reflector zone. In the outer reflector zone, local external thermalising elements not included in the DALTON model affect the agreement between calculations and experiment (even stronger than for the PNS method, see top Fig. 3.8).

3.4.3 Modal Analysis of the Spatial Correction Factor

The modal analysis of the SCF formula for the SJ method (eq. (2.70)) and the PNS area method (eq. (2.34)) is similar. The same conclusions are made for the SJ

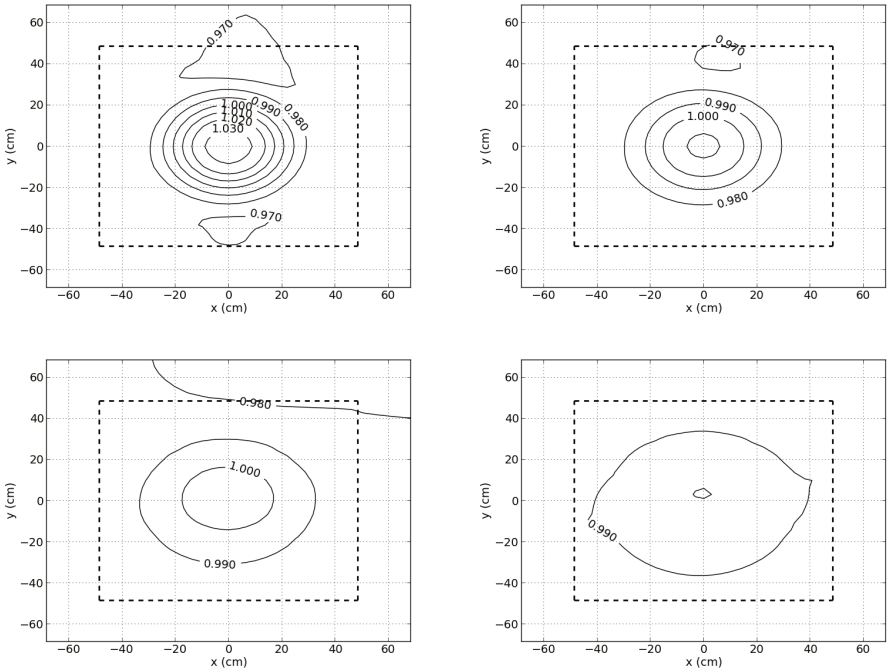

Figure 3.25: Simulated SJ SCF for the lowest energy group (i.e. group 6) at different heights in the VENUS-F SC1 configuration: 0 cm (center of the core), 20 cm (fuel), 39 cm (top reflector) and 59 cm (top reflector). The dashed line corresponds to the boundary of the 12x12 grid in which the assemblies are loaded, indicated in grey in Fig. 3.2.

method as for the area method in § 3.2.3.

3.4.4 Conclusion and Outlook

The SJ method is investigated for interim reactivity cross-checking in this section. The beam interruption experiment is simulated, analysed and validated by experimental data for the VENUS-F SC1 configuration. The spatial dependence for this method is similar to one for the PNS method, which allows a fixed detector positioning for absolute reactivity measurements during start-up and operation of a zero-power ADS.

Again, a safe overestimation of the reactivity level is found in the reflector ($SCF_{SJ} < 1$). For the SJ experiments in the VENUS-F SC1 configuration, around 10^5 beam

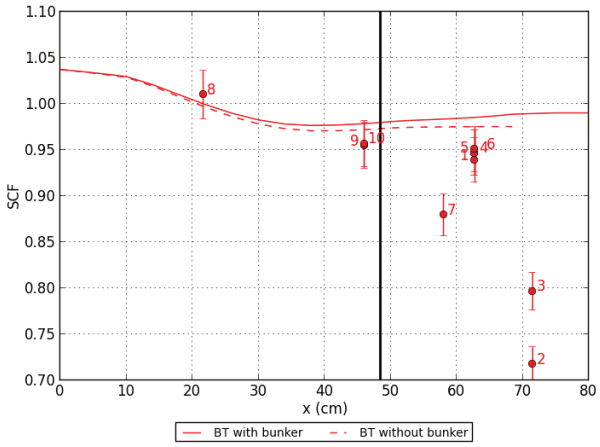

Figure 3.26: Simulated SJ SCF (line) and measurement results (dots) across the X-axis in the centre plane of the VENUS-F SC1 configuration (Y=Z=0). As the detector locations are not on the X-axis, the corresponding radius to the centre of the core is shown in this figure. The vertical line indicates the core-reflector interface.

interruptions are needed to obtain sufficient statistics on the reactivity level, which takes about 500 s. For a power ADS with a higher flux level, less beam interruptions could be needed, but special attention should be paid to thermalising elements. This issue is discussed in § 4.3.5.

3.5 Conclusion and Outlook

In this chapter, the theoretical analysis from Chapter 2 of the spatial correction for the candidate reactivity measurement techniques is validated by experimental results from the VENUS-F zero-power facility. First, the results from a 'reference' subcritical state are presented, obtained via an alternative methodology, which allows the validation of the candidate subcriticality measurement techniques.

Concerning start-up of ADS, the PNS area method is selected, rather than the ISJ method, which shows the same spatial dependence but with higher uncertainties. Thanks to the repetitive character of the PNS area method, better statistics are gained at low flux levels or deep subcritical levels than for the ISJ method. Moreover, the uncertainty on the ISJ method always comprises the uncertainty

on the delayed neutron parameters.

Global agreement between experiments and simulations is found for the PNS area method. The reflector zone is the recommended location for detector positioning during VENUS-F start-up: a robust, safe overestimation ($SCF_{area} < 1$) is found for the different subcriticality levels, and the gradient of SCF_{area} is small. For the VENUS-F SC1 configuration, the simulated SCF_{area}=0.96-0.97, therefore the simulated $|\rho_{area}|$ is 111-148 pcm higher than $|\rho_{ref}| = 3709$ pcm. Modal analysis allows, via the study of the 9th eigenmode, the identification of the boundary between $SCF_{area} > 1$ and $SCF_{area} < 1$.

For interim cross-checking of the reactivity, the same spatial dependence is found for the SJ technique as for the PNS area method, which allows the use of the same detector locations for start-up reactivity measurements as for interim reactivity cross-checking.

The SCF of both methods are sensitive to (local and global) thermalising elements, not modelled in detail in the DALTON diffusion code models. For the SJ technique, they imply a longer beam interruption time, which could cause unacceptable thermal stresses in power ADS. To avoid this issue, the use of threshold detectors is recommended for these techniques.

ADS reactivity monitoring during operation is performed by means of the Current-to-Flux (CTF) technique. The CTF monitor aims to detect sudden changes in reactivity (due to local perturbations) for safety purposes, and the follow-up of burn-up, a global reactivity change, for operational purposes. Unfortunately, the DALTON diffusion code is not able to model quantitatively correctly the local reactivity changes. The trends in SCF_{CTF} for monitoring local perturbations are however clear, and are investigated for the control rod drop case study experiment in the VENUS-F SC1 configuration. The control rod worth in the SC1 state is (unsafely) overestimated in almost the complete reactor ($SCF_{CTF} > 1$), except in the centre of the core.

More insight into reactivity monitoring on ADS will be gained in the next chapter. Then the follow-up of burn-up in the core of a power ADS will be monitored, and local perturbations will be simulated, in order to identify and quantify incident scenarios. This will be done by means of a probabilistic transport code, able to overcome the limitations of diffusion theory and deterministic codes.

4

SUBCRITICALITY MONITORING IN A POWER ADS

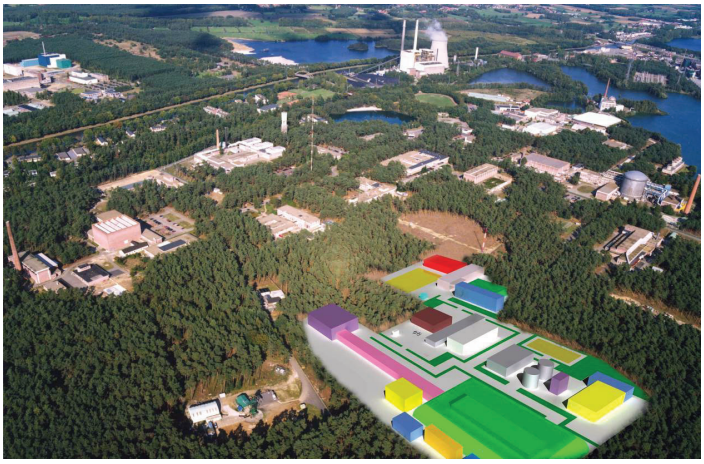

Everything should be made as simple as possible, but not one bit simpler.

Albert Einstein

Picture: The MYRRHA facility at the SCK•CEN site.

MYRRHA is the major ongoing power ADS project in Europe. In this chapter, the MYRRHA reactor will serve as an example of a power ADS to develop a detector positioning strategy for subcriticality monitoring. The development of this strategy is based on the theoretical understanding about the spatial dependence of reactivity measurements in ADS from Chapter 2, applied to the selected subcriticality measurement techniques from § 1.3.8. As an outcome of this work, the subcriticality monitoring conclusions from the zero-power VENUS-F ADS (see § 3.5) are extended to MYRRHA.

First, the PNS technique is simulated as a start-up technique. Then, the Current-to-Flux (CTF) monitor is assessed as a relative monitoring technique during the operational phases of an ADS. The need for recalibration by the source jerk interim cross-checking technique is discussed.

In order to investigate the robustness of the proposed detector positioning strategy, the combination of detector types and signals is considered for the reactivity monitoring methodology. Moreover, several hypothetical (reactivity) incident scenarios are simulated to study how they can be detected by the reactivity monitor.

4.1 Selected MYRRHA Subcritical Cores for Reactivity Monitoring

4.1.1 MYRRHA Cores

The general concept of the MYRRHA ADS is presented in § 1.5, as well as a general fuel assembly design. A detailed description and motivation for the design of the MYRRHA subcritical cores is given in Chapter 12 of [Sarotto, 2012] and in [Malambu and Stankovskiy, 2012]. In this section two typical subcritical MYRRHA-FASTEF cores are presented, used to investigate subcriticality monitoring.

The MYRRHA Beginning-Of-Life Core

The Beginning-Of-Life (BOL) core is the first core that will be loaded after construction of the MYRRHA facility. The core inventory is shown in Fig. 4.1. 58 fresh fuel assemblies with 30 wt. % enriched Pu (including 1.65 wt. % Am) are loaded, in order to obtain a k_{eff} value approximating 0.96 (this value is motivated in § 1.6.1). The core is completed by the spallation target in the central position, 6 satellite In-Pile Sections (IPS) to host experiments, 6 control rods, 38 LBE dummy assemblies and 42 YZrO reflector assemblies at the core boundary.

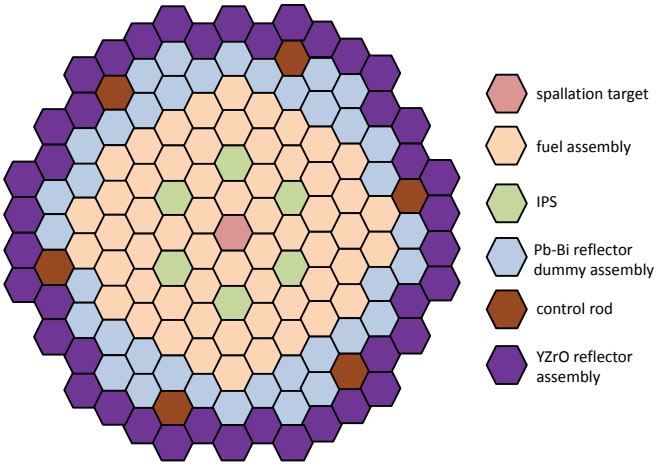

Figure 4.1: MYRRHA-FASTEF subcritical BOL core at middle height [Malambu and Stankovskiy, 2012; Sarotto, 2012].

The first MYRRHA core (BOL) has a calculated k_{eff}=0.965 [Malambu and Stankovskiy, 2012; Sarotto, 2012], decreasing towards k_{eff}=0.948 after 90 days of irradiation (i.e. the cycle duration). After the first cycle, new fuel assemblies will be added step by step, in order to obtain an equilibrium core with a fixed reactivity decrease of about 1500 pcm during the cycle. The evolution of k_{eff} in the transition from the BOL to the equilibrium Beginning-Of-Cycle (BOC) core is shown in Fig. 4.2. About 7 cycles are needed to obtain equilibrium conditions.

The MYRRHA Subcritical Equilibrium Core

The MYRRHA subcritical equilibrium core is presented in Fig. 4.3. The core consists of 72 fuel assemblies, arranged in 6 concentric zones of fuel with different burn-up levels. The equilibrium core has a calculated k_{eff}=0.967 at BOC, decreasing until 0.952 at EOC (End of Cycle). At the end of the cycle, 6 new assemblies are loaded in the second zone. The other zones are reshuffled according to the schedule presented in Fig. 4.4, and the fuel assemblies of zone 5 are discharged.

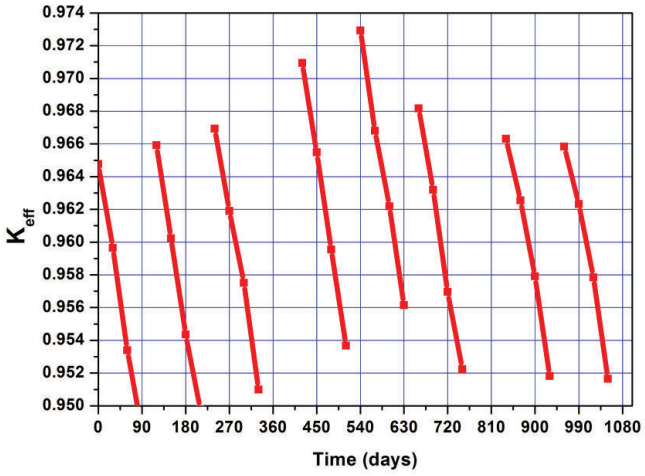

Figure 4.2: Simulated time-evolution of k_{eff} from BOL to BOC (from [Sarotto et al., 2013]).

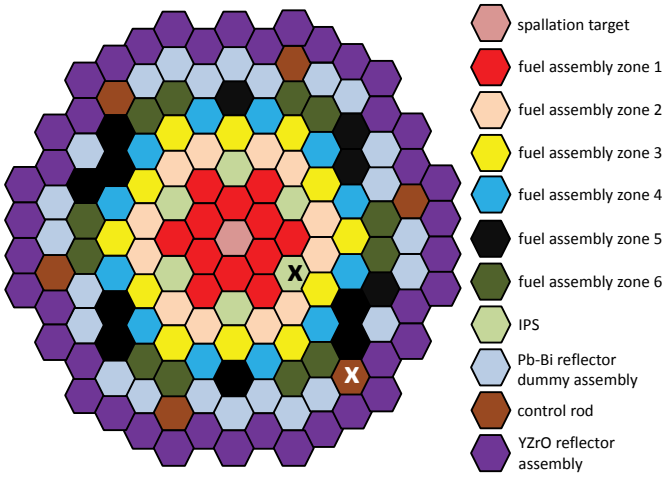

Figure 4.3: MYRRHA-FASTEF subcritical BOC core at middle height [Malambu and Stankovskiy, 2012; Sarotto, 2012]. The assemblies indicated by a cross are used in § 4.4 for incident scenario studies.

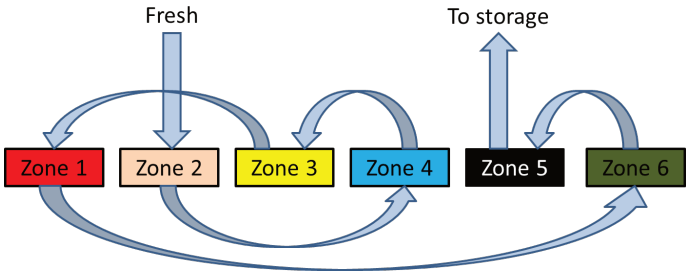

Figure 4.4: Reshuffling scheme of the MYRRHA-FASTEF subcritical equilibrium core.

4.1.2 Case Studies during Normal Operation

In this chapter, the selected subcriticality monitoring techniques from § 1.3.8 are tested for specific power ADS characteristics on the MYRRHA cores. First the PNS area method will be checked as start-up monitoring technique on the Cold Zero Power (CZP) core, i.e. the MYRRHA BOL core from Fig. 4.1 at room temperature.

Beyond the CZP state, no long beam interruptions are allowed any more during normal ADS operation. Only a few long beam interruptions are allowed per MYRRHA cycle, because they cause considerable thermal stresses in the structural materials. The reactivity will be monitored by the Current-to-Flux (CTF) monitor, eventually combined with short beam interruptions for reactivity recalibration. In this work, the need for this recalibration is investigated between three important states in ADS operation:

- during heating up of the core from CZP to Hot Full Power (HFP) on the BOL core (temperature feedback)
- during the reaching of the equilibrium core, i.e. between the BOL and the BOC core (core enlargement)
- during burn-up of an equilibrium core, i.e. between the BOC and EOC equilibrium core (core composition and thus spectrum change)

4.1.3 Calculational Tools and Methods

Two numerical codes are used for the simulation of the selected reactivity measurement techniques for MYRRHA. The DALTON code (see § 2.6.1) is used for the modelling of the PNS area method (see § 2.6.2) for **start-up reactivity monitoring** of the MYRRHA core (see § 4.2). Considering the time-dependent character of the simulations, the use of deterministic codes is recommended to reduce calculational costs. Moreover, as there is only one type of fuel assembly loaded in the core, the analysed MYRRHA BOL core is considered homogeneous (apart from the IPS). This allows the use of a diffusion code to understand the spatial dependence of this experimental technique.

For the **reactivity monitoring during operation** (see § 4.3 and further sections), static simulations are performed to investigate the CTF monitor. Therefore, precise Monte Carlo calculations are performed using MCNP(X) [MCNP Team, 2005; Pelowitz, 2011]. Flux or fission rates in a fixed source subcritical core will be simulated and compared to a reference k_{eff} value. Moreover, a mesh superimposed on the geometry (TMESH card) allows the 3D interpretation of the SCF for the different CTF experiment simulations.

4.2 Subcriticality Monitoring during Start-up

In Chapter 3 the different candidate reactivity monitoring techniques are tested on the VENUS-F ADS. The PNS area method is selected for start-up reactivity monitoring, rather than the ISJ method (see § 3.2.5). The reflector zone turned out to be a suitable detector location (see § 4.6), given the conservative SCF value ($SCF_{area} < 1$) and small spatial gradient of SCF_{area} in this region. In this section the same method will be tested on the MYRRHA BOL core (at CZP) in order to evaluate these conclusions for a power ADS.

4.2.1 Pulse Shapes

Similar to VENUS-F (see § 3.2.2) the PNS technique is simulated in DALTON by introduction of neutron pulses (of 1 μs in the highest neutron energy group) in the centre of the MYRRHA BOL core (see Fig. 4.1). The XYZ DALTON model of the MYRRHA BOL core (k_{eff}=0.97205) is described in App. B, as well as the 6 energy groups structure (representative for the MYRRHA spectrum) to perform the calculations. At steady state, i.e. after build-up of the delayed neutron contribution, the pulse shapes found in the MYRRHA core are shown in Fig. 4.5 at several locations,

for the highest (group 1, representative for threshold detectors) and the lowest energy group (group 6, representative for thermal detectors).

The outer reflector is in this case located outside the MYRRHA core barrel, whereas the inner reflector corresponds to the Pb-Bi and YZrO reflector assemblies (see Fig. 4.1). The centre core location is in the middle of the fuel zone, not at an IPS position.

Compared to the VENUS-F pulse shapes from Fig. 3.6 without bunker, the MYRRHA PNS experiments will need about a 100 μs period (i.e. the time until the prompt neutron chains from the pulse have decayed), twice as long as for VENUS-F. The delayed neutron level of the thermal energy group (indicated by the dashed line) does not vary in the MYRRHA core, whereas this level increases further away from the centre of the core for the VENUS-F pulse shapes. Without taking into account influencing (thermalising) elements outside the reactor, the detector type influence on the PNS pulse shape is slightly smaller for the MYRRHA core than for the VENUS core. The presence of the IPS does not affect the PNS pulse shapes in the core.

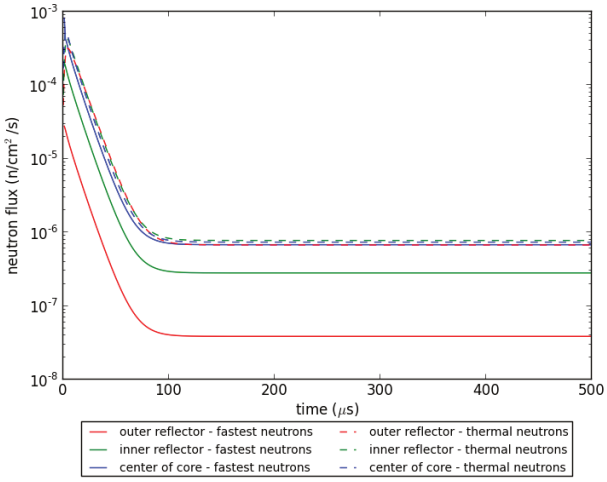

Figure 4.5: Simulated PNS responses for different neutron energies at different locations along the X-axis (Y=Z=0 cm) in the MYRRHA BOL core (at CZP). The flux level corresponds to a unit source strength implemented in the highest energy group during the first time step of 1 μs.

4.2.2 Spatial Correction Factors

The simulated SCF for the area method is shown for the detectors that monitor the six energy groups of the MYRRHA BOL core model (see App. A) in Fig. 4.6 at centre height. The choice of the centre height for detector positioning for start-up reactivity monitoring is motivated by modal analysis in § 2.2.2. Although the MYRRHA spallation neutron source is not a point source, the modelling as a point source in the centre core is an acceptable approximation for simulations [Malambu and Stankovskiy, 2012], which motivates the choice of the centre plane for detector positioning.

The behaviour of SCF_{area} for the MYRRHA BOL core is similar to the one of the VENUS-F SC1 core (presented in Fig. 3.7 for the lowest energy group). Inside a sphere in the centre of the core with radius 25 cm, $SCF_{area} > 1$. Outside this sphere, the absolute reactivity value is (safely) underestimated ($SCF_{area} < 1$[1]). For higher energy groups, one notices a local decrease in SCF (still smaller than unity) around the IPS locations.

For all energy groups, SCF_{area} shows a small gradient in the outer reflector, varying from 0.96-0.97 for the highest energy group up to 0.97-0.99 for the lowest energy group. Therefore, with thermal detectors, the absolute reactivity is underestimated by 3 % at maximum, i.e. 86 pcm on a value of 2875 pcm.

Similar to VENUS-F (see § 3.2.3), the profile of the MYRRHA SCF_{area} for the PNS experiment can be explained by modal analysis. The typical shapes of the MYRRHA eigenfunctions are similar to the ones of VENUS-F. Also the zero crossings of the 9th eigenfunction (see Fig. 4.7) are for the MYRRHA core at about the same radius from the centre of the core than for the VENUS-F core for the different energy groups. This is due to the similar radial dimensions for fuel and reflector of the considered VENUS-F and MYRRHA cores.

4.2.3 Recommendations for Subcriticality Monitoring during Start-up

Based on PNS experiment simulations for the MYRRHA power ADS, we confirm the conclusions from the zero-power VENUS-F experiment in § 3.2.5 for start-up

[1] For absolute measurement techniques (such as the area method), SCF<1 indicates an underestimation of the true absolute reactivity level. Indeed, as defined in eq. (2.17), $SCF_{area} = \frac{\rho_{area}}{\rho_{ref}}$. If $SCF_{area} < 1$, $|\rho_{area}| < |\rho_{ref}|$, therefore via the area method, a k_{eff} value higher than the true one is measured, which is a safe approach.

reactivity monitoring. The reflector is the appropriate zone for detector positioning during start-up. In that region, the gradient of the SCF for the area method is small and SCF_{area} remains smaller than unity (a safe underestimation of the absolute reactivity level) during core loading. Thermal detectors are most suitable for the reactivity measurements (if no thermalising elements are present), as their SCF_{area} is closest to (but smaller than) unity.

For the MYRRHA core, we can add that local perturbations in the fuel zone (such as IPS) do not influence the global profile of the SCF for the PNS area method. The first higher eigenmode with a maximum in the core remains a considerable contributor to the full flux profile, and its zero crossing remains the boundary between SCF_{area} smaller or bigger than unity.

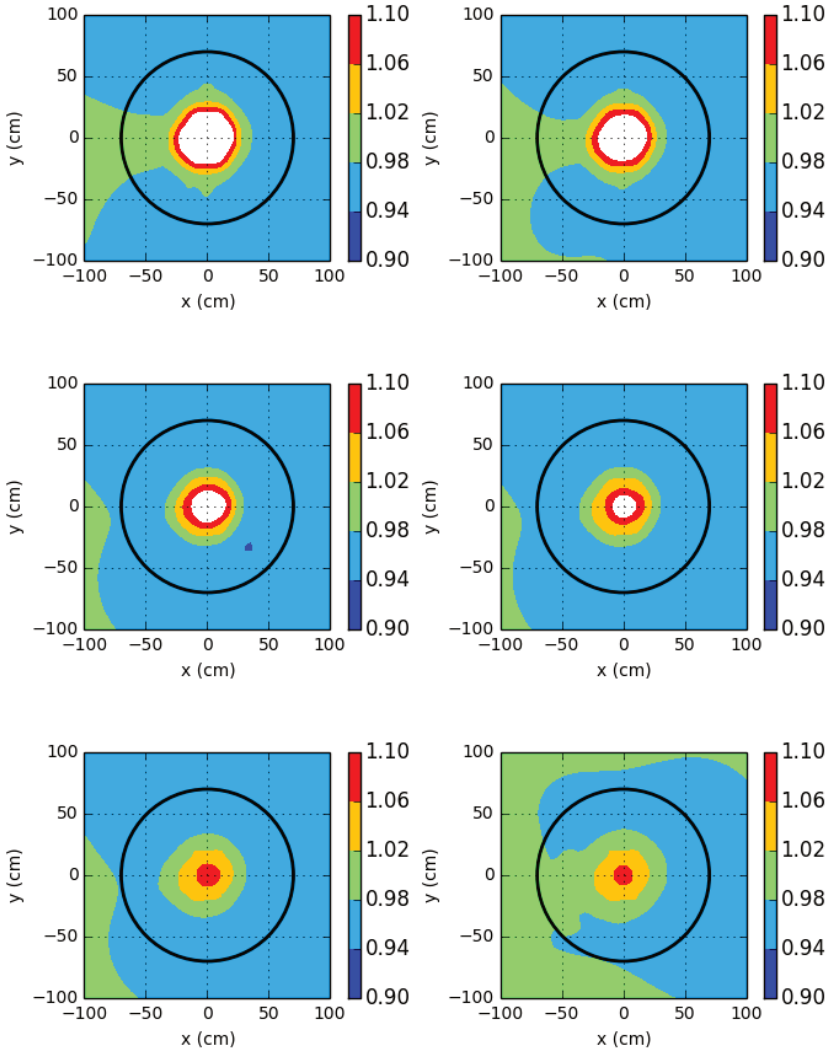

Figure 4.6: Simulated SCF_{area} for highest (i.e. group 1, top left) to the lowest (i.e. group 6, bottom right) energy group in the MYRRHA BOL core at centre height. The black circle indicates the MYRRHA core barrel.

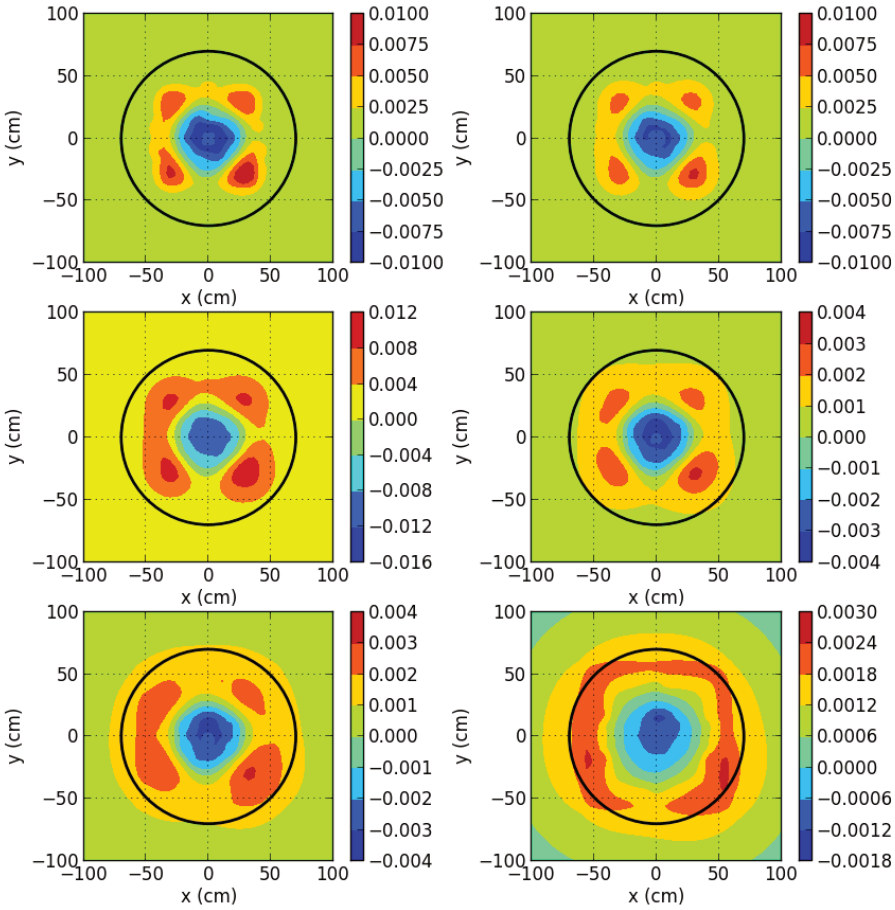

Figure 4.7: XY (z=0) plots of the 9th eigenfunction for each energy group of the MYRRHA model of the BOL core, from the highest (top left) to the lowest (bottom right) energy level. The black circle indicates the MYRRHA core barrel.

4.3 On-line Subcriticality Monitoring during Normal Operation

4.3.1 Aim and Method

In this section the evolution of the SCF of the CTF monitor is assessed during normal operation. Therefore, SCF_{CTF} is studied for the three phenomena during normal operation, presented in § 4.1.2: temperature feedback, core enlargement and core burn-up.

For each operational stage, the SCF_{CTF} is examined for 3600 sampling points in a 100x100 cm^2 square in the centre plane of the MYRRHA core, as shown in the next figures. For an ADS with source in the centre of the core, the midplane is most suitable having the lowest SCF_{CTF} (see Chapter 2, in particular § 2.3.2). Due to the high computational time, it is difficult to obtain SCF values with an acceptable uncertainty (smaller than 1 %) outside this square area. Deterministic (mode) calculations show however the constant SCF value in the outer reflector if no perturbation occurs in that region.

All reference reactivity values as well as CTF fission rates are obtained via MCNPX calculations (see § 4.1.3), using the MYRRHA-FASTEF model from [Stankovskiy and Malambu, 2011] presented in [Malambu and Stankovskiy, 2012].

As detector signals can be combined for reactivity monitoring, 5 zones of detector locations are identified: the outer reflector (outside the core barrel, 64 samples), the inner reflector (inside the core barrel, 64 samples), the complete reflector (i.e. with the core barrel region, 256 samples), the core (i.e. without the spallation target zone, 256 samples) and the total reactor (i.e. core and complete reflector, 1024 samples).

This exercise is performed with as much as possible detector locations, in order to define the SCF boundaries via the minimum and maximum values, and to estimate the variance of the SCFs per zone. In reality, a limited number of positions are available for monitoring because of practical and technological constraints. Therefore, in-core instrumentation will become difficult to install in the MYRRHA core [Vermeeren, 2015].

At the writing of this thesis, the detector type and operation mode for the MYRRHA reactor are not yet defined. Most probably, fission chambers will be chosen, seen their flexibility in mass, operation mode and spectrum [Vermeeren,

2015]. Therefore, the reactivity monitoring is simulated in this section for a thermal (U-235) and a threshold (Np-237) detector, to investigate the influence of the detector spectrum on the SCF_{CTF}.

4.3.2 From Cold Zero Power to Hot Full Power at Beginning Of Life

As a first step the CTF is assessed for the monitoring of the temperature feedback effect during start-up, which causes a decrease on k_{eff} level. Suppose the reference reactivity level is obtained (at room temperature) via the PNS technique (see § 4.2), by applying the proper SCF for the PNS technique. From this level the reference proportionality coefficient c of the CTF technique can be obtained at each position in the reactor via eq. (1.14).

The SCF_{CTF}[2] to be applied on c is shown in Fig. 4.8 for the 2 detector types at centre height, supposing $\left|\rho_{CTF}\right|=\left|\rho_{ref}\right|$=2875 ± 5 pcm (calibrated) and $\left|\rho'_{ref}\right|$=3696 ± 5 pcm. The prime state concerns the new HFP reactivity level at the MYRRHA operating temperatures (see [Malambu and Stankovskiy, 2012]). Without recalibrating c, SCF varies between 0.95 and 1.03 for the U-235 detector, and from below 0.9 to 1.03 for the Np-237 detector in the centre plane of the core.

Table 4.1 shows $SCF_{CTF,av}$ for this case study for different detector types and zones defined in § 4.3.1. The threshold detectors provide (unsafe) overestimations of $SCF_{CTF,av}$ by 1.1 % at maximum, whereas the thermal detectors overestimate up to 2.2 %.

By monitoring with threshold detectors only in the core, the reactivity monitoring is almost correct ($SCF_{CTF,av}$=0.999) with a 0.011 standard deviation on the SCF value. This location will be excluded however as a candidate monitoring zone, due to practical constraints [Vermeeren, 2015]. Therefore, the (inner) reflector zone will be chosen. In this region $SCF_{CTF,av}$=1.011 for threshold detectors, which means an unsafe overestimation of the absolute reactivity decrease by 41 ± 7 pcm. On the reference reactivity of 3696 ± 5 pcm in the prime state, this means an error of 1.1 %.

The temperature feedback effect would not be noticed at locations where $\frac{\rho_{CTF}}{\rho'_{CTF}}$=1, i.e. at locations where $SCF_{CTF,av}=\frac{\rho_{ref}}{\rho'_{ref}}$, being 1.344. This will nowhere be the case.

[2] SCF_{CTF} is defined in eq. (2.48). $SCF_{CTF} > 1$ indicates in this case an unsafe overestimation of the new absolute reactivity value, $SCF_{CTF} < 1$ a safe underestimation.

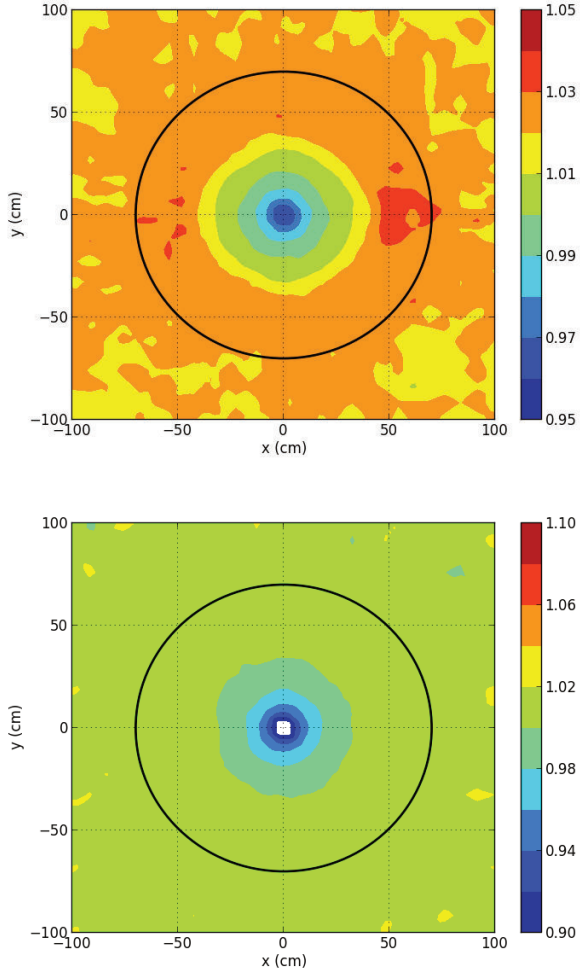

Figure 4.8: SCF_{CTF} for the MYRRHA BOL core temperature feedback at centre height, for a U-235 (top) and Np-237 detector (bottom). The maximum relative uncertainty on SCF_{CTF} is 1 %. The black circle indicates the MYRRHA core barrel.

Reactor Zone		U-235			
	$\left\|\rho'_{CTF,av}\right\|$	$SCF_{CTF,av}$	σ	max	min
outer reflector	3770	1.020	0.004	1.031	1.012
inner reflector	3777	1.022	0.004	1.029	1.013
total reflector	3774	1.021	0.004	1.031	1.008
core	3751	1.015	0.011	1.029	0.985
total reactor	3774	1.021	0.007	1.034	0.985
		Np-237			
	$\left\|\rho'_{CTF,av}\right\|$	$SCF_{CTF,av}$	σ	max	min
outer reflector	3737	1.011	0.007	1.029	0.994
inner reflector	3737	1.011	0.003	1.016	1.002
total reflector	3737	1.011	0.005	1.029	0.994
core	3692	0.999	0.011	1.011	0.954
total reactor	3729	1.008	0.008	1.029	0.954

Table 4.1: Overview of SCF_{CTF} between the CZP core ($\left|\rho_{ref}\right|$=2875 ± 5 pcm) and the HFP BOL core ($\left|\rho'_{ref}\right|$=3696 ± 5 pcm) in the centre plane of the MYRRHA core for a U-235 (thermal) and Np-237 (threshold) detector. For the different reactor zones, the average SCF and its standard deviation σ is given, as well as the minimum and maximum SCF value.

4.3.3 From Beginning Of Life to Begining Of Cycle

Before reaching the MYRRHA equilibrium core (from Fig. 4.3), different cores with increasing amount of fuel assemblies (and increasing fuel burn-up) are loaded. The evolution of k_{eff} for these cores is shown in Fig. 4.2. The monitoring of the increase in k_{eff} between the first (BOL, calibrated e.g. via source jerk, $\left|\rho_{CTF}\right|=\left|\rho_{ref}\right|$=3696 ± 5 pcm) and last (BOC, $\left|\rho'_{ref}\right|$=3193 ± 5 pcm) core at power, before reaching equilibrium, is evaluated by SCF_{CTF} in Fig. 4.9 for both thermal (U-235) and threshold (Np-237) detectors.

In this case, a different behaviour is noticed between thermal and threshold detectors. Whereas the U-235 detectors unsafely overestimate the increase in k_{eff} ($SCF_{CTF,av} > 1$, up to 1.612 in the core), the Np-237 detectors show $SCF_{CTF,av}$ lower and higher than unity in the different reactor zones.

Table 4.2 shows the average SCF_{CTF} for different detector types and zones. The

average of the set of threshold detectors in the outer reflector provides the reactivity level correctly ($SCF_{CTF,av}$=0.991), although the difference between the minimum and maximum SCF is considerable. At locations with $SCF_{CTF}=\frac{\rho_{ref}}{\rho'_{ref}}$=1.16 (e.g. in the core with a thermal detector), the change in reactivity is not detected.

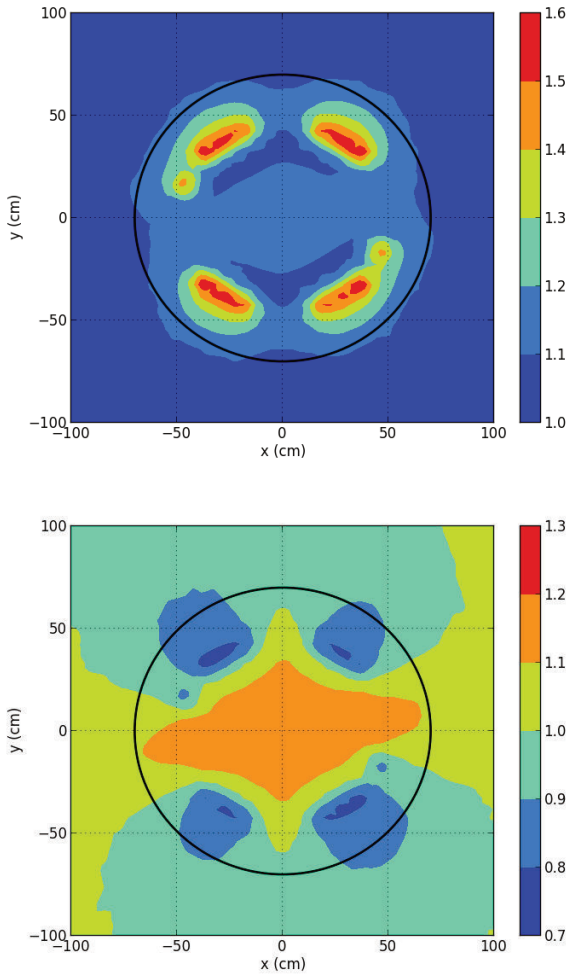

Figure 4.9: SCF_{CTF} from the MYRRHA BOL to BOC core, at centre height, for a U-235 (top) and a Np-237 (bottom) detector. The maximum relative uncertainty on SCF_{CTF} is 1 %. The black circle indicates the MYRRHA core barrel.

Reactor Zone	U-235				
	$\left\|\rho'_{CTF,av}\right\|$	$SCF_{CTF,av}$	σ	max	min
outer reflector	3397	1.064	0.007	1.082	1.047
inner reflector	3487	1.092	0.024	1.177	1.069
total reflector	3429	1.074	0.017	1.177	1.047
core	3864	1.210	0.148	1.612	1.082
total reactor	3605	1.129	0.103	1.612	1.047
	Np-237				
	$\left\|\rho'_{CTF,av}\right\|$	$SCF_{CTF,av}$	σ	max	min
outer reflector	3164	0.991	0.017	1.031	0.954
inner reflector	2944	0.922	0.030	0.983	0.860
total reflector	3081	0.965	0.036	1.042	0.860
core	3238	1.014	0.131	1.192	0.761
total reactor	3129	0.980	0.085	1.192	0.761

Table 4.2: Overview of SCF_{CTF} between the BOL core ($\left|\rho_{ref}\right|$=3696 ± 5 pcm) and the BOC equilibrium core ($\left|\rho'_{ref}\right|$=3193 ± 5 pcm) in the centre plane of the MYRRHA core, for a U-235 (thermal) and Np-237 (threshold) detector. For the different reactor zones, the average SCF_{CTF} and its standard deviation σ is given, as well as the minimum and maximum SCF value.

4.3.4 Monitoring the burn-up of an equilibrium cycle

During a MYRRHA equilibrium cycle, the reactivity decreases from $\left|\rho_{ref}\right|$=3193 ± 5 pcm (BOC) to $\left|\rho'_{ref}\right|$=4987 ± 5 pcm (EOC). The impact on SCF_{CTF} is shown in Fig. 4.10 for the two different detector types at centre height.

Although the reactivity variation is considerably higher in this case than between the BOL and BOC cores (in § 4.3.3), SCF_{CTF} slightly smaller than unity (a safe approach) is found, except close to the centre of the core.

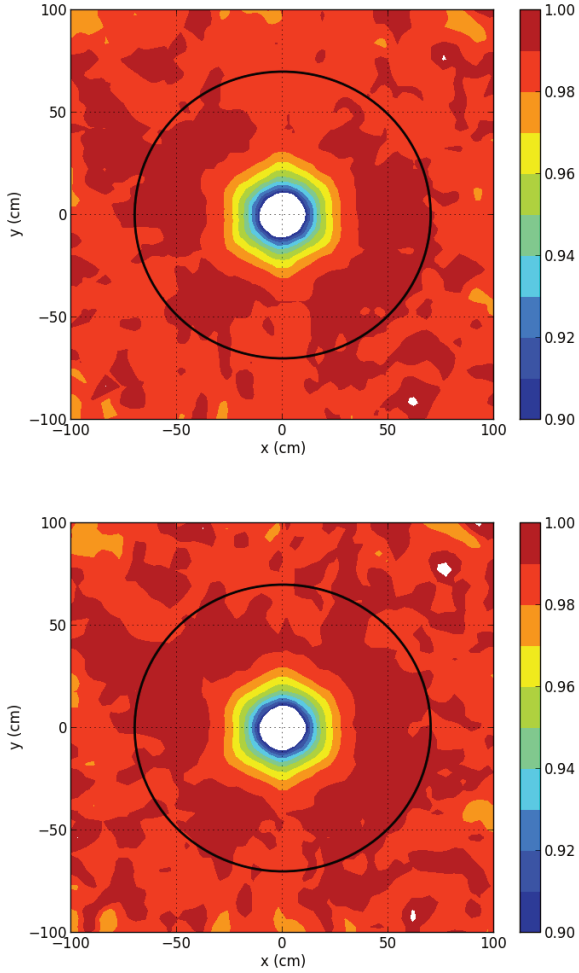

Figure 4.10: SCF_{CTF} between BOC and EOC of the MYRRHA equilibrium core, in the MYRRHA centre plane, for a U-235 (top) and a Np-237 (bottom) detector. The maximum relative uncertainty on SCF_{CTF} is 1 %. The black circle indicates the MYRRHA core barrel.

Table 4.3 shows SCF_{CTF} in different zones of the MYRRHA core with different types of detectors. One notices a similar behaviour of both detectors in the different regions of the reactor. The average SCF_{CTF} varies between 0.971 and 0.982 for a U-235 detector, and between 0.981 and 0.989 for a Np-237 detector. A noticeable

difference between the reactor core and the reflector can be found, due to the higher gradient of SCF_{CTF} in the centre of the core. Therefore, for both detectors, the smallest standard deviation for SCF_{CTF} can be found in the (inner) reflector (σ=0.004).

For this case, threshold detectors in the inner reflector are the optimal choice, as they safely underestimate the decrease in absolute reactivity by 55 pcm.

Reactor Zone	U-235				
	$\left\|\rho'_{CTF,av}\right\|$	$SCF_{CTF,av}$	σ	max	min
outer reflector	4892	0.981	0.005	0.990	0.966
inner reflector	4897	0.982	0.003	0.991	0.973
total reflector	4897	0.982	0.004	0.994	0.966
core	4842	0.971	0.011	0.983	0.929
total reactor	4882	0.979	0.008	0.998	0.929
	Np-237				
	$\left\|\rho'_{CTF,av}\right\|$	$SCF_{CTF,av}$	σ	max	min
outer reflector	4912	0.985	0.008	1.003	0.969
inner reflector	4932	0.989	0.003	0.998	0.983
total reflector	4922	0.987	0.006	1.004	0.969
core	4892	0.981	0.018	0.996	0.896
total reactor	4922	0.987	0.010	1.004	0.896

Table 4.3: Overview of the SCF_{CTF} for burn-up monitoring between BOC ($\left|\rho_{ref}\right|$=3193 ± 5 pcm) and EOC ($\left|\rho'_{ref}\right|$=4987 ± 5 pcm) in the centre plane of the MYRRHA core for a U-235 (thermal) and Np-237 (threshold) detector. For the different reactor zones, the average SCF_{CTF} and its standard deviation σ is given, as well as the minimum and maximum SCF value.

4.3.5 Role of the Interim Cross-checking of the Absolute Reactivity Level

At the time of writing of this thesis, the MYRRHA accelerator beam interruption time and frequency still need to be specified. If a short beam interruption could be repeated on the continuous MYRRHA beam, the source jerk method (see § 1.3.2) is a candidate for interim cross checking. This method allows the operator to obtain an absolute reactivity value (in dollars). The applicability of this method on a power ADS depends however on several issues.

At first, the maximum allowable beam interruption time needs to be defined. This time is limited by the maximum allowable thermal stresses in the core and structural materials. As the beam for the source jerk method behaves inversely to the PNS method, we can conclude that for the actual MYRRHA model (defined in App. B), a beam interruption time of 200 μs could be sufficient (see Fig. 4.6). This model however does not take into account the thermalising elements outside the core, which can considerably influence the beam interruption time (see the bunker effect in VENUS-F, Fig. 3.6). This effect could be reduced by using threshold detectors.

Secondly, the time for the beam to restore to its initial level plays a role. The beam should be stable again after interruption before a next beam interruption can be performed. This stabilisation time determines the source jerk period, i.e. the beam interruption time and the time to restore the beam to its original stable level.

Thirdly, the frequency of the beam interruption is under study. Depending on the number of beam interruptions needed for sufficient statistics, this parameter determines the time needed for an interim reactivity cross-check. The measurement time will, seen the nature of the method, always be significantly longer than the time needed to measure the current-to-flux ratio.

Finally, the required measurement time for acceptable accuracy depends also on the type and position of the detector, and its efficiency. Therefore, the related conclusions from VENUS-F on the required measurement time for the SJ method (see § 3.4.4) cannot directly be extrapolated to MYRRHA.

The spatial dependence of the source jerk method (see § 2.4.2) is similar to the PNS area method, developed in § 4.2.2 for the MYRRHA BOL core. Also for other cores (e.g. the BOC core), one expects the same behaviour of SCF_{area}, and thus also for SCF_{SJ}.

One concludes that at this time, it is too early to draw conclusions about the importance of the source jerk method for absolute reactivity cross-checking. It is in any case useful to estimate SCF_{CTF} not only during normal operation, but also in incident conditions. Although specific instrumentation is foreseen to detect incidents, it is useful to know how the reactivity monitor reacts on different incident scenarios. This question is studied in the next section.

4.4 Robustness of the Reactivity Monitoring against Incident Scenarios

In this section, the ability of the CTF monitor to detect and identify incidents in a power ADS is checked. From a safety point of view, the maximum operational subcriticality level is limited by the maximum positive reactivity insertion during incidents (see § 1.6.1) in order to avoid criticality and large power excursions through source multiplication. The role of reactivity monitoring in incident conditions is therefore different for power ADS than for critical power reactors: in addition to other instrumentation, the CTF monitor could help to detect abnormal situations, and to understand the response of detectors to an incident scenario.

In order to understand the behaviour of the CTF monitor during incident scenarios, three classes of incident scenarios are studied: a local perturbation in the reflector (see § 4.4.1), a local perturbation in the core (see § 4.4.2) and a global perturbation without reactivity change (see § 4.4.3). All scenarios are applied on the MYRRHA EOC core ($|\rho_{ref}|$=4987 ± 5 pcm, determined by MCNPX criticality calculations) as example.

4.4.1 Control Rod Expulsion

One of the incident scenarios studied for the MYRRHA core is the control rod expulsion. In normal operation, the MYRRHA control rods are latched below the core. When the control system fails, the control rod is propelled by buoyancy forces upwards completely through the core until the upper plenum, as it is lighter than LBE.

As a first study, the effect of one expulsed control rod (indicated by a cross in Fig. 4.3) is studied here. This incident scenario (e.g. in the EOC core) corresponds to a positive reactivity insertion $\Delta\rho_{ref}$ of 81 ± 7 pcm.

The measured change in reactivity $\Delta\rho_{CTF}$ for this incident is shown in Fig. 4.11 for a thermal and threshold detector at centre height. Both detectors show the same behaviour, i.e. an unsafe underestimation of the reactivity increase (SCF_{CTF} > 1) in the core, a (safe) overestimation of the reactivity increase (SCF_{CTF} < 1) close to the perturbation in the outer reflector, and an (unsafe) underestimation of the reactivity increase (SCF_{CTF} > 1) far away from the perturbation in the reflector.

The effect of combining detector signals is shown in Table 4.4. For each detection zone, the average reactivity change is calculated. All zones provide with both

detector types a good monitoring of the reactivity insertion, i.e. maximum of 42 pcm error on $|\rho_{ref}|$=4987 pcm (i.e. 0.9 %). The incident in the outer reflector can be identified by a larger spread in outer reflector SCF_{CTF} values for both detectors. Close to the perturbation, SCF_{CTF} is significantly smaller than unity.

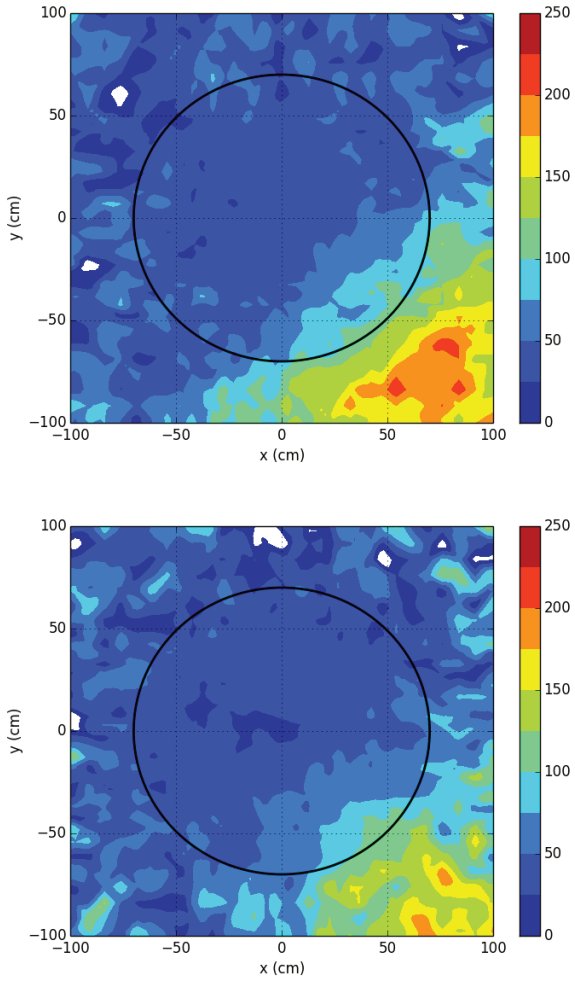

Figure 4.11: Measured change in reactivity $\Delta\rho_{CTF}$ after control rod expulsion in the MYRRHA equilibrium core at EOL, at centre height, for a U-235 (top) and a Np-237 (bottom) detector. The maximum relative uncertainty on $\Delta\rho_{CTF}$ is 1 %. The black circle indicates the MYRRHA core barrel.

Reactor Zone	U-235	Np-237
outer reflector	+76	+81
inner reflector	+66	+61
total reflector	+71	+66
core	+42	+42
total reactor	+61	+56

Table 4.4: Overview of the average reactivity increase $\Delta\rho_{CTF,av}$ in the different reactor zones for the monitoring of a CR expulsion ($\Delta\rho_{ref}$=+81 ± 7 pcm) in the centre plane of the MYRRHA EOC core for a U-235 (thermal) and Np-237 (threshold) detector.

4.4.2 IPS Sensitivity

In order to study a case of a positive reactivity insertion in the centre of the MYRRHA core, the IPS indicated by a cross in Fig. 4.3 is replaced by LBE in the equilibrium core at EOC. This incident scenario (e.g. in the EOC core) corresponds to a positive reactivity insertion $\Delta\rho_{ref}$ of 161 ± 7 pcm.

The related measured change in reactivity $\Delta\rho_{CTF}$ for this incident is shown in Fig. 4.12 for a thermal and a threshold detector at centre height. Only close to the perturbation a considerable overestimation of the reactivity increase is measured.

The combination of signals leads for both detector types to an acceptable monitoring of the reactivity change, presented in Table 4.5. The incident can be identified by a contradictory behaviour of thermal and threshold detector close to the perturbation.

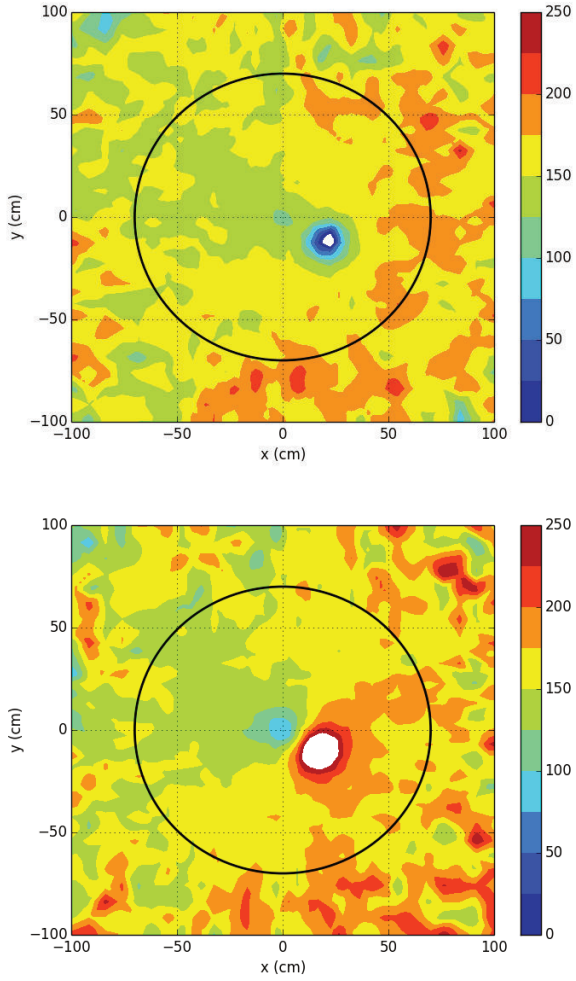

Figure 4.12: Measured change in reactivity $\Delta\rho_{CTF}$ after a positive reactivity insertion in the MYRRHA equilibrium core at EOL, at centre height, for a U-235 (top) and a Np-237 (bottom) detector. The maximum relative uncertainty on $\Delta\rho_{CTF}$ is 1 %. The black circle indicates the MYRRHA core barrel.

Reactor Zone	U-235	Np-237
outer reflector	+151	+166
inner reflector	+166	+161
total reflector	+161	+166
core	+151	+166
total reactor	+161	+166

Table 4.5: Measured change in average reactivity $\Delta\rho_{CTF,av}$ in the different reactor zones for the monitoring of an ADS source height increase ($\Delta\rho_{ref}$=0 pcm) in the centre plane of the MYRRHA EOC core for a U-235 (thermal) and Np-237 (threshold) detector.

4.4.3 Source Height Variation

Not only reactivity variations need to be interpreted correctly by the CTF monitor. Also incident scenarios without reactivity changes need to be identified. In this paragraph the influence of a source height increase of 5 cm (e.g. after beam window break, see [Keyers, 2010]) is studied for the MYRRHA EOC core.

The influence of this incident on the estimated reactivity is shown in Fig. 4.13 for both a thermal and a threshold detector at centre height. This incident is characterised by a homogeneous small increase of the measured reactivity through the complete core (except close to the spallation source), also shown by the average values $\Delta\rho_{CTF,av}$ in the different reactor zones in Table 4.6.

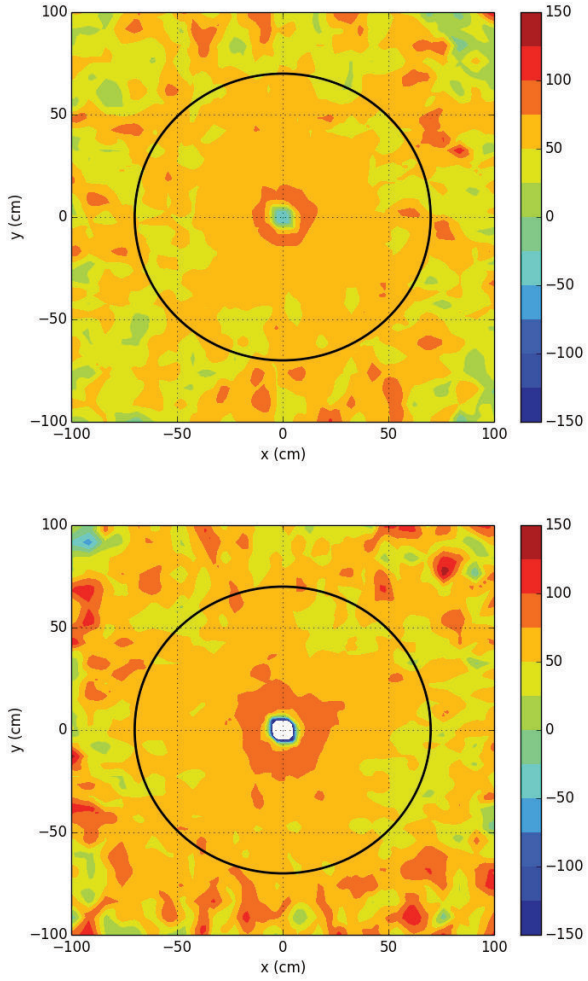

Figure 4.13: $\Delta\rho_{CTF}$ after a source height increase in the MYRRHA equilibrium core at EOL, at centre height, for a U-235 (top) and a Np-237 (bottom) detector. The maximum relative uncertainty on the $\Delta\rho_{CTF}$ is 1 %. The black circle indicates the MYRRHA core barrel.

Reactor Zone	U-235	Np-237
outer reflector	+35	+50
inner reflector	+55	+60
total reflector	+45	+55
core	+60	+65
total reactor	+55	+60

Table 4.6: Overview of $\Delta\rho_{CTF,av}$ for monitoring a source height variation in the centre plane of the MYRRHA EOC core ($\Delta\rho_{ref}$=0) for a U-235 (thermal) and Np-237 (threshold) detector.

4.5 Discussion

A combination of relative reactivity monitoring via the CTF monitor and absolute measurements via the SJ method is investigated in this thesis for reactivity monitoring during operation of an ADS. For the MYRRHA ADS, the feasibility of reproducible stable short accelerator beam interruptions is still under discussion today. Therefore, in this chapter the accuracy of the CTF monitor is checked during different stages of operation without recalibration to determine the boundaries of the measurement accuracy.

For the MYRRHA ADS, the CTF monitor provides good reactivity estimates (without recalibration) by intelligent detector positioning. Indeed, for the different phases of operation, (average) SCF_{CTF} close to unity can be found, when detectors are simulated in the complete centre plane of the MYRRHA core. In reality, the installed number of detectors will be limited by practical constraints and the required accuracy of the measurement.

To deal with the limitation in number of detectors in a conservative way, the extreme SCF value in the considered detection zone is applied as a boundary. For the three stages considered for normal operation, this is SCF_{CTF}=0.860 (for a threshold detector in the outer reflector core enlargement case, see Table 4.2), indicating an absolute estimated reactivity value of 2746 pcm instead of 3193 pcm, i.e. 447 pcm error in monitoring. Therefore, 500 pcm could be a suitable order of magnitude for the accuracy of the CTF monitoring in the MYRRHA core during ADS operation without any recalibration, independent of the detector type.

This first estimation of the accuracy of the CTF monitor shows the methodology to follow, but needs of course to be finetuned. If possible, the accuracy value could

be reduced by interim cross-checking of the absolute reactivity value. Moreover, once the detailed MYRRHA core design is available, this work can be performed in detail, and the evolution of the estimated reactivity during operation can be simulated with additional intermediate steps.

The identification and quantification of reactivity incidents in § 4.4 are more complicated than the normal reactivity monitoring presented in § 4.3. In this work, three types of incident scenarios are studied to show the reaction of the reactivity monitor to each of them. We conclude that thanks to a combination of detector signals at different locations, one is able to identify each of these scenarios.

In reality, too much detectors are required to identify (and quantify) each incident scenario (only 3 typical scenarios are studied here). Moreover, specific instrumentation is foreseen to detect the considered types of incidents. This exercise shows however the behaviour of the CTF monitor of each of the types of incidents. If needed, detectors could be installed in such a way to identify a specific type of incident, complementary to other instrumentation.

4.6 Conclusion

In this chapter the reactivity monitoring is investigated for the operation of a power ADS. Different positions and types of detectors are investigated to set-up a monitoring tool for the MYRRHA ADS. In order to assure robust reactivity monitoring, the combination of detector signals in a specific reactor zone is recommended.

For the start-up of MYRRHA at CZP (k_{eff}=0.97205), the same conclusions can be drawn as for the zero power VENUS-F ADS. The outer reflector in the centre plane of the reactor is the appropriate zone for detector positioning given the small spatial gradient in the SCF. In this region the absolute reactivity level (in pcm) is (safely) underestimated by maximum 3 % (i.e. 86 pcm on a reference absolute reactivity of 2875 pcm), using thermal detectors. Using threshold detectors, SCFs closer to unity are found, indicating a lower (but still safe) underestimation of the absolute reactivity level. The use of threshold detectors is however recommended, as it avoids the issue of thermalising elements (see Chapter 3).

For the reactivity monitoring during operation, the use of both thermal and threshold detectors is studied in different zones of the reactor. During the three

phases of operation of a power ADS, the detector recommendations are shown in Table 4.7, excluding the core as detector location zone for practical reasons. Using the appropriate detector type in the inner or outer reflector zone, the (absolute) reactivity can be correctly monitored or the SCF_{CTF} is slightly (safely) smaller than unity, except for the temperature feedback case. During temperature increase, the reactivity decrease is unsafely overestimated by 1.1 % (i.e. 41 pcm on a reference level of 3737 pcm).

Operation Phase	$\lvert\rho_{ref}\rvert$	$\lvert\rho'_{ref}\rvert$	Detectors	Positioning	$\lvert\rho'_{CTF}\rvert$	SCF_{CTF} (σ)
Temperature feedback	2875	3696	THR	Inner refl.	3737	1.011 (0.003)
Core enlargement	3696	3193	THR	Outer refl.	3164	0.991 (0.017)
Fuel burn-up	3161	4987	THR	Inner refl.	4932	0.989 (0.004)

Table 4.7: Overview of the detector type and positioning choice for optimum reactivity (ρ in pcm) monitoring of the MYRRHA full-power ADS during different phases of operation. $\lvert\rho_{ref}\rvert$ is the calibrated absolute reactivity at the beginning of the phase, $\lvert\rho'_{ref}\rvert$ and $\lvert\rho'_{CTF}\rvert$ are respectively the true and the CTF reactivity at the end of the phase. THR = Threshold detector, TH = Thermal detector. All detectors are foreseen to be positioned in the centre plane of the core.

If no SJ reactivity cross-checking can be applied, as a first approach, a conservative boundary of 500 pcm is proposed on the measured CTF reactivity during operation without correction. This value is derived from the maximum SCF value found in the MYRRHA reflector, during operation. To improve the accuracy of the measurement, a set of detectors is recommended in the reflector region. The number of detectors will however be determined by practical constraints.

The importance of the CTF monitor accuracy within the monitoring system will depend on the role of the Source Jerk (SJ) (absolute re-calibration) technique specifications. More information about the accelerator beam is required in order to estimate the required time for a precise absolute reactivity re-estimation. The spatial dependence of the SJ method is similar to the PNS area method.

Complementary to normal operation, the CTF monitor could help to detect and locate incidents. For that purpose three types of incident scenarios are studied: a local perturbation in the reflector, a local perturbation in the core (both leading to a reactivity increase) and the monitoring of an incident without reactivity change. The way in which these incidents can be detected and quantified is shown in

Table 4.8.

In reality, a considerable set of detectors will be required at different locations in the reactor to identify (and quantify) the different incident scenarios. Therefore, other instrumentation is installed. This exercise could however help to understand the behaviour of the reactivity monitoring tool on incident scenarios. Moreover, if needed, a detector could be installed at a specific location to identify one type of incident (e.g. as a back-up in case other instrumentation fails).

Incident	$\Delta\rho_{ref}$	Detectors	Identification	$\Delta\rho_{CTF}$
CR expulsion	+81	THR/TH	Close to pert.	+81
IPS ejection	+161	THR	Close to pert.	+161
Window break	0	TH/THR	Global change	+35

Table 4.8: Overview of the detector type, identification zone, and detector positioning for optimum reactivity variation (ρ in pcm) monitoring of incident scenarios in the MYRRHA power ADS EOC core ($\left|\rho\right|$=4987 pcm). THR = Threshold detector, TH = Thermal detector. All detectors are foreseen to be positioned in the centre plane of the core. Incidents can be identified close to the perturbation or globally in the core.

5

CONCLUSIONS AND RECOMMENDATIONS

This thesis provides a methodology and set-up of a robust reactivity monitoring tool for Accelerator-Driven Systems (ADS), in order to guarantee a safe margin to criticality. The robustness of the reactivity monitoring tool is defined in different fields: the choice of the measurement techniques, the evaluation methods to derive the reactivity from experimental data and the detector type and positioning.

Major achievements in this work are the analytical development of Spatial Correction Factors (SCFs), to be applied on the reactivity value obtained via point kinetics evaluation methods. Thanks to modal analysis, one is able to understand the behaviour of SCFs in a subcritical core and identify robust detector positions.

Modal analysis and experiment simulations are compared to experimental values from the VENUS-F ADS. The outcome of this work provides valuable information to set up detector positioning rules for zero-power ADS. Moreover, as a final step, an extrapolation towards a power ADS is made, in order to study the effect of specific full-power issues (such as temperature feedback and burn-up) on reactivity monitoring.

5.1 Conclusions

The Choice of Static Evaluations of the Selected Measurement Techniques

Based on an evaluation of the existing measurement techniques and experience feedback from the previous European project MUSE, a combination of different experimental techniques is proposed for ADS reactivity monitoring during all

stages of operation. The Pulsed Neutron Source (PNS) is selected as absolute reactivity measurement technique for the start-up phase (i.e. from core loading until 1 % of full power). The Current-to-Flux (CTF) relative reactivity monitor is the candidate for reactivity monitoring during operation (i.e. from 1 % of full power on, no long beam interruptions allowed). As the CTF monitor can only detect changes in reactivity, the short Source Jerk (SJ) interim cross-checking technique is included in the reactivity monitor. This proposal is successfully tested on the VENUS-F zero-power ADS during the GUINEVERE and FREYA European Framework Programmes.

To derive the reactivity value from the experimental results, static evaluation methods are used in this work: the area method for start-up, the static CTF method during operation and the static SJ method for interim cross-checking of the ADS reactivity. These methods are supposed to be more robust, as they do not depend on the knowledge of kinetic parameters (e.g. the neutron generation time).

The interpretation of the experimental results from VENUS-F using these methods is succesfully validated for the first experimental campaigns on VENUS-F. Thanks to a reference VENUS-F critical core, the experimental results can be compared to a subcriticality level obtained by an alternative methodology (i.e. a combination of the rod drop and Modified Source Multiplication (MSM) method). Moreover, an extrapolation exercise on the MYRRHA power ADS is performed by simulations in order to investigate the performance of the monitoring methodology, taking into account specific power effects.

Modal Analysis of the SCFs for Robust Detector Locations

The evaluation methods proposed in this thesis are based on point kinetics and need to be corrected with SCFs to obtain the correct reactivity value. Static modal analysis is applied in this work to derive analytical expressions of SCFs for the selected experimental techniques. The DALTON diffusion code is extended to both simulate the selected experimental techniques and perform the modal analysis of subcritical cores.

The first higher eigenmode with a maximum in the centre of the core is important for the modal analysis to study the detector positioning of ADS with source in the centre of the core. In the VENUS-F and MYRRHA ADS, this is the 9th mode, showing one zero crossing at about 20-25 cm from the centre of the core. This mode has a considerable contribution to the total flux of typical ADS core designs,

and also to the SCF of the different selected evaluation methods. Moreover, other higher modes with a maximum in the centre of the core (with more zero crossings) have the same zero crossing location as the 9th mode.

For absolute reactivity measurements, the location without any spatial correction (SCF=1) is located at the zero-crossing of the 9th mode. Indeed, at this position, the contribution to the SCF of modes with a high contribution to the full flux (and SCF) is eliminated, and the relative contribution of the fundamental mode to the total flux increases. The zero crossing position of this mode identifies the boundary between a SCF < 1 (a safe underestimation of the absolute reactivity value) and SCF > 1 (an unsafe overestimation of the absolute reactivity value).

Robust detector locations for absolute reactivity measurement techniques are not necessarily locations with SCF=1 for the different experimental methods. A better criterion is the spatial gradient of the SCF. Therefore, we will look for zones with a low gradient in SCF, and with SCF < 1, preferably close to unity if one wants to avoid to calculate correction factors. Moreover, for the relative CTF monitor, the small shift of the zero crossing of the 9th mode between two states can cause high spatial gradients of SCF_{CTF} close to the zero crossing location of this mode. As a consequence, this location is not robust for relative reactivity monitoring.

As a general rule, all proposed detector positions are in the same plane as the ADS source, i.e. (close to or) at the centre height of the core. At this height, the SCFs are closest to unity.

Reactivity Monitoring Tool Specifications for ADS Start-up

For the start-up phase of an ADS , the **reflector zone** is the recommended zone for detector locations. During core loading, SCF_{area} is significantly smaller than unity (i.e. a safe underestimation of the absolute reactivity value), rising with increasing subcriticality level. As SCF_{area}=0.96-0.97, the absolute reactivity level in the VENUS-F SC1 core ($|\rho|$=3709 pcm, a typical subcriticality level for ADS operation) is safely underestimated by 111-148 pcm.

Experimental results from VENUS-F show a clear influence of local thermalising elements (in this case the VENUS-F bunker) on the profile of SCF_{area}. This issue can be avoided by the use of **threshold detectors**, but no experimental results with this type of detector are available yet.

Moreover, thermalising elements extend the required pulse period for the area

method. Typical values for the area method are between 200 and 500 μs. Periods up to 1 ms are needed to reach the delayed neutron level for the area method, if thermalising elements are present. This increases the measurement time for good statistics, in particular for zero-power ADS or at deep subcritical states.

For the MYRRHA ADS, the same conclusions are found, with similar SCF_{area} values for the (outer) reflector.

Reactivity Monitoring Specifications for ADS Operation

The reactivity monitoring tool for an ADS during operation comprises the relative CTF monitor and the SJ interim cross-checking method. Depending on the beam interruption capability of a full power ADS accelerator, interim cross-checking of the absolute reactivity level is possible via the SJ method. The CTF monitor can be recalibrated using this information.

MYRRHA is used as a case study for the static CTF monitor, taking into account the power ADS reactivity monitoring during normal operation. Three stages of operation are identified: the monitoring of the temperature feedback during heating of the core, the core enlargement during the first MYRRHA cores, and the monitoring of the burn-up of the MYRRHA equilibrium core.

Based on deviations from unity of $SCF_{CTF,av}$, the core is the optimum location to monitor temperature feedback, whereas the reflector is the optimum location for core enlargement and burn-up monitoring. $SCF_{CTF,av}$ values between 0.989 and 0.999 are found, with standard deviation σ=0.005-0.017. This corresponds to deviations of the measured reactivity from the real value of maximum 0.9 % for the three stages of operation.

For technical reasons, it will be difficult to install detectors inside the MYRRHA core. If for all stages of operation the **reflector zone** is chosen for CTF monitoring, one should take into account a positive $SCF_{CTF} = 1.011$ (σ=0.005) for the monitoring of temperature feedback, i.e. an unsafe overestimation by 41 pcm of the absolute reactivity increase of 821 pcm (i.e. 1.1 % on the HFP reactivity).

The variance σ on $SCF_{CTF,av}$ is calculated supposing a number of detectors corresponding to the mesh grid in the simulations (e.g. 64 for the outer reflector). In reality, the number of detectors will depend on the required accuracy of the reactivity monitoring tool and the reliability of the detectors. Using a limited number of detectors, it is recommended to take the most extreme SCF_{CTF} **value**

in the reflector as a boundary for the CTF reactivity without recalibration. This value is 0.860 (threshold detector in the outer reflector core enlargement case, see Table 4.2), indicating an absolute reactivity value of 2746 pcm instead of 3193 pcm, i.e. 447 pcm error in monitoring. Therefore, **500 pcm** could be a suitable **order of magnitude** for the accuracy of the CTF monitoring in the MYRRHA core during ADS operation without any recalibration, independent of the detector type. The use of threshold detectors is however recommended to avoid the effect of thermalising elements.

The combination of many detector signals will be needed for the identification of reactivity incidents in MYRRHA. Specific (more straightforward) instrumentation is foreseen to identify the different incident scenarios. In case of a specific incident that needs follow-up by the reactivity monitoring tool, a dedicated detector can be installed, e.g. close to the perturbation.

Finally, the spatial dependence of the static SJ interim cross-checking method is similar to the PNS area start-up monitoring method, and the outer reflector is thus the preferred location. The beam interruption time at power needs to be minimised to reduce thermal stresses in the ADS. This is an additional motivation for the use of threshold detectors, similar to the PNS area method.

5.2 Recommendations

Required Accuracy of the Reactivity Monitoring Tool

The ADS reactivity monitoring tool will have different final specifications depending on the safety function it fullfills. If the safety function of the reactivity monitoring tool is related to normal operation, the number of detectors determines the accuracy of the measurement. If many detectors are installed, one is also able to identify different incidents by studying the response of each detector (group) to the simulated incident. For the latter purpose, it is obvious that other (more straightforward) detection systems will be installed.

Another question related to the measurement accuracy concerns the use of the SCFs for the different methods used for reactivity monitoring. Will they be applied as an envelope to determine the uncertainty margin to be applied on the non-corrected reactivity value, or will they be calculated and applied on the non-corrected value? In the latter case an uncertainty on the calculational tools and models will be taken into account. These licensing questions need to be clarified

before making conclusions about the accuracy of the reactivity measurement tool. The higher the accuracy, the higher the allowed operational k_{eff} level, which is beneficial for the operational cost of the ADS.

Importance of the Interim Cross-Checking Technique

At the time of writing, it is not yet clear if (and how frequent) the accelerator beam of a power ADS can be interrupted to perform the static SJ evaluation of the absolute reactivity level. An important factor is also the beam restoration time, i.e. the time the beam needs to restabilise at its original level. This time determines the period of the interruptions.

The performance of the static SJ method determines the importance of the CTF monitor. If short beam interruptions can be continuously performed with a reasonable period of interruption, absolute reactivity measurement are often available during operation of the ADS. The availability depends on the number of repetitions to achieve satisfying precision on the non-corrected reactivity value. The importance of the CTF monitor decreases if frequent recalibrations of the CTF monitor can be performed on-line. The safety function of the CTF monitor is in that case limited to the quick detection of abnormal events. Needless to say that also the SJ interim cross-checking method is subject to its own SCFs.

Additional Measurements on VENUS-F

As an outcome of this work, several conclusions are drawn from simulations on VENUS-F, which can be validated with additional measurements on VENUS-F that are currently ongoing or planned. At first, measurements with threshold detectors can be performed to check the sensitivity of the SCFs to thermalising elements. Also measurements at different subcriticality levels are foreseen to check the start-up reactivity monitoring approach. A sound validation of simulations is indispensable for the licensing of the reactivity monitoring tool.

Secondly, different aspects proper to power ADS need special attention, and are envisaged for (representative) experiments in VENUS-F: inhomogenities such as IPS, core enlargement exercises, and the simulation of burn-up. Finally, the simulations in this work are performed using a general MYRRHA design, and two types of detectors. Specific calculations should be performed with the final design of the ADS, taking into account the selected detector design. Special attention should be paid to new design changes that can affect the behaviour of the SCFs.

A

THE VENUS-F MODELS IN DALTON

This appendix describes the calculational models of the VENUS-F core used in the DALTON diffusion code, which is presented in § 2.6.1. Both the geometry description as well as the methodology to generate the cross sections are discussed.

A.1 Geometry Description

Two models of VENUS-F are made in order to perform modal analysis and experiment simulations with the DALTON code. The first (basic) model comprises the reactor only, as described in § 1.5.3. The second model extends the first one with the (approximately modelled) VENUS-F barite bunker surrounding the reactor. The model is not accurate, but represents the main elements that determine the VENUS-F reactor physics parameters (for subcriticality monitoring).

Because of the square geometry of the VENUS-F assemblies, a cartesian (XYZ) model structure is applied. Therefore a square lead reflector outside the 12x12 grid is applied in this approximated model equivalent (i.e. with a similar average outer reflector thickness) to the cylindrical outer reflector. The vacuum in the beam line is not modelled, and the 4 central assemblies are completely filled by lead reflector. The number of cells is chosen in such a way to obtain at least 3 cells per fuel assembly along the X and Y axis. The number of cells is limited to allow time-dependent calculations with DALTON in a reasonable calculational time. The basic model therefore consists of 75645 (41x41x45) cells, the extended model of 557685 (81x81x85) cells.

The structure of the VENUS-F geometry in DALTON is shown in Fig. A.1 for the

extended model. A detail zoom on the core at different heights is shown in Fig. A.2.

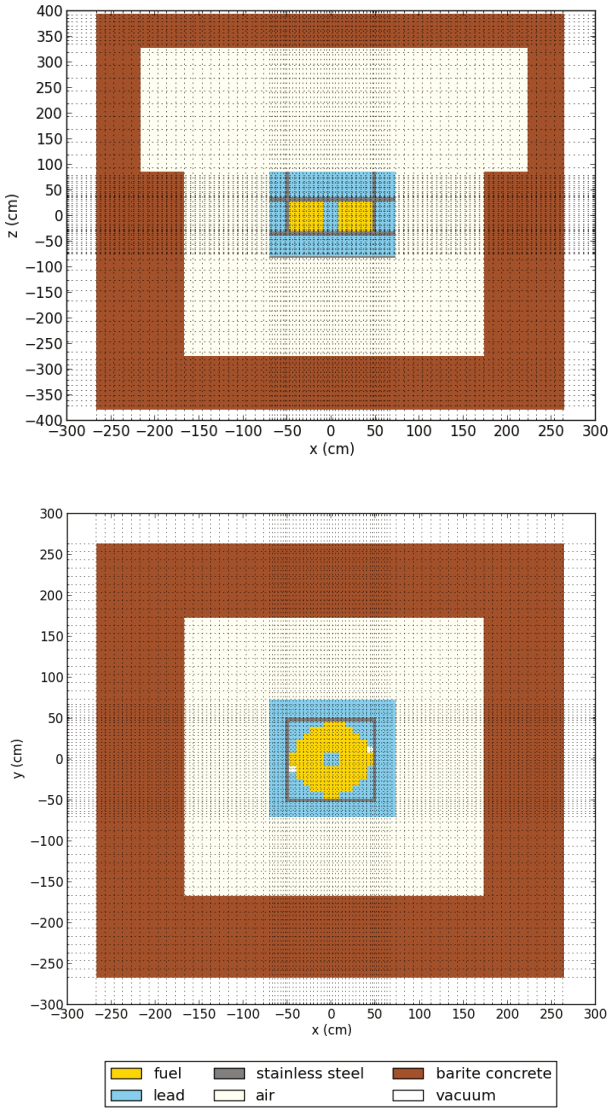

Figure A.1: Extended VENUS-F model for calculations in DALTON: vertical cut (y=0 cm, top figure) and horizontal cut (z=0 cm, bottom figure) at middle height. The gridlines on the plot correspond to the cells of the model.

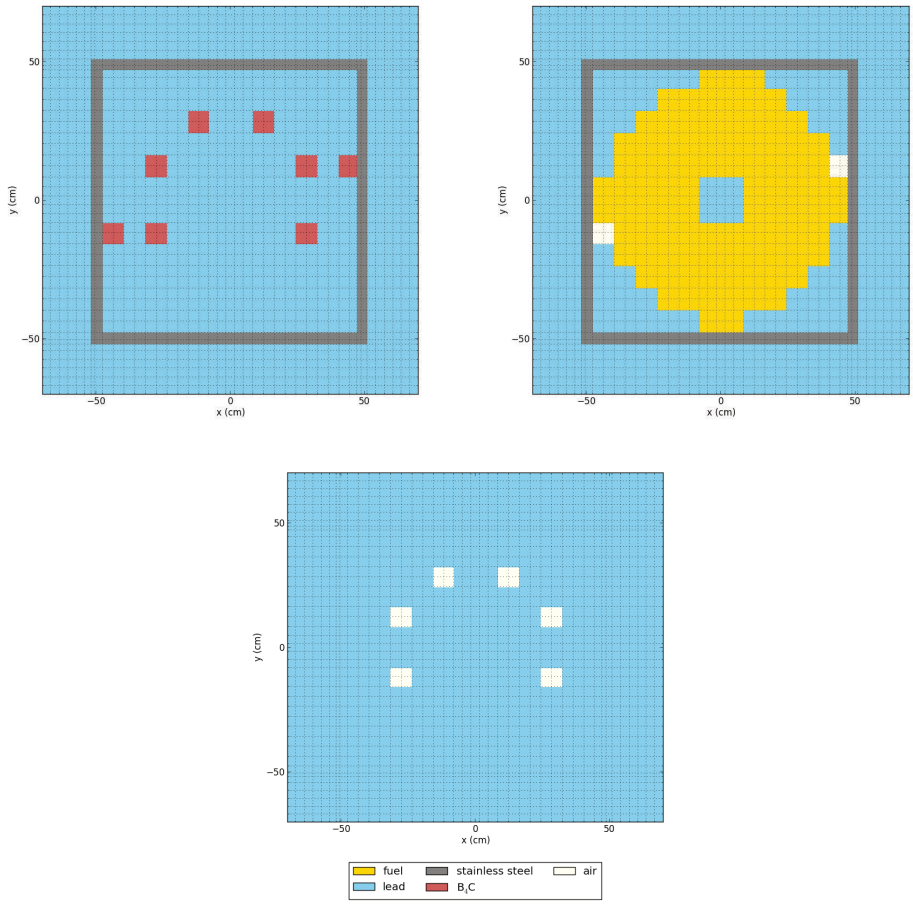

Figure A.2: VENUS-F Reactor model for calculations in DALTON: horizontal cuts at z=-39 cm (bottom reflector, top figure), at middle height z=0 cm (reactor core, middle figure) and at z=39 cm (top reflector, bottom figure). The gridlines on the plot correspond to the cells of the model.

A.2 Cross Section Generation

The cross sections of VENUS-F used for DALTON calculations are determined similar to the ones used for VENUS-F simulations with other deterministic codes (e.g. [Bianchini et al., 2010]). The ECCO module of ERANOS [Rimpault, 2002] is used. For DALTON a condensation into 6 energy groups is performed, in order to reduce the calculational time (for time dependent calculations in particular).

The structure of the 6 energy groups is shown in Table A.1. The choice of the boundaries is made based on the analysis of the neutron energy spectrum in VENUS-F [Uyttenhove et al., 2011a] (which is similar in critical mode to the subcritical mode spectrum [Krasa et al., 2014]). Sensitivity checks were carried out on the group boundaries, and comparison with experimental k_{eff} values (for the CR0 and SC1 cores) are in good agreement with experimental values (see Table A.2). Also by probabilistic MCNP calculations [Uyttenhove and Steckmeyer, 2014] similar results are obtained, e.g. for the VENUS-F bunker effect on the reactivity.

Energy Group	Range
1	$E > 1$ MeV
2	497.8 keV $< E \leq 1$ MeV
3	111.1 keV $< E \leq$ 497.8 keV
4	55.2 keV $< E \leq$ 111.1 keV
5	9.12 keV $< E \leq$ 55.2 keV
6	$E \leq$ 9.12 keV

Table A.1: Boundaries of the 6 neutron energy groups for the VENUS-F calculation in DALTON.

	model with bunker	model without bunker	experiment (i.e. with bunker)
CR0	1.00467	1.00150	1
SC1	0.96424	0.96078	0.964 ± 0.001 [Lecouey et al., 2015b]

Table A.2: Comparison of the k_{eff} results for the VENUS-F CR0 and SC1 cores: DALTON calculations versus experiments. The SC1 core has the control rods positioned out of the core, i.e. at 600 mm.

B

THE MYRRHA MODEL IN DALTON

This appendix describes the calculational model of the VENUS-F MYRRHA used in the DALTON diffusion code, which is presented in § 2.6.1. Both the geometry description as well as the methodology to generate the cross sections are discussed.

B.1 Geometry Description

A simplified model of MYRRHA is made in order to perform modal analysis and experiment simulations with the DALTON code. The MYRRHA core consists of hexagonal assemblies (see e.g. Fig. 4.1). In DALTON an equivalent XYZ model is set up. In order to guarantee a correct reactor modelling, the different hexagonal rings in the core are transferred to rectangular rings in DALTON, assuring the same corresponding volume per ring.

Per ring the proportion of different types of assemblies is maintained. E.g. for the first ring in the MYRRHA Beginning Of Life (BOL) core in Fig. 4.1, half the assemblies is fuel and the other half is In-Pile Sections. In DALTON a rectangular ring is created with the same volume as the first ring. Half the volume is taken by fuel and the other half by IPS. The vacuum in the beam line is modelled as air.

The number of cells is chosen in such a way to obtain at least 3 cells per fuel assembly along the X and Y axis. The number of cells is limited to allow time-dependent calculations with DALTON in a reasonable calculational time. The model therefore consists of 220932 (57x57x68) cells.

The structure of the MYRRHA geometry in DALTON is shown via a vertical cut (y=0 cm) in Fig. B.1. The reactor modelling at different heights is shown in Fig. B.2.

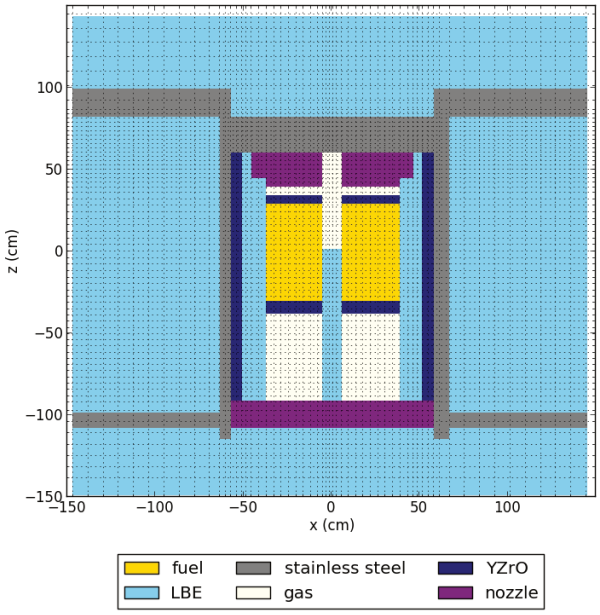

Figure B.1: Vertical cut (y=0 cm) through the MYRRHA model. The gridlines on the plot correspond to the cells of the model.

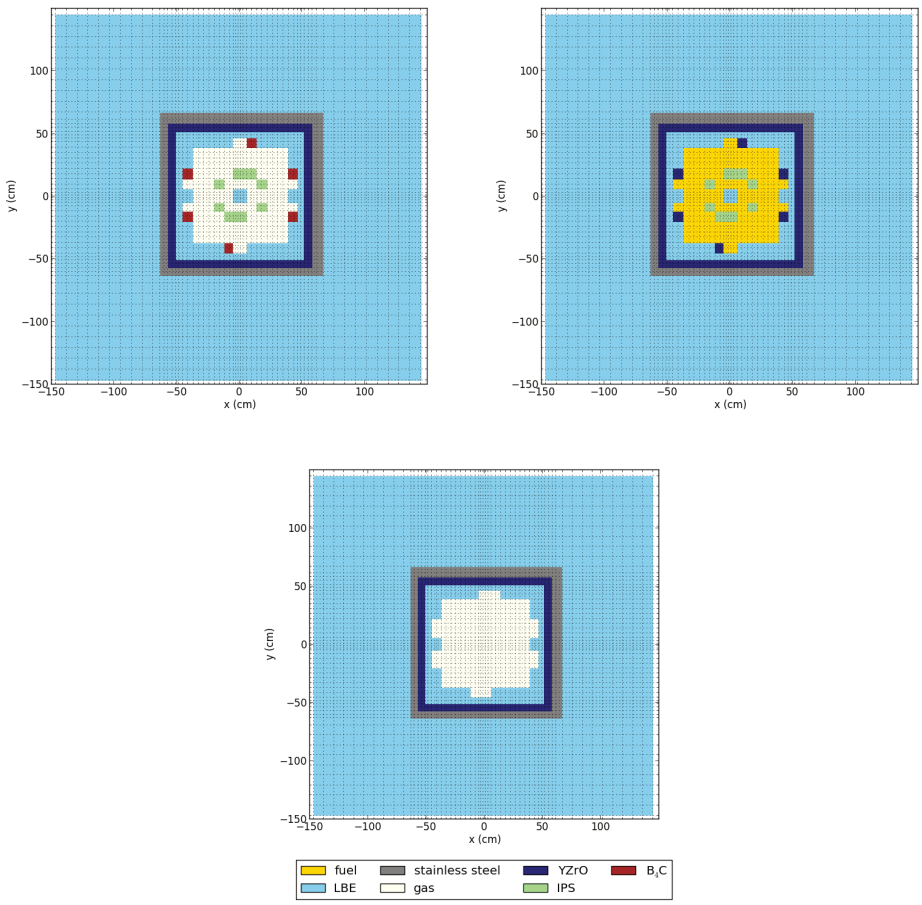

Figure B.2: Horizontal cut at different heights through the MYRRHA model for calculations in DALTON: z=-58 cm (top figure), z=0 cm(middle figure) and z=39 cm (bottom figure). The gridlines on the plot correspond to the cells of the model.

B.2 Cross Section Generation

The cross sections of MYRRHA used for DALTON calculations are calculated similar to the ones used for MYRRHA determistic calculations in [Sarotto et al., 2013]. The ECCO module of ERANOS [Rimpault, 2002] is used. Similar homogenisation of the reactor materials is used as presented in [Sarotto, 2012].

For DALTON a condensation into 6 energy groups is performed, in order to reduce the calculational time (for time dependent calculations in particular). The structure of the 6 energy groups is made similarly to VENUS, as shown in Table A.1, seen the consistency in neutron spectra between VENUS-F and MYRRHA (see [Krasa, 2013]).

Sensitivity checks are carried out on the group boundaries, and comparison with probabilistic MCNP calculations is done for the MYRRHA BOL core. Whereas for the MYRRHA BOL core, k_{eff}=0.95375 is found, MCNP (v1.4 of the MYRRHA input file, see [Stankovskiy and Malambu, 2011]) provides k_{eff}=0.96436.

C

List of Abbreviations

ADONIS	Accelerator Driven Operated New Irradiation System
ADS	Accelerator-Driven System
BARC	Bhaba Atomic Research Centre
BOC	Beginning-Of-Cycle
BOL	Beginning-Of-Life
BWR	Boiling Water Reactor
CAS	Chinese Academy of Science
CDT	Central Design Team
CIAE	Chinese Institute of Atomic Energy
CLEAR	China LEad Alloy cooled Reactor
CPSD	Cross Power Spectral Density
CR	Control Rod
CTF	Current-To-Flux
CZP	Cold Zero Power
EFIT	European Fast Industrial Transmuter
EOC	End-Of-Cycle
ESFRI	European Strategy Forum on Research Infrastructure
FA	Fuel Assembly
FASTEF	FAst Spectrum Transmutation Experimental Facility
FEED	Front End Engineering Design

FR	Fast Reactor
FREYA	Fast Reactor Experiments for hYbrid Applications
GUINEVERE	Generator of Uninterrupted Intense NEutrons at the VEnus REactor
HFP	Hot Full Power
HLM	Heavy Liquid Metal
IPS	In-Pile Section
ISJ	Integrated Source Jerk
KIPT	Kharkov Institute of Physics and Technology
LBE	Lead-Bismuth Eutectic
MA	Minor Actinides
MCNP	Monte Carlo N-Particle
MIRT	MYRRHA International Review Team
MOX	Mixed OXide
MSM	Modified Source Multiplication
MTA	Material Testing Accelerator
MUSE	MUltiplication avec Source Externe
MYRRHA	Multi-purpose hYbrid Research Reactor for High-tech Applications
NEA	Nuclear Energy Agency
PE	PolyEthylene
PEAR	PEllet Absorber Rod
PNS	Pulsed Neutron Source
SCF	Spatial Correction Factor
SCK•CEN	StudieCentrum voor Kernenergie - Centre d'étude de l'Energie Nucléaire
SJ	Source Jerk
SNETP	Sustainable Nuclear Energy Technology Platform
SR	Safety Rod
TH	THermal (detector)
THR	THReshold (detector)

REFERENCES

S. Andriamonje, A. Angelopoulos, A. Apostolakis, F. Attale, L. Brillard, S. Buono, J. Calero, F Carminati, F . Casagrande, P. Cennini, S. Charalambous, R. Del Moral, C . Eleftheriadis, E . Gallego, J. Galvez, L. Garcia-Tabares, C. Geles, I. Goulas, A . Giorni, E. Gonzalez, M. Hussonnois, J. Jaren, R. Klapisch, P. Kokkas, F . Lemeilleur, G . Lindecker, A . Liolios, J.M. Loiseaux, C. Lopez, A. Lorente, M. Macri, J.M. Martinez-Val, H. Nifenecker, J. Oropesa, P. Pavlopoulos, J.A. Pinston, J-P. Revol, C. Roche, C. Rubbia, J .A. Rubio, K. Sakelariou, L . Sakelliou, F . Saldana, F . Schussler, J. Tarnarit, D. Trubert, J.B. Viano, S. Vieira, S. Vlachos, Xuan Li, and G. Zarris. Experimental determination of the energy generated in nuclear cascades by a high energy beam. *Phys. Lett. B*, 348:697–709, 1995.

B. Ariën. Determination of the required anti-reactivity margin for the reference core 1.4 of MYRRHA for both critical and subcritical operation. Technical Report 3583712, SCK-CEN, 2014.

H. Arnould, C.A. Bompas, R. Del Moral, V. Lacoste, V. Vlachoudis, J. Aleixandre, J. Bueno, E. Cerro, O. Gonzalez, J. Tamarit, S. Andriamonje, D. Brozzi, S. Buono, F. Carminati, F. Casagrande, P. Cennini, J.I. Collar, L. Dumps, C. Geles, I. Goulas, R. Fernandez, Y. Kadi, R. Klapisch, J. Oropesa, A. Placci, J.-P. Revol, C. Rubbia, J.A. Rubio, F. Saldana, M. Embid, J. Galvez, C. Lopez, E. Perez-Enciso, M. Poza, C. Sirvent, S. Vieira, A. Abanades, J. Garcia, J.M. Martinez-Val, M. Perlado, E. Gonzalez, M. Hussonnois, C. Le Naour, D. Trubert, E. Belle, A. Giorni, D. Heuer, J.M. Loiseaux, O. Meplan, H. Nifenecker, F. Schussler, J.B. Viano, A. Angelopoulos, A. Apostolakis, P. Karaiskos, L. Sakelliou, P. Kokkas, P. Pavlopoulos, C. Eleftheriadis, G. Kitis, I. Papadopoulos, E. Savvidis, A. Tzima, K. Zioutas, S. Diez, and A. Perez-Navarro. Experimental verification of neutron phenomenology in lead and transmutation by adiabatic resonance crossing in accelerator driven systems. *Phys. Lett. B*, 458:167–180, 1999.

C. Artioli, X. Chen, F. Gabrielli, G. Glinatsis, P. Liu, W. Maschek, C. Petrovich, A. Rineiski, M. Sarotto, and M. Schikorr. Minor Actinide Transmutation in ADS: the EFIT Core Design. In *International Conference of the Physics of Reactors, Nuclear Power: A Sustainable Resource (PHYSOR'08), Interlaken, Switzerland*, 2008.

H. Aït Abderrahim and P. Baeten. MYRRHA: a Multi-purpose hYbrid Research Reactor for High-tech Applications. In *Proceedings of PHYSOR2012 - Advances in Reactor Physics - Knoxville (TN), USA, April 15-20, 2012*, 2012.

H. Aït Abderrahim, A. Al Mazouzi, B. Arien, P. Baeten, D. De Bruyn, M. Dierckx, J. Heyse, E. Malambu, K. Rosseel, P. Schuurmans, V. Sobolev, G. Van den Eynde, S. Van Dyck, K. Van Tichelen, and M. Verwerft. MYRRHA Technical Description (for the OECD MYRRHA Review Team). Technical report, SCK•CEN, 2008.

H. Aït Abderrahim, P. Baeten, D. De Bruyn, and R. Fernandez. MYRRHA - A Multi-purpose Fast Spectrum Research Reactor. *Energy Conversion and Management*, 63:4–10, 2012.

P. Baeten. Heuristic derivation of the Rossi-alpha formula for a pulsed neutron source. *Annals of Nuclear Energy*, 31/1:43–53, 2003.

P. Baeten, R. Brissot, Y. Rugama, A. Billebaud, C. Le Brun, E. Liatard, J. Vollaire, and C. Destouches. Analytical Investigation and Experimental Application of the Source Modulation Technique to measure $\frac{\rho}{\beta_{eff}}$. *Progress in Nuclear Energy*, 48:550–558, 2006.

P. Baeten, H. Aït Abderrahim, G. Bergmans, J. Heyse, D. Maes, B. Verboomen, F. Vermeersch, G. Vittiglio, G. Ban, M. Baylac, A. Billebaud, D. Bondoux, J. Bouvier, J.-M. De Conto, P. Dessagne, G. Gaudiot, J.-M. Gautier, D. Grondin, G. Heitz, M. Kerveno, B. Laune, F.-R. Lecolley, J.-L. Lecouey, D. Marchand, N. Marie, Y. Merrer, R. Micoud, M. Planet, D. Reynet, C. Ruescas, J.-C. Steckmeyer, G. Granget, F. Mellier, G. Rimpault, and T. Aoust. The GUINEVERE Project at the VENUS Facility. In *Proceedings of the International Conference on the PHYSics Of Reactors (PHYSOR2008), Interlaken, Switzerland*, 2008.

L.H. Baetslé. Application of Partitioning/Transmutation of Radioactive Materials in Radioactive Waste Management. In *Workshop on Hybrid Nuclear Systems for Energy Production, Utilisation of Actinides and Transmutation of Long-lived Radioactive Waste, Trieste, September 3-7*, 2001.

G.A. Bartholomew and P.R. Tunnicliffe. The AECL Study for an Intense Neutron Generator. Technical Report Report No. AECL-2600, Atomic Energy of Canada Limited, 1966.

M. Baylac, H. Aït Abderrahim, P. Baeten, P.-B. Bard, A. Billebaud, G. Bergmans, P. Boge, D. Bondoux, J. Bouvier, T. Cabanel, Y. Carcagno, G. Dargaud, J.-M. De Conto, P. Desrues, E. Froidefond, G. Gaudiot, J.-M. Gautier, Y. Gómez, G. Granget, G. Heitz, M. Heusch, B. Laune, D. Marchand, F. Mellier, Y. Merrer, R. Micoud, E. Perbet, M. Planet, P. Poussot, D. Reynet, C. Ruescas, D. Tourrès, D. Vandeplassche, F. Vermeesch, and G. Vittiglio. The GENEPI-3C Accelerator for the GUINEVERE Project. In *Proceedings of International Topical Meeting on Nuclear Research Applications and Utilization of Accelerators, Vienna, May 4-8*, 2010.

V. Becares and J. Blazquez. Detector dead time determination and optimal count rate for a detector near a spallation source or a subcritical mulitplying system. *Science and Technology of Nuclear Installations*, 2012, 2012.

V. Becares, D. Villamarin, M. Fernandez-Ordonez, E.M. Gonzalez-Romero, C. Berglof, V. Bournos, Y. Fokov, S. Mazanik, and I. Serafimovich. Validation of ADS reactivity monitoring techniques in the Yalina-Booster subcritical assembly. *Annals of Nuclear Energy*, 53:331–341, 2013.

G.I. Bell and S. Glasstone. *Nuclear Reactor Theory*. Van Nostrand Reinhold Company, 1970.

G.I. Bell and S. Glasstone. *Nuclear Reactor Theory*. Robert E. Krieger Publishing Company, Malabar, Florida, 1985.

C. Berglof, M. Fernandez-Ordonez, D. Villamarin, V. Becares, E.M. Gonzalez-Romero, V. Bournos, and J.-L. Munoz-Cobo. Auto-correlation and variance-to-mean measurements in a subcritical core obeying multiple alpha-modes. *Annals of Nuclear Energy*, 38:194–202, 2011.

F. Bianchi, C. Artioli, K.W. Burn, G. Gherardi, S. Monti, L. Mansani, L. Cinotti, D. Struwe, M. Schikorr, W. Maschek, H. Aït Abderrahim, D. De Bruyn, and G. Rimpault. Status and Trend of Core Design Activities for Heavy Metal Cooled Accelerator-Driven Systems. *Energy Conversion and Management*, 47(17):2698–2709, 2006.

G. Bianchini, M. Carta, F. Pisacane, M. Frisoni, and V. Peluso. Set-up of a Deterministic Model for the Analysis of the GUINEVERE Experience. In *Proceedings*

of the International Conference on the PHYSics Of Reactors (PHYSOR2010) - Advances in Reactor Physics to Power the Nuclear Renaissance, Pittsburgh, Pennsylvania, USA, May 9-14, 2010.

A. Billebaud, R. Brissot, C. Le Brun, E. Liatard, and J. Vollaire. Prompt multiplication factor measurements in subcritical systems: from MUSE experiment to a demonstrator ADS. *Progress in Nuclear Energy*, 49:142–160, 2009.

A. Billebaud, J.-L. Lecouey, G.Ban, S.Chabod, F.-R. Lecolley, N.Marie, H.-E.Thyébault, and J.-C.Steckmeyer. GENEPI-3C Neutron Source Monitoring. Technical Report GUI-SPE-2.2-0001-LPSC, v.1, CNRS, 2010.

P. Blaise, F. Mellier, and P. Fougeras. Application of the Modified Source Multiplication (MSM) Technique to Subcritical Reactivity Worth Measurements in Thermal and Fast Reactor Systems. *IEEE Transactions on Nuclear Science*, 58(3): 1166–1176, 2011.

B. Boer, D. Lathouwers, M. Ding, and J.-L. Kloosterman. Coupled Neutronics/Thermal Hydraulics Calculations for High Temperature Reactors with the DALTON-THERMIX Code Systems. In *Proceedings of the International Conference on the PHYSics Of Reactors (PHYSOR2008), Interlaken, Switzerland*, 2008.

B. Boer, D. Lathouwers, J.-L. Kloosterman, T.H.J.J. van der Hagen, and G. Strydom. Validation of the DALTON-THERMIX Code System with Transient Analysis of the HTR-10 and Application to the PBMR. *Nuclear Technology*, 170(2):306–321, 2010.

Brookhaven National Laboratory. An introduction to PHENIX, www.phenix.bnl.gov, 2013.

Y. Cao and J.C. Lee. Spatial Corrections for Pulsed-Neutron Reactivity Measurements. *Nuclear Science and Engineering*, 165:270–282, 2010.

M. Carta and A. D'Angelo. Subcriticality-Level Evaluation in Accelerator-Driven Systems by Harmonic Modulation of the External Source. *Nuclear Science and Engineering*, 133:282–292, 1999.

S. Chabod, A. Billebaud, F.-R. Lecolley, J.-L. Lecouey, G. Lehaut, N. Marie, G. Ban, X. Doligez, A. Kochetkov, P. Baeten, A. Krasa, W. Uyttenhove, G. Vittiglio, and

J. Wagemans. Reactivity measurements at GUINEVERE facility using the integral k_p method. In *International Conference on the PHYSics Of Reactors (PHYSOR2014), Kyoto, Japan*, 2014.

N. Chauvin, S. Bejaoui, J.-M. Beonnerot, F. Delaga, G. Martin, V. Bouineau, M. Pelletier, and L. Buiron. Minor Actinide Fuels for Fast Reactor: Qualification. In *Heraeus Seminar, Bad Honeff, Germany, December 5-8*, 2011.

T. Chevret. Private e-mail communication, october 13, 2014a.

T. Chevret. Reactivity measurement using beam interruption experiments: influence of the reactor surroundings and latest results. In *FREYA WP1 Meeting, Grenoble (France), October 30-31*, 2014b.

T. Chevret, J.-L. Lecouey, N. Marie, F.-R. Lecolley, G. Lehaut, G. Ban, A. Billebaud, S. Chabod, X. Doligez, A. Kochetkov, P. Baeten, W. Uyttenhove, G. Vittiglio, J. Wagemans, F. Mellier, V. Bécares, and D. Villamarin. Reactivity Measurement of the Lead Fast Subcritical VENUS-F Reactor using Beam Interruption Experiments. In *Proceedings of the International Conference on the PHYSics Of Reactors (PHYSOR2014), Kyoto, Japan*, 2014.

D. De Bruyn and R. Fernandez. The Fast-spectrum Transmutation Experimental Facility FASTEF: Main Design Achievements (Part 1: Core & Primary System) within the FP7-CDT Project of the European Commission. In *ICAPP12, Chicago, USA, June 24-28,*, 2012.

S.B. Degweker, P. Satyamurthy, P.K. Nema, and P. Singh. Program of Development of Accelerator-Driven Systems in India. In *Technical Meeting on the Use of Low-Enriched Uranium in Accelerator-Driven Systems, IAEA, Vienna, February 4-8*, 2013.

X. Doligez, A. Billebaud, S. Chabod, T. Chevret, D. Fourmentel, A. Krasa, A. Kochetkov, F.-R. Lecolley, J.-L. Lecouey, G. Lehaut, N. Marie-Nourry, F. Mellier, G. Vittiglio, and J. Wagemans. Effective delayed neutron fraction measurement in the critical VENUS-F reactor using noise techniques. In *Proceedings of the Int. Conf. on Advancements in Nuclear Instrumentation, Measurement Methods and their Applications: ANIMMA, Lisbon, Portugal, April 20-25*, 2015.

J. J. Duderstadt and L. J. Hamilton. *Nuclear Reactor Analysis*. John Wiley and Sons, 1976.

S. Dulla, P. Ravetto, M.M. Rostagno, G. Bianchini, M. Carta, and A. D'Angelo. Some Features of Spatial Neutron Kinetics for Multiplying Systems. *Nuclear Science and Engineering*, 149:88–100, 2005.

S. Dulla, P. Picca, P. Ravetto, D. Tomatis, and M. Carta. Integral Parameters in Source-driven Systems. *Progress in Nuclear Energy*, 53:32–40, 2011.

S. Dulla, M. Nervo, P. Ravetto, G. Mila, S. Argirò, S. Beolè, M. Masera, G. Bianchini, M. Carta, V. Fabrizio, V. Peluso, F. Gabrielli, A. Rineiski, A. Kochetkov, P. Baeten, W. Uyttenhove, G. Vittiglio, and J. Wagemans. Interpretation of Experimental Measurements on the SC-1 Configuration of the VENUS-F Core. In *Proceedings of the International Conference on the PHYSics Of Reactors (PHYSOR2014), Kyoto, Japan*, 2014.

ESFRI. Strategy Report on Research Infrastructures, Roadmap 2010. Technical Report ISBN 978-92-79-16828-4, European Strategy Forum on Research Infrastructures, European Commission, 2010.

A. Gandini and M. Salvatores. The Physics of Subcritical Multiplying Systems. *Journal of Nuclear Science and Technology*, 6:673–686, 2002.

E. Garelis and J.L. Russell. Theory of Pulsed Neutron Source Measurements. *Nuclear Science and Engineering*, 16:263–270, 1963.

Y. Gohar. National and International Accelerator-Driven System Activities for Nuclear Energy. In *Project X Collaboration Meeting, Lawrence Berkeley National Laboratory, April 10-12*, 2012.

Y. Gohar and D. L. Smith. YALINA Facility: A Sub-Critical Accelerator-Driven System (ADS) for Nuclear-Energy Research Facility Description and an Overview of the Research Program (1997-2008). Technical Report ANL-10/05, Argonne National Laboratory, 2010.

W. Gudowski. Accelerator-driven Transmutation Projects. The Importance of Nuclear Physics Research for Waste Transmutation. *Nuclear Physics A*, 654: 436–457, 1999.

IAEA. Advanced reactor technology options for utilization and transmutation of actinides in spent nuclear fuel. IAEA-TECDOC-1626 ISBN 978-92-0-109309-7, International Atomic Energy Agency, 2009a.

IAEA. *Status of Minor Actinide Fuel Development*. Number NF-T-4.6. International Atomic Energy Agency, Nuclear Energy Series, 2009b.

J.A. Thie. *Reactor Noise*. Rowman and Littlefield, 1963.

C. Jammes, B. Geslot, and G. Imel. Advantage of the Area Ratio Pulsed Neutron Source Technique for ADS Reactivity Calibration. *Nuclear Instruments and Methods in Physics Research A*, 562:778–784, 2006.

Y. Kadi and J.P. Revol. *Design of an Accelerator-Driven System for the Destruction of Nuclear Waste*, volume 12 of *ICTP Lecture Notes Series*, pages 88–132. 2002.

S. Keyers. Considerations for the Design of a Spallation Target Window - From Windowless Loop to Loopless Window. Technical Report I-185, SCK•CEN, 2010.

J.L. Kloosterman, Y. Rugama, M. Szieberth, and C. Destouches. Measurement and calculation of control rod worths in MASURCA. In *Proceedings of the International Conference on the PHYSics Of Reactors (PHYSOR2002), Seoul, Korea*, 2002.

J. Knebel. Integrated Project EUROTRANS: EUROpean research programme for the TRANSmutation of high level nuclear waste in an accelerator driven system (Contract FI6W-CT-2004-516520). In *Proceedings FISA, Luxemburg, March 13-16*, 2006.

A. Kochetkov. Fast Reactor Experiments for hYbrid Applications (FREYA), European Commission 7th Framework Programme Project 269665. Technical report, 2010.

A. Kochetkov. Source Jerk Integral Method - WP1 Summary Results. In *FREYA WP1 Meeting, Grenoble (France), October 30-31*, 2014.

A. Kochetkov, P. Baeten, A. Billebaud, S. Chabod, X. Doligez, F.-R. Lecolley, J.-L. Lecouey, G. Lehaut, N. Marie, H.-E. Thyébault, W. Uyttenhove, J. Wagemans, G. Ban, P. Dessagne, M. Kerveno, and L. Mercatali. Current Progress and Future Plans of the FREYA Project. In *Technology and Components of Accelerator-Driven Systems TCADS, Second International Workshop, Nantes, France, 21-23 May*, 2013.

A. Kochetkov, P. Baeten, W. Uyttenhove, G. Vittiglio, J. Wagemans, A. Bilebaud, S. Chabod, J.-L. Lecouey, G. Ban, F.-R. Lecolley, N. Marie, G. Lehaut, X. Doligez,

and F. Mellier. An alternative source jerk method implementation for the subcriticality estimation of the VENUS-F subcritical core in the FREYA project. In *Proceedings of the International Conference on the PHYSics Of Reactors (PHYSOR2014), Kyoto, Japan, September 28 - October 3*, 2014.

A. Krasa. New candidate configurations of MYRRHA-like VENUS-F cores. In *FREYA WP2 technical meeting, Brussels, Belgium, November 13*, 2013.

A. Krasa, A. Kochetkov, P. Baeten, W. Uyttenhove, G. Vittiglio, and J. Wagemans. Axial traverses in CR0, SC1 with long and short thimble. In *FREYA WP1 technical meeting, Grenoble, France, October 30-31*, 2014.

KUCA. The Kyoto University Critical Assembly, http://www.rri.kyoto-u.ac.jp/CAD/english/, 2013.

J.-L. Lecouey. Recommended value for ρ(SC1) and related business. In *FREYA WP1 Meeting, Grenoble (France), October 30-31*, 2014.

J.-L. Lecouey, A. Kochetkov, A. Krasa, P. Baeten, V. Bécares, A. Billebaud, S. Chabod, T. Chevret, X. Doligez, F.-R. Lecolley, G. Lehaut, N. Marie, F. Mellier, W. Uyttenhove, D. Villamarin, G. Vittiglio, and J. Wagemans. Monte Carlo MSM Correction Factors for Control Rod Worth Estimates in Subcritical and Near-critical Fast Neutron Reactors. In *ICAPP 2015, Nice, France, May 3-6*, 2015a.

J.-L. Lecouey, N. Marie, G. Ban, A. Billebaud, S. Chabod, A. Kochetkov, F.-R. Lecolley, G. Lehaut, F. Mellier, H.-E. Thyébault, W. Uyttenhove, C. Van Grieken, and G. Vittiglio. Estimate of the Reactivity of the VENUS-F Subcritical Configuration using a Monte Carlo MSM Method. *Annals of Nuclear Energy*, 83:65–75, 2015b.

R.B. Lehoucq, D.C. Sorensen, and C. Yang. *ARPACK Users' Guide, Solution of Large-Scale Eigenvalue Problems by Implicitly Restarted Arnoldi Methods*. Society of Industrial and Applied Mathematics, Philadelphia, 1998.

E. Malambu and A. Stankovskiy. Proposals for MYRRHA core configurations with 30 at% (Pu-Am)-enriched MOX fuel. Technical Report I-260, SCK•CEN, 2012.

L. Mansani, C. Artioli, M. Schikorr, G. Rimpault, C. Angulo, and D. De Bruyn. The designs of an experimental ADS facility (XT-ADS) and of a European Industrial Transmutation Demonstrator (EFIT). In OECD, editor, *Proceedings of the Conference on Technology and Components of Accelerator-Driven Systems (TCADS)*, number ISBN 978-92-64-11727-3, 2011.

N. Marie, G. Lehaut, J.-L. Lecouey, A. Billebaud, S. Chabod, X. Doligez, F.-R. Lecolley, A. Kochetkov, W. Uyttenhove, G. Vittiglio, J. Wagemans, F. Mellier, G. Ban, H.-E. Thyébault, and D. Villamarin. Reactivity Monitoring Using the Area Method for the Subcritical VENUS-F Core within the Framework of the FREYA Project. In *Technology and Components of Accelerator-Driven Systems (TCADS), Second International Workshop, Nantes, France, May 21-23*, 2013.

MCNP Team. MCNP 5.1.40 RSICC Release Notes. Technical Report LA-UR-05-8617, Los Alamos National Laboratory, November 2005.

F. Mellier. The MUSE Experiments for Subcritical Neutronics Validation. Final Report Deliverable 8, FP5 MUSE Project, FIKW-CT-2000-0063, CEA Cadarache, 2005.

L. Mercatali, A. Serikov, P. Baeten, W. Uyttenhove, A. Lafuente, and P. Teles. Design Study of a Fast Spectrum Zero-power Reactor dedicated to Source-driven Subcritical Experiments. *Energy Conversion and Management*, 51:1818–1825, 2010.

NEA. Accelerator-Driven Systems (ADS) and Fast Reactors (FR) in Advanced Nuclear Fuel Cycles. Technical Report 3109, Nuclear Energy Agency, 2003.

H. Nifenecker, S. David, J.-M. Loiseaux, and O. Meplan. Basics of Accelerator-driven Subcritical Reactors. *Nuclear Instruments and Methods in Physics Research A*, 463:428–467, 2001.

H. Nifenecker, O. Meplan, and S. David. *Accelerator Driven Subcritical Reactors*. Number ISBN 0-7503-0743-9. Institute of Physics Publishing Ltd, 2003.

OECD/NEA. Independent Evaluation of the MYRRHA Project. Technical Report ISBN 978-92-64-99114-9, NEA no. 6881, The OECD Nuclear Energy Agency, 2009.

K.O. Ott and R.J. Neuhold. *Introductory Nuclear Reactor Dynamics*. American Nuclear Society, 1985.

A. Pautz and A. Birkhofer. DORT-TD: A Transient Neutron Transport Code with Fully Implicit Time Integration. *Nuclear Science and Engineering*, 145:299–319, 2003.

D.B. Pelowitz. MCNPX 2.7.A Extensions. Technical Report LA-UR-08-07182, Los Alamos National Laboratory, 2008.

D.B. Pelowitz. MCNPX 2.7.0 Extensions. Technical Report LA-UR-11-02295, Los Alamos National Laboratory, 2011.

F. Perdu, J.-M. Loiseaux, A. Billebaud, R. Brissot, D. Heuer, C. Lebrun, E. Liatard, O. Meplan, E. Merle, H. Nifenecker, and J. Vollaire. Prompt reactivity determination in a subcritical assembly through the response to a dirac pulse. *Progress in Nuclear Energy*, 42:107–120, 2003.

C.-M. Persson, P. Seltborg, A. Ahlander, W. Gudowki, T. Stummer, H. Kiyavitskaya, V. Bournos, Y. Fokov, I. Serafimovich, and S. Chigrinov. Analysis of Reactivity Determination Methods in the Subcritical Experiment YALINA. *Nuclear Instruments and Methods in Physics Research A*, 554:374–383, 2005.

C.H. Pyeon. Status of Research and Development of Accelerator-Driven Systems and Nuclear Transmutation Technology in Asian Countries. Technical Report ISSN 1349-7960, Research Reactor Institute, Kyoto University, 2013.

G. Rimpault. The ERANOS code and data system for fast reactor neutronic analyses. In *Proc. PHYSOR 2002, Seoul, South-Korea*, 2002.

C. Rubbia, J.A. Rubio, S. Buono, F. Carminati, N. Fiétier, J. Galvez, C. Gelès, Y. Kadi, R. Klapisch, P. Mandrillon, J.-P. Revol, and Ch. Roche. Conceptual Design of a Fast Neutron Operated High Power Energy Amplifier. Technical Report CERN/AT/95-44 (ET), CERN, 1995.

M. Salvatores, I. Slessarev, and M. Uematsu. A Global Physics Approach to Transmutation of Radioactive Nuclei. *Nuclear Science and Engineering*, 116:1–18, 1994.

P. Saracco, S. Dulla, and P. Ravetto. On the spectrum of the multigroup diffusion equations. *Progress in Nuclear Energy*, 59:86–95, 2012.

M. Sarotto. Critical Core Design of MYRRHA-FASTEF: Refinement of Shutdown Systems and Neutronic Characterisation of the Equilibrium Sub-Cycle Core. CDT Task 2.2 REP007-2011, ENEA, 2011.

M. Sarotto. FASTEF design changes to operate in critical mode. CDT/FASTEF Deliverable 2.2, ENEA, 2012.

M. Sarotto, D. Castelliti, R. Fernandez, D. Lamberts, E. Malambu, A. Stankovskiy, W. Jaeger, M. Ottolini, F. Martin-Fuertes, L. Sabathé, L. Mansani, and P. Baeten.

The MYRRHA-FASTEF cores design for critical and sub-critical operational modes (EU FP7 Design Team Project). *Nuclear Engineering and Design*, 265: 184–200, 2013.

B.E. Simmons and J.S. King. A Pulsed Neutron Technique for Reactivity Determination. *Nuclear Science and Engineering*, 3:595–608, 1958.

N.G. Sjöstrand. Measurements on a Subcritical Reactor using a Pulsed Neutron Source. *Arkiv för Fysik*, 11, 13, 1956.

SNETP. Strategic Research and Innovation Agenda. Technical report, Sustainable Nuclear Energy Technology Platform, www.snetp.eu, 2013.

V. Sobolev, B. Boer, M. Verwerft, S. Keijers, W. Lowet, R. Fernandez, and A. Woaye-Hune. Preliminary Design and Specifications for MYRRHA Driver Fuel. SCK•CEN Technical Report R-5151, SCK•CEN, 2011a.

V. Sobolev, W. Uyttenhove, R. Thetford, and W. Maschek. Prognosis and Comparison of Composite CERCER and CERMET Fuels dedicated to Transmutation of TRU in an EFIT ADS. *Journal of Nuclear Materials*, 414:257–264, 2011b.

R. Soule, W. Assal, P. Chaussonnet, C. Destouches, C. Domergue, C. Jammes, J.-M. Laurens, J.-F. Lebrat, F. Mellier, G. Perret, G. Rimpault, H. Servière, G. Imel, G.M. Thomas, D. Villamarin, E. Gonzalez-Romero, M. Plaschy, R. Chawla, J.-L. Kloosterman, Y. Rugama, A. Billebaud, R. Brissot, D. Heuer, M. Kerveno, C. Le Brun, E. Liatard, J.-M. Loiseaux, O. Méplan, E. Merle, F. Perdu, J. Vollaire, and P. Baeten. Neutronic Studies in Support of Accelerator-Driven Systems: the MUSE Experiments in the MASURCA Facility. *Nuclear Science and Engineering*, 148:124–152, 2004.

A. Stankovskiy and E. Malambu. Myrrha bol reference core (v1.4, september 30, 2011). MCNPX Input File, September 2011.

R.E. Uhrig. *Random Noise Techniques in Nuclear Reactor Systems*. Ronald Press, 1956.

W. Uyttenhove. VENUS-F Re-Evaluation of 4 Typical Cores for the Envelope Parameters. Technical report, SCK•CEN, July 5 2012.

W. Uyttenhove. GUINEVERE: Experimental Programme - C/E Analysis of the VENUS-F Critical Core Characterisation Experiments. Technical Report R-5425, SCK•CEN, 2013.

W. Uyttenhove and A. Krasa. Status of the Analysis of Current-to-Flux Monitor Data. In *FREYA WP1 Data Analysis Meeting, October 1-2, CNRS Caen, France*, 2013.

W. Uyttenhove and J.-C. Steckmeyer. VENUS-F MCNP(X) Input File, Version 8, February 2014.

W. Uyttenhove and G. Van den Eynde. Physics of Subcritical Systems: Transposition towards a Full-scale ADS. In *Atelier GEDEPEON, Paris, France, July 5-6*, 2012.

W. Uyttenhove, P. Baeten, and A. Kochetkov. GUINEVERE: Experimental Programme - Description of the VENUS-F Reactor for Neutronics Calculations. Technical Report R-4914, SCK•CEN, December 2009.

W. Uyttenhove, P. Baeten, G. Van den Eynde, A. Kochetkov, D. Lathouwers, and M. Carta. The Neutronic Design of a Critical Lead Reflected Zero-power Reference Core for On-line Subcriticality Measurements in Accelerator-Driven Systems. *Annals of Nuclear Energy*, 38:1519–1526, 2011a.

W. Uyttenhove, V. Sobolev, and W. Maschek. Optimisation of Composite Metallic Fuel for Minor Actinide Transmutation in an Accelerator-Driven System. *Journal of Nuclear Materials*, 416:291–299, 2011b.

W. Uyttenhove, P. Baeten, G. Ban, A. Billebaud, S. Chabod, P. Dessagne, M. Kerveno, A. Kochetkov, F.-R. Lecolley, J.-L. Lecouey, N. Marie, F. Mellier, J.-C. Steckmeyer, H.-E. Thyébault, G. Vittiglio, and J. Wagemans. Experimental Results from the VENUS-F Critical Reference State for the GUINEVERE Accelerator Driven System Project. *IEEE Transactions on Nuclear Science*, 59(6):pp. 3194–3200, 2012a.

W. Uyttenhove, G. Van den Eynde, P. Baeten, A. Kochetkov, G. Vittiglio, J. Wagemans, D. Lathouwers, J.-L. Kloosterman, T.J.H.H. van der Hagen, F. Wols, A. Billebaud, S. Chabod, H.-E. Thyébault, J.-L. Lecouey, G. Ban, F.-R. Lecolley, N. Marie, J.-C. Steckmeyer, P. Dessagne, M. Kerveno, and F. Mellier. Detector Positioning for the Initial Subcriticality Level Determination in Accelerator-Driven Systems. In *Proceedings of the International Conference on the PHYSics Of Reactors (PHYSOR2012), Knoxville (TN), USA, April 15-20*, 2012b.

W. Uyttenhove, D. Lathouwers, J.-L. Kloosterman, T.H.J.J. van der Hagen, G. Van den Eynde, and P. Baeten. Methodology for Modal Analysis at Pulsed Neutron

Source Experiments in Accelerator-Driven Systems. *Annals of Nuclear Energy*, 72:286–297, 2014.

C.M. Van Atta. A brief history of the MTA Project. In *ERDA Information Meeting on Accelerator Breeding, January 19-29*, 1977.

G. Van den Eynde. XT-ADS Core Neutronics & Cycle Analysis. IP EUROTRANS Deliverable D1.34 & D1.35, SCK•CEN, March 2009.

G. Van den Eynde, H. Aït Abderrahim, and D. De Bruyn. Progress of the MYRRHA ADS Project in Belgium. In *OECD-NEA Exchange Meeting, Prague, September 25-27*, 2012.

G. Van den Eynde, E. Malambu, A. Stankovskiy, R. Fernandez, and P. Baeten. An Updated Core Design for the Multi-purpose Irradiation Facility MYRRHA. In *Proceedings of the International Conference on the PHYSics Of Reactors (PHYSOR2014), Kyoto, Japan*, 2014.

R. G. Vassylkov, V. I. Goldanskii, B. A. Pimenov, Yu. N. Pokotilovskii, and L. V. Chistyakov. Neutron multiplication in uranium bombarded with 300-660 MeV protons. *Sovjet Atomic Energy*, 44(4):377–383, 1978.

G. Verdu, D. Ginestar, V. Vidal, and J.-L. Munoz-Cobo. 3D λ-Modes of the Neutron-Diffusion Equation. *Annals of Nuclear Energy*, 21 (7):405–421, 1994.

L. Vermeeren. Personal communication. e-mail, May 2015.

Summary

This thesis provides a methodology and set-up of a reactivity monitoring tool for Accelerator-Driven Systems (ADS). The reactivity monitoring tool should guarantee the operation of an ADS at a safe margin from criticality. Robustness is assured in different aspects of the monitoring tool: the choice of the measurement techniques, the evaluation methods to derive the reactivity from experimental data, and the detector type and positioning.

In the first chapter of the work, the experience from previous research programmes (mainly MUSE and YALINA) is used to select appropriate experimental techniques for reactivity monitoring. A combination of three techniques is assessed to monitor reactivity: The Pulsed Neutron Source (PNS) technique (with the Integrated Source Jerk (ISJ) method as alternative) for start-up (until 1 % of nominal power) and the Current-to-Flux (CTF) combined with the Source Jerk (SJ) technique during ADS operation.

Static evaluation methods are used to derive the reactivity from the experimental value: the area method for start-up, the static CTF method during operation, and the static SJ method for the interim cross-checking of the ADS reactivity. These are more robust than dynamic evaluation techniques, as they do not depend on the knowledge of kinetic parameters. In the second chapter of this thesis, the spatial correction factors (SCFs) are defined that need to be applied on the reactivity values obtained by point kinetics. Via modal analysis, the SCFs are derived analytically for the selected evaluation methods.

Extensions are made to the existing DALTON diffusion code in order to perform modal analysis and time-dependent experiment simulations. In this way modal analysis helps to understand the behaviour of the simulated SCFs of the complete subcritical core.

In the third chapter the proposed reactivity monitoring methods are tested on the zero-power VENUS-F ADS. Thanks to the modular core, VENUS-F can operate in both critical and subcritical mode. The experimental reactivity results can therefore be compared to a value obtained by an alternative methodology, starting from a critical core. The experimental results confirm the modal analysis and experiment simulations. For both absolute reactivity measurement techniques (PNS area method and SJ method) SCF < 1, i.e. a safe overestimation of the absolute reactivity value, is found outside a sphere at the centre of the core with a

radius of about 20 to 25 cm, depending on the energy group. The SCF=1 location corresponds to the zero crossing of the first eigenfunction (different from the fundamental one) with a zero crossing outside the centre of the core.

The outer reflector is chosen as robust location for the detectors during start-up and interim cross-checking reactivity monitoring during operation, as in this zone SCF < 1 with a small spatial gradient. For the VENUS-F first subcritical core SC1, SCF_{area}=SCF_{SJ}=0.96-0.97 (depending on the detector type), which corresponds to an overestimation of $|\rho|$=3709 pcm by 111-148 pcm. Special attention should be paid to (local) thermalising elements, considerably influencing the SCF. This issue could be solved by the use of threshold detectors.

Finally, reactivity monitoring during operation in the MYRRHA ADS is studied in order to take into account the full-power aspects of reactivity monitoring. For the start-up reactivity monitoring and interim reactivity cross-checking MYRRHA behaves similar to VENUS concerning the SCFs for the evaluation methods. The (outer) reflector is therefore the recommended detector zone, preferably using threshold fission chambers as instrumentation.

For the simulation of reactivity monitoring during operation, MCNP is used as appropriate simulation tool to deal with the MYRRHA core inhomogeneities. The relative CTF monitor is evaluated between three stages of operation: the temperature feedback during core start-up (from 1 % nominal power on), the core enlargement during the first MYRRHA cores, and the burn-up during the MYRRHA equilibrium core.

Again, the MYRRHA outer reflector turns out to be a suitable detector location for reactivity monitoring also during operation, independent of the detector type. A safe (under)estimation of the absolute reactivity decrease is obtained for all stages of operation, except for the temperature feedback case. For practical reasons, only a limited number of detectors will be installed in the reflector. Therefore, a conservative boundary value of 500 pcm could be appropriate to take into account the locations with extreme SCFs, in case no re-calibration of the relative CTF monitor via the SJ method is possible.

As a conclusion, it is possible to measure the reactivity in an ADS by combining different experimental techniques. The accuracy of the reactivity monitor will depend on the safety function it has to fulfill and the related licensing requirements. If it is possible to perform short (in the order of hundreds of μs) reproducible accelerator beam interruptions with a stable beam restoration, the absolute re-

activity during operation can be determined via the SJ cross checking technique. In that case, the accuracy of the reactivity monitoring tool can be improved. The higher the accuracy, the higher the operational k_{eff} level, which is beneficial for the operational cost of an ADS.

Samenvatting

Dit proefschrift levert een methodologie en het ontwerp van een systeem om de reactiviteit van een Accelerator-Driven System (ADS) te monitoren. Dit systeem moet de veilige werking van een ADS garanderen, met een veilige marge om kritikaliteit te vermijden. De robuustheid van het systeem wordt verzekerd op verschillende vlakken: de keuze van de meettechnieken, de evaluatiemethodes om de reactiviteitswaarde af te leiden uit experimentele data, het type detectoren en hun locatie.

In het eerste hoofdstuk van het proefschrift wordt de ervaringsterugkoppeling van voorgaande onderzoeksprojecten (hoofdzakelijk de MUSE en YALINA projecten) gebruikt om geschikte experimentele technieken te selecteren voor reactiviteitsmonitoring. Een combinatie van drie technieken is hiervoor onderzocht: de gepulste neutronenbron (PNS) techniek (met de Integrated Source Jerk (ISJ) techniek als alternatief) voor de opstart (tot 1 % van het nominaal vermogen), en de Current-To-Flux (CTF) techniek gecombineerd met de Source Jerk (SJ) techniek tijdens de werking van het ADS.

Om de reactiviteit af te leiden uit de experimentele data worden statische evaluatiemethodes gebruikt: de oppervlaktemethode voor opstart, de statische CTF methode tijdens bedrijf, en de statische SJ methode voor het tussentijds controleren van de reactiviteit van het ADS. Deze methodes zijn meer robuust dan dynamische methodes, aangezien ze niet afhangen van de kennis van de kinetische parameters. In het tweede hoofdstuk van dit proefschrift worden de ruimtelijke correctiefactoren (SCFs) gedefinieerd die worden toegepast op de reactiviteitswaarden verkregen via de puntkinetiek. Via modale analyse worden de SCFs voor de geselecteerde evaluatiemethodes analytisch afgeleid.

De reeds bestaande DALTON code werd uitgebreid om modale analyse en tijdsafhankelijke simulaties van experimenten uit te voeren. Zo kan modale analyse helpen om het gedrag van de gesimuleerde SCFs te begrijpen in de volledige subkritische kern.

In het derde hoofdstuk worden de voorgestelde methodes voor reactiviteitsmonitoring getest op het nulvermogen VENUS-F ADS. Dankzij de modulaire kern kan VENUS-F in zowel kritische als subkritische toestand bedreven worden. Daardoor kunnen de experimentele reactiviteitswaarden vergeleken worden met een waarde verkregen via een alternatieve methodologie, die vertrekt van een kritische

kern. De experimentele waarden bevestigen de modale analyse en de simulatie van de experimenten. Voor beide methodes (PNS en SJ) die een absolute waarde van de reactiviteit opleveren wordt SCF < 1 (dit is een veilige overschatting van de absolute reactiviteitswaarde) verkregen buiten een bol in het centrum van de kern met een straal van 20-25 cm, afhankelijk van de energiegroep. De locatie waar SCF=1 komt overeen met de nuldoorgang van de eerste eigenfunctie met een nuldoorgang die niet in het centrum van de kern ligt (en verschillend van de fundamentele eigenfunctie).

De buitenste reflector wordt gekozen als robuuste detectorlocatie tijdens opstart en voor de tussentijdse reactiviteitscontrole tijdens bedrijf, aangezien in deze zone de SCF < 1 met een kleine ruimtelijke gradiënt. Voor de eerste subkritische VENUS-F kern SC1, is SCF_{area}=SCF_{SJ}=0.96-0.97 (afhankelijk van het type detector), wat overeenkomt met een overschatting van $|\rho|$=3709 pcm met 111-148 pcm. Speciale aandacht dient te worden besteed aan (lokale) thermaliserende elementen die de SCF aanzienlijk kunnen beïnvloeden. Deze kwestie kan opgelost worden door het gebruik van detectoren met een drempelwaarde.

Tot slot wordt de reactiviteitsmonitoring tijdens bedrijf van het MYRRHA ADS bestudeerd, om de aspecten met betrekking tot vol vermogen in rekening te brengen bij reactiviteitsmonitoring. Voor de opstart en de tussentijdse reactiviteitscontrole gedraagt MYRRHA zich zoals VENUS met betrekking tot de SCFs van de evaluatiemethodes. Daarom is de (buitenste) reflector de aangewezen zone voor de detectoren. Er worden bij voorkeur splijtingskamers met een drempelwaarde als instrumentatie gebruikt.

Voor de simulatie van de reactiviteitsmonitoring tijdens uitbating is MCNP gebruikt als simulatiecode, om de sterk inhomogene MYRRHA kern te modelleren. De relatieve CTF reactiveitsmonitoring wordt geëvalueerd tijdens drie fases in bedrijf: de temperatuursterugkoppeling tijdens opstart (vanaf 1 % nominaal vermogen), de kernvergroting tijdens de eerste MYRRHA kernen en de opbrand tijdens de MYRRHA equilibrium kern.

Opnieuw blijkt de buitenste reflector de aangewezen locatie voor de detectoren voor reactiviteitsmonitoring, ook tijdens bedrijf, onafhankelijk van het detectortype. Een veilige (onder)schatting van de daling van het absolute reactiviteitsniveau wordt voor alle uitbatingsfases verkregen, behalve voor de temperatuursterugkoppeling. Omwille van praktische redenen worden maar een beperkt aantal detectoren in de reflector geïnstalleerd. Daarom zou een conservatieve grenswaarde van 500 pcm geschikt kunnen zijn om rekening te houden met locaties

met extreme SCFs, in het geval geen hercalibratie van de relatieve CTF reactiviteitscontrole mogelijk is via de SJ methode.

Het blijkt mogelijk om de reactiviteit van een ADS te meten door verschillende experimentele technieken te combineren. De vereiste nauwkeurigheid van de reactiviteitsmonitoring hangt af van de veiligheidsfunctie van het systeem en van gerelateerde vereisten om een uitbatingslicentie te verkrijgen. Als het mogelijk is om korte (in de orde van honderden μs) repetitieve onderbrekingen van de deeltjesbundel van de accelerator uit te voeren met een stabiel herstel van de bundel, kan de absolute reactiviteit bepaald worden door tussentijdse controle via de SJ techniek. In dat geval kan de nauwkeurigheid van het reactiviteitsmonitoringsysteem verbeterd worden. Hoe hoger de nauwkeurigheid, hoe hoger het k_{eff} niveau tijdens bedrijf, wat voordelig is voor de exploitatiekost van een ADS.

Acknowledgements

Core

This thesis is realised thanks to the support of many people. First of all, I would like to thank Tim van der Hagen, the promotor of this work. Thanks to his constructive fundamental analysis mode during our monthly meetings, he was the efficient core manager of this work. Even after becoming dean of the Faculty of Applied Sciences, he continued to devote the necessary time to the management of this PhD work.

Secondly, the support of my copromotor Danny Lathouwers is invaluable. He focused my research scope into a strong (beam) line, and accelerated the daily management of this work by his computational and theoretical reactor physics knowledge. Finally, Jan-Leen Kloosterman provided the required coupling of both tools into a successful system by his all-round management, technical and moral support.

Back to the basics, the drivers of this work are at SCK•CEN, who I am grateful. They offered me the (financial) possibility to make a PhD in combination with a 'normal' job. Hamid Aït Abderrahim's mind created so many research questions in our institute, and Peter Baeten translated one of them into a precise PhD topic. It is a privilege to validate in this work theoretical calculations and simulations with unique experimental results.

An important acknowledgement goes to Gert Van den Eynde, my daily manager at SCK•CEN. Gert was a real mentor of this PhD. He reconciled the daily project work with the fundamental PhD research. He created the work environment to combine a PhD with the day-to-day job and patiently provided a continuous support.

Support

Thanks to the fruitful collaboration between TUDelft and SCK•CEN, my work was supported by many interesting and warm people in the field.

From TUDelft side, thanks go to Hugo van Dam and Eduard Hoogenboom for the interesting discussions, to the PhD and Postdoc colleagues for all kinds of support (Bart, Gertjan, Frank, Luca, Zoltan, Jozsef, Jurriaan, Valentina, Matteo, Denis, Sara, Aldo, Karo, Dimitrios), to the administrative support by Ine and Thea,

and to the other members of the NERA team (Martin, Peter, Dick, Norbert, ...) for all-round support.

At SCK•CEN, I am grateful for the support of my colleagues from the Nuclear System Physics group: Simon, Bart, Luca, Nadia, Edouard, Alexey, Alberto, Baudoin, Radu, David, Guy, Simone, Francesco, Dario, Diego, Tewfik, Camilla, Margot and Carine. Also the Research Reactor Operation group and the GUINEVERE and FREYA project teams helped me for this work via the experimental results.

SCK•CEN is a unique research institute where personal development is encouraged, thanks to the group of warm colleagues. Many of them supported me: colleagues from the train, administrative staff, the SCK•CEN Academy, the communication department and many more.

The outside world

Last but not least, I would like to thank my parents, family and friends for their continuous support in my life. They know what they mean to me without explanation.

Thank you!

List of Publications

Journal Publications

Main Author

- W. Uyttenhove, D. Lathouwers, J.-L. Kloosterman, T.H.J.J. van der Hagen, G. Van den Eynde, and P. Baeten. Methodology for Modal Analysis at Pulsed Neutron Source Experiments in Accelerator-Driven Systems. *Annals of Nuclear Energy*, 72: 286–297, 2014.
- W. Uyttenhove, P. Baeten, G. Ban, A. Billebaud, S. Chabod, P. Dessagne, M. Kerveno, A. Kochetkov, F.-R. Lecolley, J.-L. Lecouey, N. Marie, F. Mellier, J.-C. Steckmeyer, H.-E. Thyébault, G. Vittiglio, and J. Wagemans. Experimental Results from the VENUS-F Critical Reference State for the GUINEVERE Accelerator Driven System Project. *IEEE Transactions on Nuclear Science*, 59(6):pp. 3194–3200, **Invited Lecture at ANIMMA2011, Gent, Belgium**, 2012.
- W. Uyttenhove, P. Baeten, G. Van den Eynde, A. Kochetkov, D. Lathouwers, and M. Carta. The Neutronic Design of a Critical Lead Reflected Zero-power Reference Core for On-line Subcriticality Measurements in Accelerator-Driven Systems. *Annals of Nuclear Energy*, 38:1519–1526, 2011.
- W. Uyttenhove, V. Sobolev, and W. Maschek. Optimisation of Composite Metallic Fuel for Minor Actinide Transmutation in an Accelerator-Driven System. *Journal of Nuclear Materials*, 416:291–299, 2011.

Co-Author

- J.-L. Lecouey, N. Marie, G. Ban, A. Billebaud, S. Chabod, A. Kochetkov, F.-R. Lecolley, G. Lehaut, F. Mellier, H.-E. Thyébault, W. Uyttenhove, C. Van Grieken, and G. Vittiglio. Estimate of the Reactivity of the VENUS-F Subcritical Configuration using a Monte Carlo MSM Method. *Annals of Nuclear Energy*, 83:65–75, 2015.
- H. Imawoto, A. Stankovskiy, and W. Uyttenhove. Sensitivity and uncertainty analysis of the VENUS-F critical core. *Energy Procedia*, 71:33–41, 2015.
- V. Sobolev, W. Uyttenhove, R. Thetford, and W. Maschek. Prognosis and Comparison of Composite CERCER and CERMET Fuels dedicated to Transmutation of TRU in an EFIT ADS. *Journal of Nuclear Materials*, 414:257–264, 2011.
- L. Mercatali, A. Serikov, P. Baeten, W. Uyttenhove, A. Lafuente, and P. Teles. Design Study of a Fast Spectrum Zero-power Reactor dedicated to Source-driven Subcritical Experiments. *Energy Conversion and Management*, 51:1818–1825, 2010. *Oral Presentation at ICENES, Ericeira, Portugal June 29-July 3, 2009.*

Publications from Oral Presentations at International Conferences

Main Author

- W. Uyttenhove, P. Baeten, A. Kochetkov, G. Vittiglio, J. Wagemans, D. Lathouwers, J.-L. Kloosterman, T.H.J.J. van der Hagen, A. Billebaud, S. Chabod, F. Mellier, J.-L. Lecouey, F.-R. Lecolley, G. Lehaut, N. Marie, X. Doligez, M. Carta, V. Bécares, and D. Villamarin. Static Modal Analysis of the Current-to-Flux Subcriticality Monitor for Accelerator-Driven Systems. In *Proceedings of the International Conference on the PHYSics Of Reactors (PHYSOR2014), Kyoto, Japan*, 2014. **Best Paper Award.**
- W. Uyttenhove, P. Baeten, D. Lathouwers, J.-L. Kloosterman, A. Kochetkov, A. Krasa, G. Van den Eynde, T.H.J.J. van der Hagen, G. Vittiglio, and J. Wagemans. Reactivity Monitoring in Accelerator-Driven Systems. In *International Youth Nuclear Congress (IYNC), Burgos, Spain, July 6-12,*, 2014.
- W. Uyttenhove. Past and Future Activities on the VENUS Facility. In *Technical Meeting on Collaborative Work on Accelerator Driven Systems (ADS) and Use of Low-Enriched Uranium (LEU) in ADS, IAEA, Vienna, 4-7 February*, 2013.
- W. Uyttenhove, G. Van den Eynde, P. Baeten, A. Kochetkov, G. Vittiglio, J. Wagemans, D. Lathouwers, J.-L. Kloosterman, T.J.H.H. van der Hagen, F. Wols, A. Billebaud, S. Chabod, H.-E. Thyébault, J.-L. Lecouey, G. Ban, F.-R. Lecolley, N. Marie, J.-C. Steckmeyer, P. Dessagne, M. Kerveno, and F. Mellier. Detector Positioning for the Initial Subcriticality Level Determination in Accelerator-Driven Systems. In *Proceedings of the International Conference on the PHYSics Of Reactors (PHYSOR2012), Knoxville (TN), USA, April 15-20*, 2012.
- W. Uyttenhove and G. Van den Eynde. Physics of Subcritical Systems: Transposition towards a Full-scale ADS. In *Atelier GEDEPEON, Paris, France, July 5-6*, 2012.
- W. Uyttenhove and M. Carta. Challenges and Opportunities for modelling an Accelerator-Driven System with ERANOS. In *2nd ERANOS Users' Workshop , Aix-en-Provence, France, October 19-21*, 2009.

Co-Author

- J.-L. Lecouey, A. Kochetkov, A. Krasa, P. Baeten, V. Bécares, A. Billebaud, S. Chabod, T. Chevret, X. Doligez, F.-R. Lecolley, G. Lehaut, N. Marie, F. Mellier, W. Uyttenhove, D. Villamarin, G. Vittiglio, and J. Wagemans. Monte Carlo MSM Correction Factors for Control Rod Worth Estimates in Subcritical and Near-critical Fast Neutron Reactors. In *ICAPP 2015, Nice, France, May 3-6*, 2015.
- G. Lehaut, J.-L. Lecouey, N. Marie, P. Baeten, V. Becares, A. Billebaud, S. Chabod, T. Chevret, X. Doligez, A. Kochetkov, A. Krasa, F.-R. Lecolley, F. Mellier, W. Uyttenhove, D. Villamarin, G. Vittiglio, and J. Wagemans. Study of Space-Energy Effects

in a Subcritical Reactor within a Time-dependent Multi-group 1-dimensional Diffusion Approach. In *ICAPP 2015, Nice, France, May 3-6*, 2015.

- A. Kochetkov, V. Becares, G. Bianchini, M. Carta, X. Doligez, V. Fabrizio, A. Krasa, A. Krasa, G. Lehaut, and W. Uyttenhove. Control Rod Worth Measurements in a Fast Neutron VENUS-F Critical Core. In *ICAPP 2015, Nice, France, May 3-6*, 2015.
- A. Krasa, P. Baeten, A. Kochetkov, W. Uyttenhove, G. Vittiglio, J. Wagemans, L. Mercatali, G. Bianchini, M. Carta, V. Fabrizio, and V. Peluso. The FREYA Project at VENUS-F - The Next Step Towards MYRRHA. In *Advancements in Nuclear Instrumentation Measurement Methods and their Applications (ANIMMA), Lisbon, Portugal, April 20-24*, 2015.
- A. Kochetkov, P. Baeten, W. Uyttenhove, G. Vittiglio, J. Wagemans, A. Billebaud, S. Chabod, X. Doligez, F.R. Lecolley, J.L. Lecouey, G. Lehaut, N. Marie, G. Ban, and F. Mellier. VENUS-F Zero Power Experiments to Support ADS and LFR Designs. In *Third International Scientific and Technical Conference about Innovative Designs and Technologies of Nuclear Power, ISTC NIKIET, Moscow, Russia, October 7-10*, 2014.
- T. Chevret, J.-L. Lecouey, N. Marie, F.-R. Lecolley, G. Lehaut, G. Ban, A. Billebaud, S. Chabod, X. Doligez, A. Kochetkov, P. Baeten, W. Uyttenhove, G. Vittiglio, J. Wagemans, F. Mellier, V. Bécares, and D. Villamarin. Reactivity Measurement of the Lead Fast Subcritical VENUS-F Reactor using Beam Interruption Experiments. In *Proceedings of the International Conference on the PHYSics Of Reactors (PHYSOR2014), Kyoto, Japan*, 2014.
- S. Chabod, A. Billebaud, F.-R. Lecolley, J.-L. Lecouey, G. Lehaut, N. Marie, G. Ban, X. Doligez, A. Kochetkov, P. Baeten, A. Krasa, W. Uyttenhove, G. Vittiglio, and J. Wagemans. Reactivity measurements at GUINEVERE facility using the integral k_p method. In *International Conference on the PHYSics Of Reactors (PHYSOR2014), Kyoto, Japan*, 2014.
- V. Becares, D. Villamarin, E.M. Gonzalez-Romero, A. Kochetkov, P. Baeten, W. Uyttenhove, G. Vittiglio, J. Wagemans, A. Billebaud, S. Chabod, J.-L. Lecouey, F.-R. Lecolley, G. Lehaut, N. Marie, X. Doligez, and F. Mellier. Monte Carlo Assessment of Spatial and Energy Effects in the VENUS-F Subcritical Configurations and Application for Reactivity Determination. In *International Conference on the PHYSics Of Reactors (PHYSOR2014), Kyoto, Japan*, 2014.
- S. Dulla, M. Nervo, P. Ravetto, G. Mila, S. Argirò, S. Beolè, M. Masera, G. Bianchini, M. Carta, V. Fabrizio, V. Peluso, F. Gabrielli, A. Rineiski, A. Kochetkov, P. Baeten, W. Uyttenhove, G. Vittiglio, and J. Wagemans. Interpretation of Experimental Measurements on the SC-1 Configuration of the VENUS-F Core. In *Proceedings of the International Conference on the PHYSics Of Reactors (PHYSOR2014), Kyoto, Japan*, 2014.

- A. Kochetkov, P. Baeten, W. Uyttenhove, G. Vittiglio, J. Wagemans, A. Bilebaud, S. Chabod, J.-L. Lecouey, G. Ban, F.-R. Lecolley, N. Marie, G. Lehaut, X. Doligez, and F. Mellier. An alternative source jerk method implementation for the subcriticality estimation of the VENUS-F subcritical core in the FREYA project. In *Proceedings of the International Conference on the PHYSics Of Reactors (PHYSOR2014), Kyoto, Japan, September 28 - October 3*, 2014.
- A. Krasa, A. Kochetkov, P. Baeten, W. Uyttenhove, G. Vittiglio, and J. Wagemans. Experimental Investigation of the Axial Neutron Flux Distribution in an Accelerator-Driven System. In *International Youth Nuclear Congress (IYNC), Burgos, Spain, July 6-12*, 2014.
- A. Kochetkov, G. Vittiglio, J. Wagemans, W. Uyttenhove, A. Krasa, and J. Hernandez. The Lead-Based VENUS-F Facility: Status of the FREYA Project. In *International Symposium on Reactor Dosimetry (ISRD), Aix-en-Provence, France, May 18-23*, 2014.
- L. Mercatali, X. Doligez, A. Kochetkov, G. Vittiglio, W. Uyttenhove, G. Bianchini, M. Carta, V. Peluso, A. Gandini, and V. Fabrizio. Optimization Studies for a MYRRHA-like Mock-up Configuration in the VENUS-F Facility. In *International Topical Meeting on Nuclear Applications of Accelerators (AccApp), Bruges, Belgium, August 5-8*, 2013.
- N. Marie, G. Lehaut, J.-L. Lecouey, A. Billebaud, S. Chabod, X. Doligez, F.-R. Lecolley, A. Kochetkov, W. Uyttenhove, G. Vittiglio, J. Wagemans, F. Mellier, G. Ban, H.-E. Thyébault, and D. Villamarin. Reactivity Monitoring Using the Area Method for the Subcritical VENUS-F Core within the Framework of the FREYA Project. In *Technology and Components of Accelerator-Driven Systems (TCADS), Second International Workshop, Nantes, France, May 21-23*, 2013.
- S. Chabod, X. Doligez, G. Lehaut, A. Billebaud, J.-L. Lecouey, F.-R. Lecolley, N. Marie, A. Kochetkov, W. Uyttenhove, G. Vittiglio, J. Wagemans, F. Mellier, G. Ban, H.-E. Thyébault, and D. Villamarin. Analysis of Prompt Decay Experiments for ADS Reactivity Monitoring at VENUS-F Facility. In *Technology and Components of Accelerator-Driven Systems (TCADS), Second International Workshop, Nantes, France, May 21-23*, 2013.
- A. Kochetkov, P. Baeten, A. Billebaud, S. Chabod, X. Doligez, F.-R. Lecolley, J.-L. Lecouey, G. Lehaut, N. Marie, H.-E. Thyébault, W. Uyttenhove, J. Wagemans, G. Ban, P. Dessagne, M. Kerveno, and L. Mercatali. Current Progress and Future Plans of the FREYA Project. In *Technology and Components of Accelerator-Driven Systems TCADS, Second International Workshop, Nantes, France, 21-23 May*, 2013.
- H.-E. Thyebault, P. Baeten, A. Billebaud, S. Chabod, A. Kochetkov, F.-R. Lecolley, J.-L. Lecouey, G. Lehaut, N. Marie, F. Mellier, W. Uyttenhove, G. Vittiglio, J. Wagemans, G. Ban, P. Dessagne, M. Kerveno, and J.-C. Steckmeyer. The GUINEVERE Experiment: First PNS Measurements in a Lead Moderated Sub-Critical Fast Core. In *ICAPP, Chicago, USA, June 24-28*, 2012.

- A. Kochetkov, P. Baeten, A. Billebaud, S. Chabod, F.-R. Lecolley, J.-L. Lecouey, N. Marie, F. Mellier, H.-E. Thyébault, G. Vittiglio, W. Uyttenhove, J. Wagemans, G. Ban, P. Dessagne, M. Kerveno, and J.-C. Steckmeyer. The GUINEVERE Project at VENUS-F Facility: Critical Core Configuration. In *GLOBAL, Nagoya, Japan, September 4-9*, 2011.
- P. Baeten, H. Aït Abderrahim, G. Bergmans, A. Kochetkov, W. Uyttenhove, D. Vandeplassche, F. Vermeersch, G. Vittiglio, G. Ban, M. Baylac, A. Billebaud, D. Bondoux, J. Bouvier, S. Chabod, J.M. de Conto, P. Dessagne, G. Gaudiot, J.M. Gautier, G. Heitz, M. Kerveno, B. Launé, F.R. Lecolley, J.-L. Lecouey, N. Marie, Y. Merrer, A. Nuttin, D. Reynet, J.-C. Steckmeyer, and F. Mellier. The GUINEVERE project at the VENUS-F facility. In *European Nuclear Conference (ENC), Barcelona, Spain, May 30 - June 2*, 2010.
- L. Mercatali, P. Baeten, A. Kochetkov, W. Uyttenhove, and G. Vittiglio. The GUINEVERE Experiments at the VENUS Facility: Status and Perspectives. In *European Nuclear Conference (ENC), Barcelona, Spain, May 30 - June 2*, 2010.
- A. Billebaud, P. Baeten, H. Aït Abderrahim, G. Ban, M. Baylac, G. Bergmans, D. Bondoux, J. Boouvier, S. Chabod, J.-M. De Conto, P. Dessagne, G. Gaudiot, J.-M. Gautier, G. Granget, G. Heitz, M. Kerveno, A. Kochetkov, B. Laune, F.-R. Lecolley, J.-L. Lecouey, N. Marie, F. Mellier, Y. Merrer, A. Nuttin, D. Reynet, J.-C. Steckmeyer, W. Uyttenhove, D. Vandeplassche, F. Vermeersch, and G. Vittiglio. The GUINEVERE Project for Accelerator-Driven System Physics. In *GLOBAL, Paris, France, September 6-11*, 2009.

Curriculum Vitae

Wim Uyttenhove (1980, Ghent, Belgium) is a mechanical and nuclear engineer from Ghent University.

In 2005, he started his professional career as a safety engineer at AVN (Association Vinçotte Nuclear), the Belgian nuclear safety inspection body at that time. He performed safety analyses and assisted resident inspectors in the Belgian nuclear power plants of Doel and Tihange.

From 2008 to 2015, he worked as a research and licensing engineer for advanced nuclear systems at SCK•CEN, the Belgian nuclear research centre. He was in charge of the core design, licensing, and commissioning of the VENUS-F installation, a unique accelerator-driven system.

From 2010 onwards, Wim has been a professional trainer of nuclear engineering to junior engineers, senior management, reactor operators, and master students in industry and academia.

In October 2015, Wim launched The Binding Energy. The company offers strategic engineering and communication services, focusing on companies dealing with risks, or active in the energy sector. Wim is passionate about transparent communication and a common sense safety approach.